SEABED MAPPING USING MULTIBEAM SONAR AND COMBINING WITH
FORMER BATHYMETRIC DATA

A THESIS SUBMITTED TO
THE GRADUATE SCHOOL OF NATURAL AND APPLIED SCIENCES
OF
MIDDLE EAST TECHNICAL UNIVERSITY

BY

FATİH FURKAN GÜRTÜRK

IN PARTIAL FULFILLMENT OF THE REQUIREMENTS
FOR
THE DEGREE OF MASTER OF SCIENCE
IN
ELECTRICAL AND ELECTRONIC ENGINEERING

DECEMBER 2015

Approval of the thesis:

SEABED MAPPING USING MULTIBEAM SONAR AND COMBINING WITH FORMER BATHYMETRIC DATA

submitted by **FATİH FURKAN GÜRTÜRK** in partial fulfillment of the requirements for the degree of **Master of Science in Electrical and Electronics Engineering Department, Middle East Technical University** by,

Prof. Dr. Gülbin Dural Ünver   _____
Dean, Graduate School of **Natural and Applied Sciences**

Prof. Dr. Gönül Turhan Sayan   _____
Head of Department, **Electrical and Electronics Engineering**

Prof. Dr. Kemal Leblebicioğlu   _____
Supervisor, **Electrical and Electronics Engineering Dept., METU**

Examining Committee Members:

Prof. Dr. Tolga Çiloğlu   _____
Electrical and Electronics Engineering Dept., METU

Prof. Dr. Kemal Leblebicioğlu   _____
Electrical and Electronics Engineering Dept., METU

Assoc. Prof. Dr. Çağatay Candan   _____
Electrical and Electronics Engineering Dept., METU

Assist. Prof. Dr. Elif Vural   _____
Electrical and Electronics Engineering Dept., METU

Assist. Dr. Yakup Özkazanç   _____
Electrical and Electronics Engineering Dept., Hacettepe Uni.

Date: _____

I hereby declare that all information in this document has been obtained and presented in accordance with academic rules and ethical conduct. I also declare that, as required by these rules and conduct, I have fully cited and referenced all material and results that are not original to this work.

Name, Last name   : Fatih Furkan, Gürtürk

Signature   :

ABSTRACT

SEABED MAPPING USING MULTIBEAM SONAR AND COMBINING WITH FORMER BATHYMETRIC DATA

Gürtürk, Fatih Furkan

M.S., Department of Electrical and Electronic Engineering

Supervisor: Prof. Dr. Kemal Leblebicioğlu

December 2015, 101 pages

The most practical methods in underwater mapping are based on acoustic measurements. In this thesis, a simulation program was developed for mapping the sea depth with a multibeam echosounder. The factors affecting the mapping resolution and accuracy were shown on the simulation. The correction of the sound velocity profile, which affects the sonar's performance, with the Ray Theory was explained. The error sources were explained for measured depth values on each beam and the position assigned for depth measurements.

In transfer of the achieved data to earth reference frame, ship movement and ship's position by GPS were added to the simulation with a certain error rate. In the next phase, use of previously taken bathymetric data on improvement of new measurement is conducted using a novel method. With the use of old measurements, an optimization algorithm is applied to minimize errors caused by ship movement and position assignment. With correction of ship movement data the position errors are corrected and this approach is applied in order to improve the old map data by weighting with measurement quality.

In the conclusion part, simulation results were compared with the acceptable error quantity stated by the International Hydrography Organization (IHO). On specified

depth measurements, error amounts are given and error amount related with ship motion data was summarized. Improvement achieved by weighting of corrected new data and previous data with their measurement quality was shown. Error results were compared on the previous map, on the new measurement and on the map after the improvement. Echosounder resolution required in a bathymetry study in accordance with the IHO standards, ship movement sensor precision, and GPS positioning precision are obtained. Data achieved after improvement were compared with the acceptable error quantity stated by the IHO standards.

Keywords: Underwater Acoustics, Hydrography, Bathymetry, Multibeam Sonar

ÖZ

ÇOK IŞINLI SONAR İLE DENİZ DİBİ HARİTALAMA VE ESKİ BATİMETRİK VERİ İLE BİRLEŞTİRİMİ

Gürtürk, Fatih Furkan

Yüksek Lisans, Elektrik ve Elektronik Mühendisliği

Tez Yöneticisi: Kemal Leblebicioğlu

Aralık 2015, 101 sayfa

Deniz dibi haritalama için en pratik metotlar akustik metotlardır. Bu tezde, çok ışınlı iskandil ile harita oluşturma üzerine bir simülasyon programı geliştirilmiştir. Harita çözünürlüğü ve doğruluğunu etkileyen faktörler simülasyonda gösterilmiştir. Sonarın performansını belirleyen ses hızı profilinin Ray Teorisi ile düzeltilmesi anlatılmıştır. Elde edilen veride her bir ışın için derinlik ve bu derinliğin atanacağı konum bilgisindeki hata kaynakları anlatılmıştır.

Elde edilen derinlik bilgilerinin gerçek koordinat içerisine aktarımında gemi hareketi ve geminin GPS üzerinden alınan konumu belli bir hata oranı ile simülasyona eklenmiştir. Devam eden kısımda yeni bir metot uygulanarak, daha önceden alınmış batimetrik verilerin yeni ölçümde iyileştirme amaçlı kullanılması çalışılmıştır. Eski ölçümlerin yardımıyla gemi hareketi ve konum belirleme kaynaklı hataların azaltılmasına yönelik bir optimizasyon algoritması uygulanmıştır. Gemi hareketi verilerinin düzeltilmesi ile pozisyon hataları düzeltilmiş ve bu yaklaşım eski harita verilerini iyileştirmek amaçlı ölçüm kalitesine göre ağırlıklandırarak uygulanmıştır.

Sonuç bölümünde, simülasyon sonuçları hidrografik çalışmalarda hedeflenen uluslararası standartların belirlendiği Uluslararası Hidrografi Örgütü (IHO)'nün

kabul edilebilir hata miktarları ile kıyaslanmıştır. Belirlenen derinlikte alınan ölçümlerde, hata miktarları verilmiş ve gemi hareketi verileri kaynaklı hataların miktarı özetlenmiştir. Düzeltilmiş veri ile eski verinin ölçüm kalitesine göre ağırlıklandırılmasıyla elde edilen iyileştirmeler gösterilmiştir. Hata sonuçları eski haritada, yeni ölçüm haritasında ve iyileştirme sonrası haritada kıyaslanmıştır. IHO standardına uygun bir batimetri çalışmasında ihtiyaç duyulan iskandil çözünürlüğü, gemi hareket sensörü hassasiyeti, GPS konum bilgisi hassasiyeti çıkarılmıştır. İyileştirme sonrası elde edilen değerler IHO'nun kabul edilebilir hata miktarları ile kıyaslanmıştır.

Anahtar Kelimeler: Sualtı Akustiği, Hidrografi, Batimetri, Çok Işınlı Sonar

to my family....

ACKNOWLEDGEMENTS

members for their social support. I would like to thank to Tülay Yiğiter to make my personal life easier throughout my thesis study.

I would like to express my very great appreciation to my parents for their lifetime support. Special thanks go to my sister Feyza for being supervisor of my life and my brother Fehmi Bey for being hopes of my future.

I am particularly grateful for the assistance given by my family-in-law which are personally real family of mine.

Last but not the least, I would like to thank to my wife Zeynep for being my greatest support not only during my thesis study but also during my lifetime.

TABLE OF CONTENTS

LIST OF TABLES

TABLES

LIST OF FIGURES

FIGURES

LIST OF ABBREVIATIONS

C&GS: Coast and Geodetic Survey

DI: Receiving Directivity Index (DI)

GPS: Global Positioning System

IHO: International Hydrography Organization

LIDAR: Light Detection and Ranging

MBES: Multi-beam Echosounder Systems

NL: Noise Level (NL)

NOAA: National Oceanic Atmospheric Administration

RL: Reverberation Level (RL)

RD: Recognition Differential (RD)

SASS: Sonar Array Sounding System

SL: Source Level (SL)

TL: Transmission Loss (TL)

TS: Target Strength (TS)

CHAPTER 1

INTRODUCTION

Seabeds are the least explored parts of the world despite more than 70% of the earth surface is covered with water [1]. Studies have been progressively revealed in the last century due to advancement in the ocean depth measuring technology. Present depth-measuring techniques employ vehicles ranging from remotely operated near-bottom vehicles to ships on the sea to the satellites around the world. These vehicles can work with acoustics, optics, or radar altimetry depending on the mission and type of the vehicle in order to either directly measure or infer bathymetry [2]. Each technique supplies different spatial resolution and probe ranging from surface coastlines to the deepest trenches. The coastal estuaries and bays must be carefully evaluated in terms of tidal currents as they can change the bathymetry on hourly time scales. At this point the data and analysis techniques used for estimating bathymetry across the worldwide ocean are continuously developed [2].

1.1. Historical Development of Hydrographic Measurements

In 1807, French physicist Dominique Francois Jean Arago first proposed that water depth could be measured by sound waves [3]. Sound velocity in water was first precisely measured as 1435 m/s by Daniel Calladon and Charles Strum in Genova Lake [4]. In 1872, Sir William Thomson discovered mechanic echosounder [3]. In the following 50 years, different types of wire echosounders were developed. The most important wire echosounders were Lucas echosounder used by British ships and deep water echosounders used by Coast and Geodetic Survey (C&GS) [3].
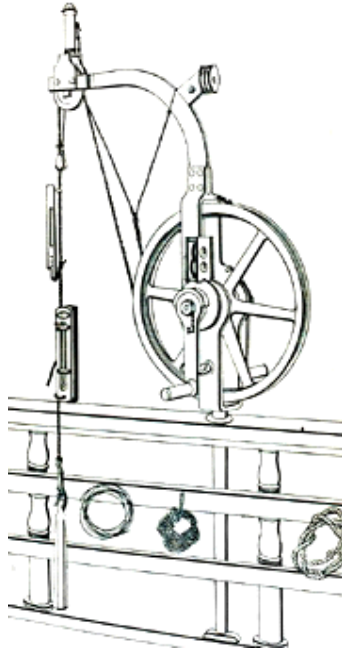
Figure 1.1. Wire echosounder [3]

In 1910, Robert Blake and William Gunn realized that sent echo comes from the seabed after two minutes. Fessenden showed that horizontal and vertical echo is formed in water [3].These turning points led to development of new technologies. In 1922, the first bathymetric map covering the current South California continent border areas was created by making depth measurements with Harvey Hayes' echosounder [5]. Following 312 Fathometer, many echosounders were produced by C&GS [3].

These developments last until the beginning of 1960's. At these years, important discoveries were made for ocean researches. One of them is Side-scanned Sonar System which was developed and used by Scripps Oceanography Institution [6].

Another discovery was Multi-beam Echosounder Systems (MBES). The first MBES known as Sonar Array Sounding System (SASS) was used in 1963. In 1968, current Sea Beam MBES were started to be produced. These developments were used in 1980's [7]. After 1990's, Light Detection and Ranging (LIDAR) echosounders enabled making measurements in shallow waters and coastal areas and creation of digital terrain models easily [8].

1.2. Application Areas of the Hydrographic Measurements

From past to present, human and freight transportation between continents were done by shipping. For this reason, sea depth measurement is indispensable for shipping course. Firstly, hydrographic measurements were used in the shipping course. Current hydrographic measurements are multi-disciplinary and serve to different application areas (Figure 1.2) [9].

Application Areas of the Hydrographic Measurements

Hydrographic Mapping

* Plotting navigation maps
* Placing off-shore platforms
* Laying of cables and pipes
* Military applications

Coastal Engineering

* Preservation of ports against sandblasting
* Determination of coastal erosion
* Calculation of stone fill volume in port astablishment
* Scanning studies
* Application of sea outfall projects

Research and Scientific Applications

* Measurement of wave, flow, tide
* Determination of avarage sea level
* Determination of physical properties of sea water
* Geological applications (eg. determination of sediment structure)
* Geophysic applications (eg. determinations of seabed tectonics)
* Research of underwater resources

Figure 1.2. Application area of the hydrographic measurements [10-12]

Coastal engineering is an application area where planning and engineering studies are done for the most efficient use of the natural sources at coasts and seas [13]. In order the define the hydrodynamic structure; depth, shoreline, flow, wave, and tide measurements and sea level change, sea water properties, water quality, and sediment structure identifications should be well accomplished [13].

In geophysical researches, hydrographic data by MBES and by seismic and side-scan sonar images reveal seabed underwater faults and seabed tectonics [14].

Hydrographic measuring is highly used in research of the underwater resources at oceans, seas, and lakes in determination of location of the sources, extraction of petroleum, and installation and drilling of the petroleum platforms [15]. Hydrographic measuring is also highly used in military applications such as construction of the mine maps, determination of the underwater ammunition areas, and determination of hydrographic situation of the invasion areas and the surroundings in the event of war [16].

Navigation maps used by the ships for a safer journey in the oceans, seas, and lakes are prepared by the hydrography boards of the countries [17]. In Turkey, the navigation maps are prepared by the Navigation, Hydrography, and Oceanography Board at Turkish Naval Forces according to the law published in 1973, [18].

Evaluation of environmental effects of the applications at coasts and seas are done with the hydrographic and oceanographic measurements [19].

1.3. Bathymetry Methods

The bathymetry refers to the seafloor depth relative to the sea level. On the other hand, the concepts involved in measuring bathymetry are quite far from the commonplace definition. Seabed mapping first became a demand for secure sailing at coastal waters. The first oceanographic data collection is conducted using single beam echosounders, by measuring the depth under keel of the ship [20]. Since mid-nineteenth century the shelves, canyons, mountains, and trenches of the seafloor have

been mapped with varying degree of precision. Nowadays the seafloor depth can be measured from kilometer to centimeter using the latest different techniques such as multi-beam sonar from ships, optical remote sensing from aircrafts and satellites, and satellite radar altimetry [2].

Different types of bathymetry data have been collected and modeled into gridded matrices extending the seafloor at 1 arc-minute spatial resolution per pixel (<2 km) or even better resolution for the world portions (e.g. <100 m resolution for U.S. coastal waters) [2]. Nevertheless, the remote regions of the worldwide ocean have been just accurately mapped as the errors in these modeled data sets are common. In contrary to oceans, all lands are mapped with a resolution better than 1m is provided with high tech methods like satellite imaging [21]. However, underwater world, especially deep oceans have only partial oceanographic data collected from sparse explorations. In some parts of the ocean there are only bathymetric values with 15 km horizontal resolution and 250 m vertical accuracy [22]. In fact, the topography of Mars or Venus may be better known than the earth's seafloor [2].
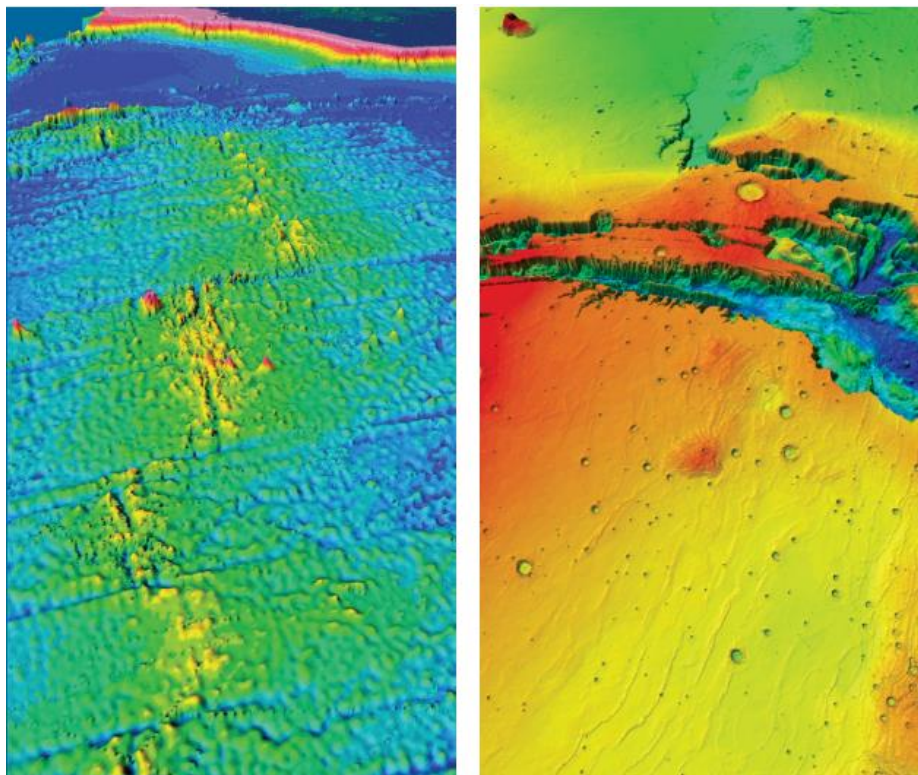
Figure 1.3. Quality of topology data for Mars is much better than ocean bathymetry data [2]

5

The surfaces of Mars, Venus, and the Moon are much better mapped than Earth's ocean floors. Topography of Earth's Mid-Atlantic Ridge (left) derived from sparse ship soundings and satellite altimeter measurements reveals the large-scale structures created by seafloor spreading (ridges and transforms) but the horizontal resolution (15 km) and vertical accuracy (250 m) is poor. Topography of Valles Marineris on Mars (right) reveals both the large-scale structure of the canyon as well as the smaller impact and fracture features. These images have the same horizontal and vertical scale. The horizontal resolution of the Mars data (1 km) is 15 times better than that of the Earth data, while the vertical accuracy (1 m) is 250 times better [2].

Bathymetry measures are done using remote sensing methods where the seafloor is investigated remotely without making physical contact. Most of the bathymetry methods are based on the concept of using the time to estimate the distance. Principally, the sensors measure the round-trip travel time of a beam of light, sound, or radio waves to be reflected from a sensor and return back to the sensor. The elapsed time is then related to the distance travelled by the beam to measure the bathymetry. The longer the elapsed time for a beam to return, the longer the distance traveled. However, in these methods the limitations are spontaneous and no single method is ideal for measuring the complexity and diversity of the underwater landscape and coastline. New techniques are required to properly measure the bathymetry and to evaluate and process the datasets [23-24].

1.4. Acoustic Bathymetry Methods

Acoustic bathymetry or echo sounding became popular in seafloor configuration determination in the 1920s. Initially a single pulse of sound was used to measure the depth by a shipboard hydrophone from elapsed time for the travel of the sound to the seafloor and to be reflected. The depth was calculated by multiplying the one half of the round time traveled and velocity of the sound in the sea [25-26].
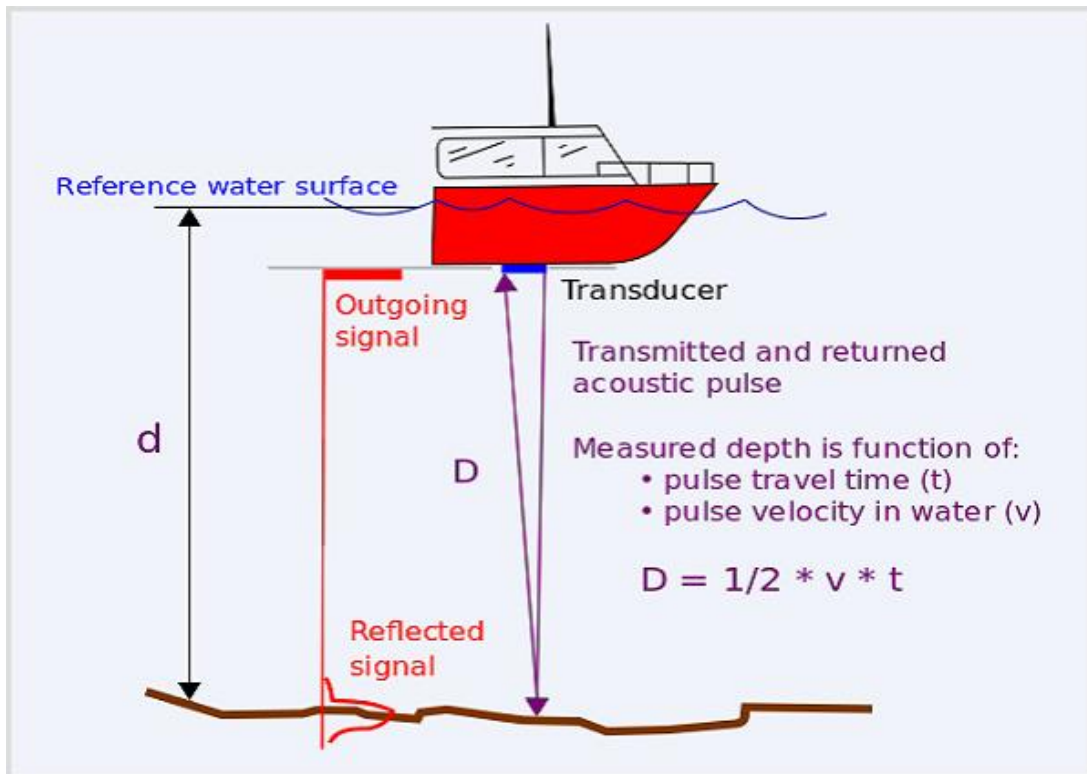
Figure 1.4. Single beam echosounder operation [27]

It is previously noted by the Leonardo da Vinci in 1490 and later by Benjamin Franklin in 1762 that in water sound travels with a little attenuation when compared it's in air [2]. Similarly in water sound travels faster than in air and so the large ocean depths can be acoustically probed without any significant degradation of the signal. Even though the velocity of the sound in seawater varies with ocean temperature, pressure, and salinity, the approximate velocity of sound in seawater is 1500 meters per second. Not only the velocity of the sound but also the character of the seabed, vegetative cover, biota and other particles in the water column may affect the precision of the measured depth [28].
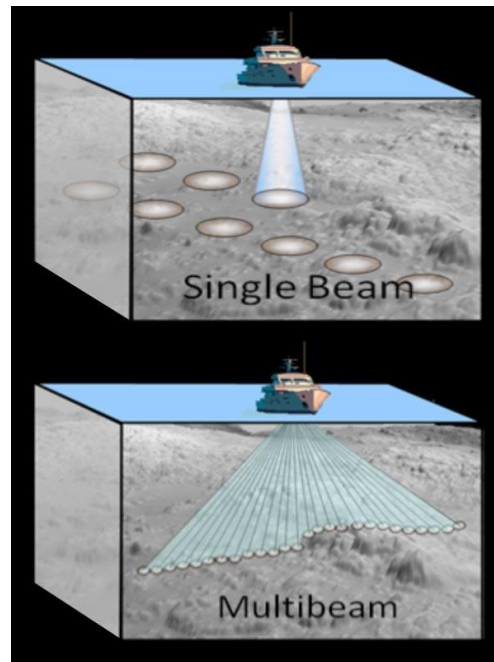
Figure 1.5. Coverage efficiency of multibeam echosounder compared to singlebeam echosounder [29]

Nowadays the multibeam sonar technology is used to produce high resolution measurements of the ocean depth. Each multibeam sonar ping emits a single wide swath of sound (i.e., up to 153 degrees) reflecting of the seafloor [30]. The returning echo is taken by a transducer array and electronically separated into a few individual beams where the depths are calculated for each beam separately. In this manner, very high resolution is achieved even in shallow water with decreasing swath width. On the other hand, the efficiency of the ship operation in deep water is increased as the swath width grows geometrically with decreasing resolution [31].
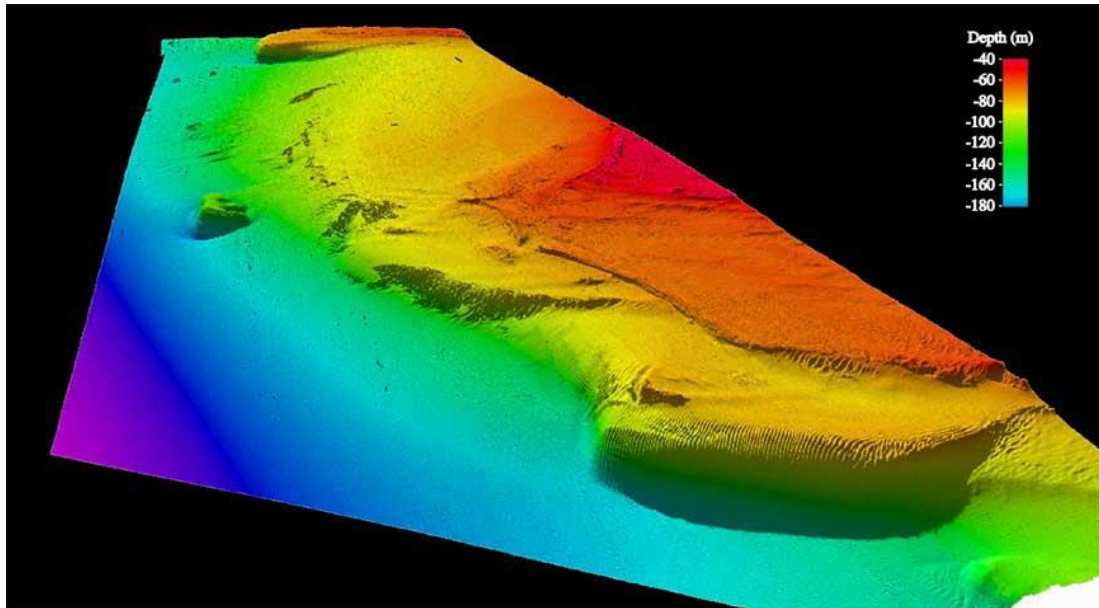
Figure 1.6. An image obtained with a multibeam echosounder [32]

In multibeam sonar technology, a swath of the seafloor is imaged with a pattern similar to "mowing the grass" where the swatch of the seafloor is acoustically imaged with a survey ship's each pass. The overlapping swaths produce a bathymetric map of the area being investigated. Different sound frequencies (e.g., 12-400 kHz) are used for different depth ranges [2]. The sound with lower frequency can measure deeper depths while high frequency sounds can measure shallower depths but with a higher resolution. The level of resolution and the accuracy estimated in bathymetry was previously unachievable. For instance, the shallow-water multibeam systems have been effectively used to map the coastal waters of the United States where the bathymetry is measured at roughly 10 cm scale in 10 m of water [33].

Moreover, the concentrated mapping programs include "sidescan" sonar for a qualitative view of the characteristics of the seafloor reflectivity. Acoustic sensors can maintain a constant position relating to the seafloor and provide high resolution bathymetry by placing them on remotely operated tethered vehicles or autonomous underwater vehicles such as gliders [34].

The acoustic measurements have time and cost associated disadvantages with making the measurements by a ship in deep waters or a small vessel in shallow

waters. Many survey lines with overlapping tracks must be run to build up high resolution consistent images. Excessive ship or glider tracks are required in coastal estuaries and bays with shallower water as the swath width decreases in shallow water. Therefore, in coastal regimes detailed surveys require remarkable time and effort to cover relatively small portions of the sea bed. To conclude, the acoustic methods can be used all along the oceanic depths from shallow estuaries to the deepest trenches. The acoustic systems are not ideal for operating shallow waters due to changes and shoreline configuration changes caused by tidal currents, storm surge, and sea level changes while even in deep water ship time is still costly [35].

1.5. Current Studies on Multibeam Echosounders

Multibeam echosounder systems are so sensitive and reliable systems that they are widely used in underwater measurements at many places of the world from shallow waters to deep waters. Figure 1.7, which is taken from National Oceanic Atmospheric Administration (NOAA), shows that the hydrographic studies are conducted around the world oceans.
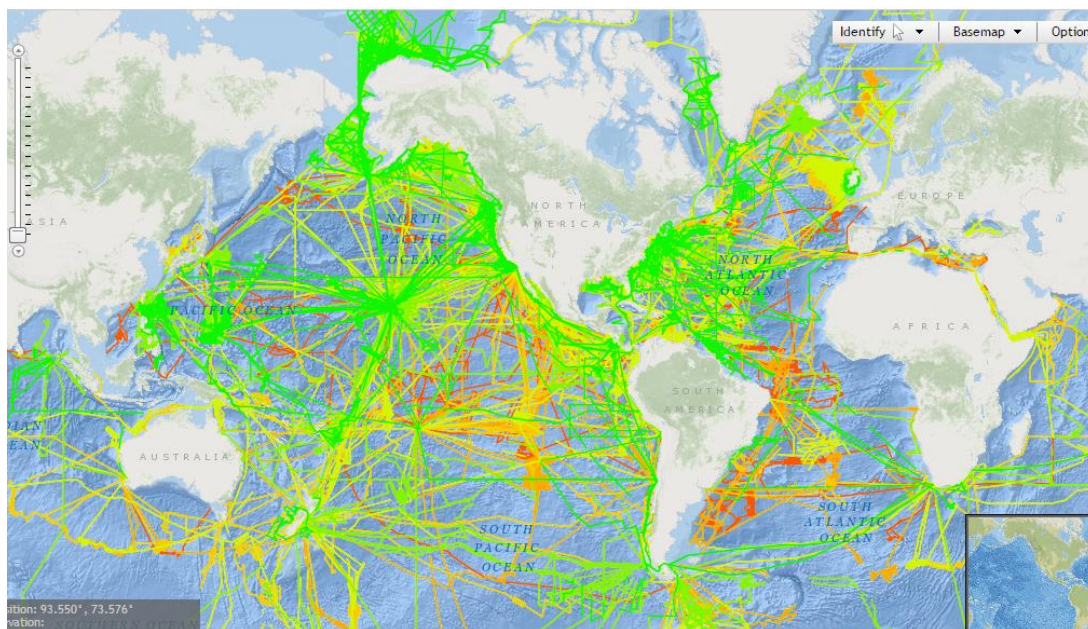
Figure 1.7. Multibeam bathymetry map showing the studies conducted around the world oceans [68]

Figure 1.8 reveals that the bathymetry measurements are repeated at critical locations. It is seen that measurements are repeated over the years. At NOAA archive, various these types of examples could be found for different locations.
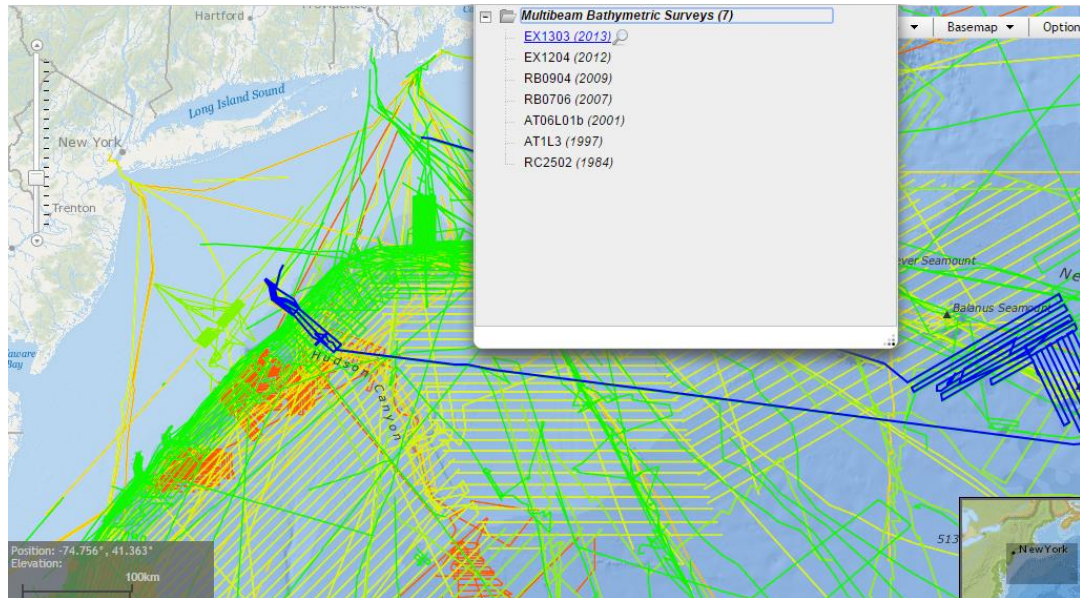
Figure 1.8. Multibeam bathymetry map showing the studies conducted over the years at the critical locations [68]

A recent study on MBS aims to weaken the effect of residual errors based on frequency-spectrum characteristics of seabed topography and multibeam bathymetric data [69]. Another recent study applied a crossover-error analysis and method of data compilation to multi-source multibeam sets, and yet revealed to have limited hydrographic capabilities in extended continental shelf regions [70]. In another recent study, consecutive MBES surveys were carried out to experience the seafloor change and to measure the corresponding volumes involved in active sedimentation processes by using the uncertainty information provided by the MBES data processing algorithm CUBE [71]. However, none of these studies were reported for error amount reduction using the bathymetry data from the same region together. To accomplish this, the maps have to have very little positional error to overlap with each other. Therefore, we apply a method to decrease the positional error.

1.6. Scope of the Thesis

Nowadays, earth's topography is achieved with high resolution and satellite images and landforms are open access to even all individuals. However, ocean bottom images, which form very large portion of the world, are achieved in limited quantities. Coordinate related depth data exist in determination of underwater landforms. In this manner, underwater mapping is a part of hydrography-bathymetry sciences and these studies serve to "hydrographic mapping", "coastal engineering", and "scientific applications" fields, which is deeply explained in Chapter 1. Depth measurement need arises due to navigational needs since underwater mapping has critical importance in ships' safety of navigation. Nowadays, the need for underwater images with high resolution arises from areas such as in underwater cable and pipe laying or coastal engineering and military application requirements. The most practical methods in underwater mapping are acoustic methods.

In this thesis study a simulation program is developed on depth measurement with multibeam sonar. On some places in the world, where navigational or under sea applications are vital, repeated multibeam echosounder measurements are documented. However, mapping process is heavily affected by the positional errors. Because of the positional errors, consecutive depth measurements are not suitable for improvement in depth accuracy. In this thesis, process of positioning the new measurements on old bathymetric data is studied. After fitting the new measurements on the old bathymetric data, different measurements taken on different time are corrected together.

In Chapter 2, the sonar simulation basics are explained. The array and parameters of multibeam echosounder geometry are modeled. Environmental parameters affecting simulation are explained mathematically and added to simulation. Ship movement and location sensors which are the positional error sources are modeled.

In Chapter 3, for each beam, conversion of the travel time information to depth value using the geometry is modeled in the simulation. The error occurred during estimation of travel time is modeled with the effect of grazing angle on the scatterer,

the effect of sound velocity and the effect of draft, collapse and sitting of the ship. The effect of ship motion and the effect of ship position information on depth reading location are modeled.

In transfer of the achieved data to earth reference frame, ship movement and ship's position by GPS were added to the simulation with a certain error rate. Usage of previously taken bathymetric data on improvement of new measurement is conducted using a novel method, which is explained in Chapter 4. In the literature survey, no study was reported for error amount reduction using the data from the same region together. This study aims to overlap the maps by decreasing the positional error. In this manner, depth error is fixed by weighted averaging method in the overlapping regions. With the use of old measurements, an optimization which is not in the literature is applied to minimize errors caused by ship movement and position assignment. With correction of ship movement data the position errors are corrected and improvement is applied with the old map data by weighting with measurement quality.

In Chapter 4, simulation results were compared with the acceptable error quantity stated by the International Hydrography Organization (IHO). On specified depth measurements, error amounts are given and error amount related with ship motion data was summarized. Results of correction with optimization of ship movement data were shown. Improvement achieved by weighting of corrected new data and previous data with their measurement quality were shown. The error amount in total result was extracted from the difference of data measured on the map and simulation absolute truth. Error results were compared on the previous map, the new measurement and the map after the improvement. Echosounder resolution required in a bathymetry study in accordance with the IHO standards, ship movement sensor precision, and GPS positioning precision are obtained. Data achieved after improvement were compared with the acceptable error quantity stated by the IHO standards.

CHAPTER 2

SONAR AND SONAR SIMULATION FUNDAMENTALS

2.1. Sound Pressure Level

For a wave to be a plane wave, pressure changes only in the direction of propagation of the sound; pressure is the same at all points in any plane normal to this direction. Wave fronts are those normal planes - separated by one wavelength, λ where p is at a maximum [56].

The speed of sound which is the longitudinal motion of the wave fronts in the medium is calculated by multiplying wavelength and frequency as follows:

$$c = f\lambda$$

The speed of sound is a parameter different from particle velocity, u. Particle velocity is one of the propagating amplitudes (p,u). Speed of sound is denoted as c and, u refers to the movement of the molecules in the medium [57].

$$p = (\rho c)u$$

p = pressure (Pa or N/m2)

u = particle velocity (m/s)

p = fluid density = 10^3 kg/m^3 for sea water

c = velocity of sound wave propagation = 1.5 x 10^3 m/s in sea water

pc = specific acoustic impedance = Z = 1.5 x 10^6 kg m^{-2} s^{-1} for sea water

The sound wave carries mechanical energy with it in the form of the kinetic energy of the particles and the potential energy of the stresses in the medium. Because the wave is propagating, a certain amount of energy per second will flow across unit area normal to the direction of propagation.

This energy per second (power) crossing unit area is known as the intensity of the wave (power per unit area). For a plane wave, the intensity is related to the pressure as follows [58]:

$$I = p^2 / \rho c$$

The reference intensity (I_r) in underwater sound is the intensity of a plane wave having a root mean square (RMS) pressure equal to 1 µPa (one micropascal). Inserting 1 µPa = 10^{-6} Pa and pc = 1.5 x 10^{-6} in the above equation for I, the formula below is obtained:

$$I_r = 0.67 \text{ x } 10^{-18} \text{ W/m}^2$$

2.2. Source Level

The source level (SL) is defined as follows:

$$SL = 10\log \left(\frac{\text{intensity of source at standard range}}{\text{reference intensity}} \right)$$

At 1 meter, the acoustic center of an omnidirectional source is surrounded by a sphere of surface area of $4\pi r^2$ or omnidirectional power output of P watts, I_r and I_I. The SL is calculated as follows [58]:

$$SL = 10\log \left(\frac{I_I}{I_r} \right)$$

2.3. Sonar Equation

The sonar equation is an expression used to quantify various aspects of sonar performance. Equations vary according to active or passive sonars. Active sonars are differentiated according to noise or reverberation limited conditions.

Table 2.1. Sonar parameters and definitions [58]

Parameter	Definition
Source Level (SL)	$10\log_{10}\dfrac{intensity\ of\ source}{reference\ intensity^{4}}$
Transmission Loss (TL)	$10\log_{10}\dfrac{signal\ intensity\ at\ 1\ m}{signal\ intensity\ at\ target\ or\ receiver}$
Target Strength (TS)	$10\log_{10}\dfrac{echo\ intensity\ at\ 1\ m\ from\ target}{incident\ intensity}$
Noise Level (NL)	$10\log_{10}\dfrac{noise\ intensity}{reference\ intensity^{4}}$
Receiving Directivity Index (DI)	$10\log_{10}$ $\dfrac{noise\ power\ generated\ by\ an\ equivalent\ nondirectional\ hydrophone}{noise\ power\ generated\ by\ actual\ hydrophone}$
Reverberation Level (RL)	$10\log_{10}\dfrac{reverberation\ power\ at\ hydrophone\ terminals}{power\ generated\ by\ signal\ of\ reference\ intensity^{4}}$
Recognition Differential (RD)	$10\log_{10}\dfrac{signal\ power\ to\ just\ perform\ a\ certain\ function}{noise\ power\ at\ display}$

Table 2.2. Terminology of various combinations of the sonar parameters [58]

Name	Parameters
Echo level	SL-2TL+TS
Noise-masking level	NL-DI+DT
Reverberation-masking level	RL+DT
Echo excess	SL-2TL+TS-(NL-DI+DT)
Performance figure	SL-(NL-DI)
Figure of merit	SL-(NL-DI+DT)

2.4. Sonar Simulation Models

2.4.1. Propagation Models

Sonar propagation models aim using three dimensional, time dependent wave equation. Sound propagation solution is conducted using boundaries as surface and bottom. Moreover it specifically uses sound speed variation in the volume. Propagation model techniques can be listed as ray models to calculate ray tracing with propagation loss. Normal mode solutions are simulating the solution of wave equation from the form of integral representation. Multipath techniques use a set of rays to be solved on infinite set of integrals. Far field theory is another propagation

model mostly used in seismology, and may also be called discrete wavenumber method. Another technique for propagation model solution is the parabolic approximation approach which solves the wave equation with a simplification to elliptic approximation [72].

2.4.2. Sonar Performance Models

The aim of sonar performance model is to solve the sonar equations using environmental parameters, propagation parameters, noise and reverberation estimations and signal-processing models. Sonar performance models are used to estimate the sonar detection capabilities. Sonar performance models mainly categorized with sonar characteristics. Passive sonars, active sonars, mono and bi-static sonars, noise limited or reverberation limited conditions determine the type of sonar performance model [68].

2.4.3. Noise & Reverberation Models

Noise is unwanted background sound and depends on location, time and frequency of operation. Underwater noise mostly occurs by natural sources. Noise from ship propellers is a good example of man-made noise, if the propeller is not the signal that is to be detected. Noise models aim to calculate ambient noise levels, which are critical for sonar performance models. Noise models use noise simulations induced from surface waves, biological sources and man-made sources [68].

Reverberation is underwater sound reflections and scattering effects due to sea surface and sea floor. Volume reverberation is also defined for reflection caused by small particles which have significance near acoustic source. Bottom and sea have mostly higher levels of reflection than object to be detected. However, volume reverberation stays under noise level in distances far away from acoustic source. Reverberation models are built on summation of cell reflections or summation of point reflections. Reverberation calculation using cells is done by dividing the volume to small cells which consists uniformly distributed scatterers. Point scatterers are modeled with assumption of random distributed scatterers in the volume [68].

2.5. Acoustic Plane Wave Equation

Acoustic wave equation is a second order differential equation, which can be written using Hooke's law and conservation of mass [59]. It is assumed that there is an infinite homogeneous medium in equilibrium, where a rigid plane is boundary to the right of the applied force. For simplicity, it is assumed that the applied force is not varying with time. The excess pressure (relative to the equilibrium condition) remains everywhere the same. Between the plane at x_0 and the rigid boundary, there is no net force across any small volume of water. Accordingly, there is no particle motion and particle speed $u(x, t)$. Nevertheless, the compressional force, acting in the positive x-direction against the rigid boundary, will cause a particle displacement in the x-direction, at the location x_0. This displacement decreases linearly when x increases, to zero at the rigid boundary [60].

It is assumed to be the small volume element with original length dx and unit area in the plane of the applied force. The equilibrium volume V of the element is hereby equal to dx. The application of the compressional force changes the volume of the element as in the following equation:

$$V' = dx + d\xi = dx + \frac{\partial \xi}{\partial x} dx$$

The change in volume is as follows:

$$dV = V' - V = \frac{\partial \xi}{\partial x} dx$$

The produced strain in the volume element is defined as the ratio of the volume change to the original volume and is calculated as:

$$\text{Strain} = \frac{dV}{V} = \frac{\frac{\partial \xi}{\partial x} dx}{dx} = \frac{\partial \xi}{\partial x}$$

The ratio of stress to strain in an elastic medium is constant according to Hooke's Law. In this equation, the stress is the static applied pressure and the constant is the bulk modulus of elasticity, B. In case of a positive pressure in the x-direction, the strain is negative as follows:

$$\frac{p(x)}{\frac{\partial \xi}{\partial x}} = -B \qquad \text{OR} \qquad p(x) = -B \frac{\partial \xi}{\partial x}$$

Rather than static pressure, generally the applied pressure is varying in time. Accordingly, the pressure magnitude will be a function of distance (x) as well as time (t). In general, there will be a pressure differential across a volume element of length dx as shown in the following formula:

$$dp = \frac{\partial p(x, t)}{\partial x} \, dx$$

This net pressure causes an acceleration of the element, or particle as defined by Newton's second law of motion.

$$\frac{\partial p(x, t)}{\partial x} \, dx = -(\rho \, dx) \frac{\partial u(x, t)}{\partial t}$$

The negative sign in this equation is resulted from the fact that a net acceleration to the right requires a negative spatial pressure gradient. In this equation, ρ is the medium density, and ρdx is the mass of the volume element. The particle acceleration is calculated by the partial derivative of the particle speed u(x,t) with respect to time. Consequently, as dx appears on both sides of the previous equation, the equation becomes as follows:

$$\frac{\partial p}{\partial x} = -\rho \frac{\partial u}{\partial t} \qquad (*)$$

This equation represents the inertial reaction. Particle mass stands against a change in speed under influence of an applied force. Similar to a time-varying applied pressure,

the strain produced in a volume element is also time varying. A second differential equation is achieved by taking the partial derivative with respect to time.

$$\frac{\partial p(x,t)}{\partial t} = -B\frac{\partial}{\partial t}\left(\frac{\partial \xi(x,t)}{\partial x}\right) = -B\frac{\partial}{\partial x}\left(\frac{\partial \xi(x,t)}{\partial t}\right)$$

The particle speed u(x,t) is defined as the time rate of change of particle displacement as shown in the following formula:

$$u(x,t) = \frac{\partial \xi(x,t)}{\partial t}$$

After substitution of u(x,t) to the equation and rearranging the equation, following equation is achieved:

$$\frac{\partial u}{\partial x} = -\frac{1}{B}\frac{\partial p}{\partial t} \qquad (**)$$

In this equation, the time rate of change of pressure to the differential speed across an element is related by means of the elastic properties of the medium [60].

Equations (*) and (**) could be solved simultaneously for either pressure or particle velocity in exactly the same way as used for the electrical transmission line. Accordingly the following equation is achieved:

$$\frac{\partial^2 p}{\partial t^2} = \frac{B}{\rho}\frac{\partial^2 p}{\partial x^2}$$

This equation has the form of the differential acoustic plane wave equation. This equation has mechanical analog of the electrical lossless transmission line. The analogous relationship between the electrical and mechanical parameters is listed in Table 2.3.

Table 2.3. Analogy of electrical and acoustic wave parameters [60]

Electrical Parameter		Mechanical Parameter	
Voltage	v	Pressure	p
Current	i	Particle speed	u
Inductance/unit length	L	Density	ρ
Capacitance/unit length	C	Inverse of bulk modulus of elasticity	B^{-1}

The solutions to differential acoustic plane wave equation have the following form:

$$p(x,t) = p_1 \left[t - (x + k_1)\sqrt{\frac{\rho}{B}} \right] + p_2 \left[t + (x + k_2)\sqrt{\frac{\rho}{B}} \right]$$

In this equation, the functions of p_1 and p_2 represent forward and backward traveling waves, respectively. Moreover, the propagation speed can be observed in the water [60].
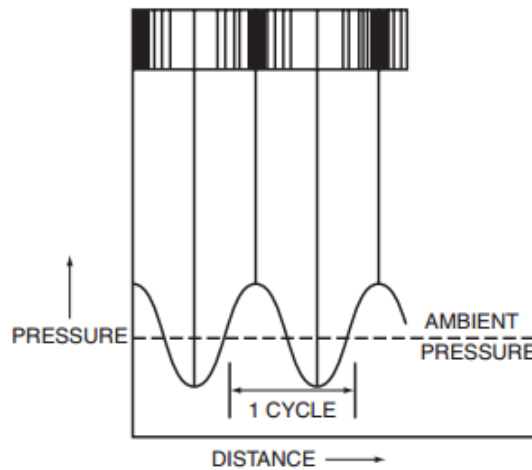
Figure 2.1. Acoustic wave [59]

2.6. Array Beamforming

Arrays are beneficial as the signals arrive at the different sensors at different times because of the array geometry and signal angle. The time delay for a signal incident on two sensors is illustrated below.
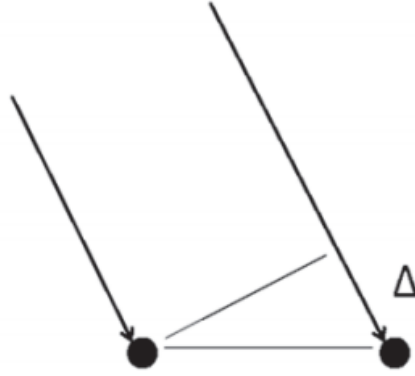
Figure 2.2. Time delay, Δ, associated with a signal incident on a two-sensor array [61]

The signal interaction with the array can be modeled using matrices. The measured data, y(t), over an array of n sensors is expressed as a mapping of the signal, s(t), onto the array with the addition of noise.

$$\begin{pmatrix} y_1(t) \\ y_2(t) \\ \vdots \\ y_n(t) \end{pmatrix} = \begin{pmatrix} 1 \\ \Delta_2 \\ \vdots \\ \Delta_n \end{pmatrix} s(t) + noise$$

The mapping covers a series of time delays, which are functionally symbolized by Δ. The signal is referenced to the first array sensor, and similarly the time delays are referenced to the first array sensor. It is convenient to entitle this mapping vector, D [61].

The basis of beamforming involves inverting the equation to ensure the best estimate of the signal from the measured data. The optimum solution in a least-squares sense can be arranged using the Moore-Penrose inverse. This inverse equation is widely used in a variety of applications. It is applied by first left multiplying the matrix above by the complex transpose of the mapping vector, D†. Afterwards, as D†D is a square matrix (in this case a scalar), left multiplying by (D†D)⁻¹. This allows to predict the signal, s(t), to be expressed in terms of the measured sensor data, y(t), and the mapping vector, D. As D†D = n, the matrix becomes as follows:

23

$$s(t) = (D^\dagger D)^{-1} D^\dagger \begin{pmatrix} y_1(t) \\ y_2(t) \\ \vdots \\ y_n(t) \end{pmatrix}$$

The mathematical interpretation of this equation is commonly called as delay-and-sum beamforming. This equation forms the basis for beamforming methods.

In the mapping matrix, the required time shifts have a particularly simple representation for narrowband signals. This phenomenon is based on the observation of that shifting the phase of a narrowband signal approximates a time shift. The resulting equations bring about high resolution beamforming and direction-of-arrival estimation [61].

According to the Figure 2.2 (Time delay, Δ, associated with a signal incident on a two-sensor array), the extra distance (Δ) that the signal (s) has to travel to the second array element is geometrically determined by the distance between the sensors (a) and the angle of incidence (θ). This extra distance is calculated as follows:

$$\Delta = a \sin(\theta)$$

For narrowband signals, it is convenient to state this distance as the radian measure of the fraction of a wavelength extra distance that the signal travels.

$$\Phi = \frac{2\Pi}{\lambda} a \sin(\theta)$$

Afterwards, this phase angle can be used to simulate a progressive or delayed narrowband signal by simple multiplication of the phase term.

$$e^{i\varphi} e^{i\omega t} = e^{i(\omega t + \varphi)}$$

It should be noted that this approach is just an approximation, not actually shift the signal in time. In fact, it only changes the phase to match a signal shifted in time.

This phase-shifted signal starts and stops at the same time samples as the original signal. Therefore, it is not actually time shifted in fact it approximates a time-shifted signal over part of its interval. This could cause some problems in short signal pulses and large time shifts. The general sonar problem includes multiple sensors and multiple signals. This could be expressed as a mapping, D, of the m signals onto the n sensors in the array [61].

$$
\begin{pmatrix} y_1(t) \\ y_2(t) \\ \vdots \\ y_n(t) \end{pmatrix} = D \begin{pmatrix} s_1(t) \\ s_2(t) \\ \vdots \\ s_m(t) \end{pmatrix} + noise
$$

The narrowband mapping or steering matrix, D, could be represented in terms of the phase shifts, φ, associated with the various directions of arrival. In this matrix, each column corresponds to a different signal. For a uniform linear array, which is often encountered, the steering matrix has the following Vandermonde structure:

$$
D = \begin{pmatrix} 1 & 1 & \cdots & 1 \\ e^{i\varphi_1} & e^{i\varphi_2} & \cdots & e^{i\varphi_m} \\ \vdots & \vdots & \ddots & \vdots \\ e^{i(n-1)\varphi_1} & e^{i(n-1)\varphi_2} & \cdots & e^{i(n-1)\varphi_m} \end{pmatrix}
$$

Other array geometries can be easily established with this approach by correctly modeling the various phase delays related with the various time delays. Beamforming requires inverting. Therefore, the following representation for the signals is achieved when Moore-Penrose inverse is used:

$$
\begin{pmatrix} s_1(t) \\ s_2(t) \\ \vdots \\ s_m(t) \end{pmatrix} = (D^\dagger D)^{-1} D^\dagger \begin{pmatrix} y_1(t) \\ y_2(t) \\ \vdots \\ y_n(t) \end{pmatrix}
$$

25

2.7. Simulation Block Diagram

A projector line array transmits sound preferably in all directions perpendicular to the axis of the array, ensonifying a strip of the ocean bottom. Similarly, a hydrophone array aligned parallel to the projector array gets echoes from all locations along a similar strip of the ocean floor. This method is not adequate to locate echoes on the ocean floor. The projector array will cause echoes throughout the ensonified strip, and the hydrophone array will collect echoes from a similar strip. It is impossible to state whether or not the echoes occur along these strips [62].
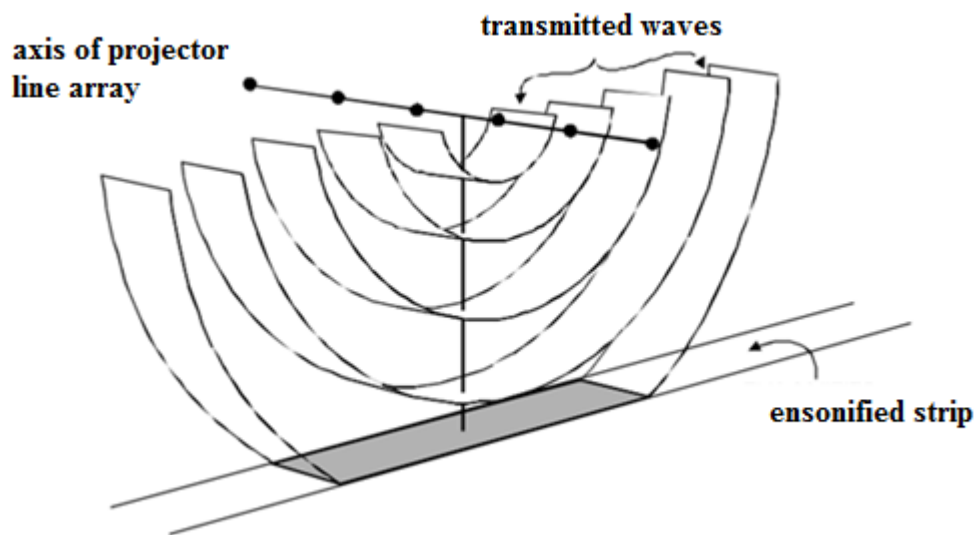
Figure 2.3. Projector array ensonifying as strip of the ocean floor [63]

On the other hand, if the projector and hydrophone arrays are perpendicular to each other, the strip of the ocean floor ensonified by the projectors will intersect with the strip of the ocean floor observed by the hydrophones. This only occurs in a small area with dimensions that approximately correspond to the projector and hydrophone array beamwidths [63].

While echoes occur along the all ensonified area, and sound may be taken from the all observed area, the only part of the bottom both ensonified by the projector array and observed by the hydrophone array beam is the area where the two strips overlap.

The amplitude trace from the hydrophone array will only have those echoes from the transmitted ping occurring in this area. The perpendicular arrangement of the projector and hydrophone line arrays is entitled as Mills Cross, which is named after a pioneering radio astronomy instrument built in New South Wales, Australia [63].
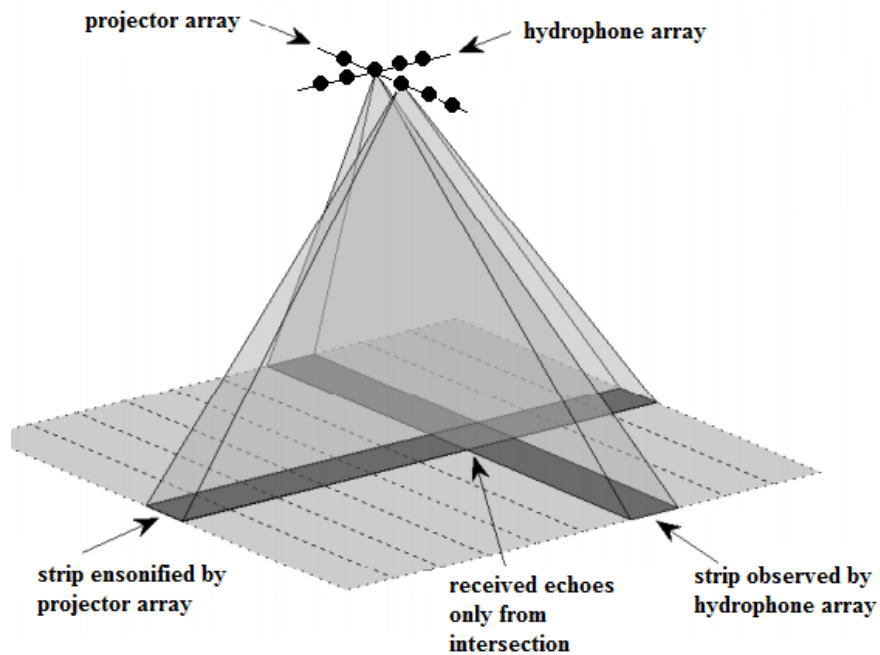
Figure 2.4. Mills cross arrangement of the projector and hydrophone arrays [63]

Beam steering is applied to hydrophone array to generate echoes from multiple angles. For a given angle, echo reply corresponds to parallel strips of the bottom. Ensonified area which is perpendicular to this strip gives out the position of measurement.

Using this arrangement, multiple beams are created simultaneously and, from all along the ensonified area, a number of depth measurements are obtained which is equal to number of beams formed. This method is common in current multibeam sonar products [62].
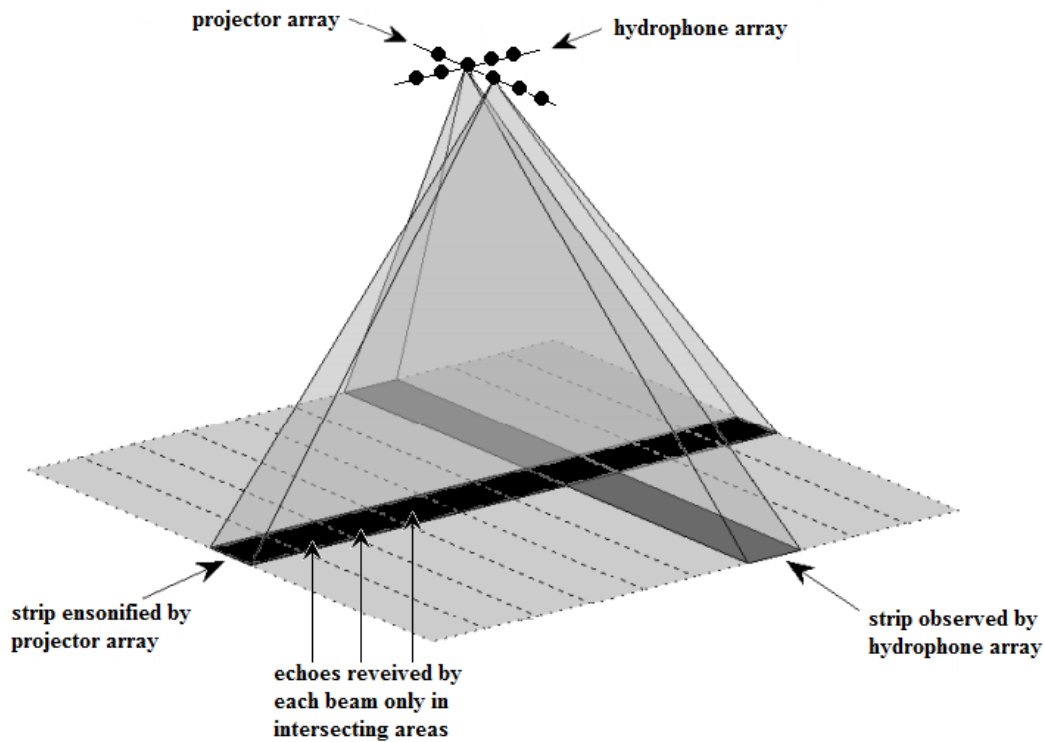
Figure 2.5. Mills cross with multiple steered beams [62]

With Mills Cross technique, the projector array ensonifies a strip as shown in Figure 2.5. Therefore, the return echoes on receiver array will be only from the ensonified area. After beam steering applied to return echo on the hydrophone array, beams generated for each angle will receive from the steered angle. Beamforming is applied on the received data set which is time versus amplitude functions for hydrophone. The beamformer output becomes time versus amplitude functions for each beam direction.

A block diagram is shown in Figure 2.6. In the simulation, parameters are set for once. Map generation, setting multibeam echosounder parameters and environmental parameters are conducted in the first stage of the simulation. These parameters affect one ping cycle of multibeam echosounder. While running a ping cycle, the ship position and motion data is generated. Also, sensor data for position and motion is generated by adding zero mean Gaussian noise. Depth readings from ping cycle and outputs of position and motion sensors are kept for data assignment. At the data

assignment part, the ensonified positions for each beam are calculated using position and motion sensor data. Then, depth readings are assigned to these beam positions. The block diagram of multibeam simulation is shown in Figure 2.6.
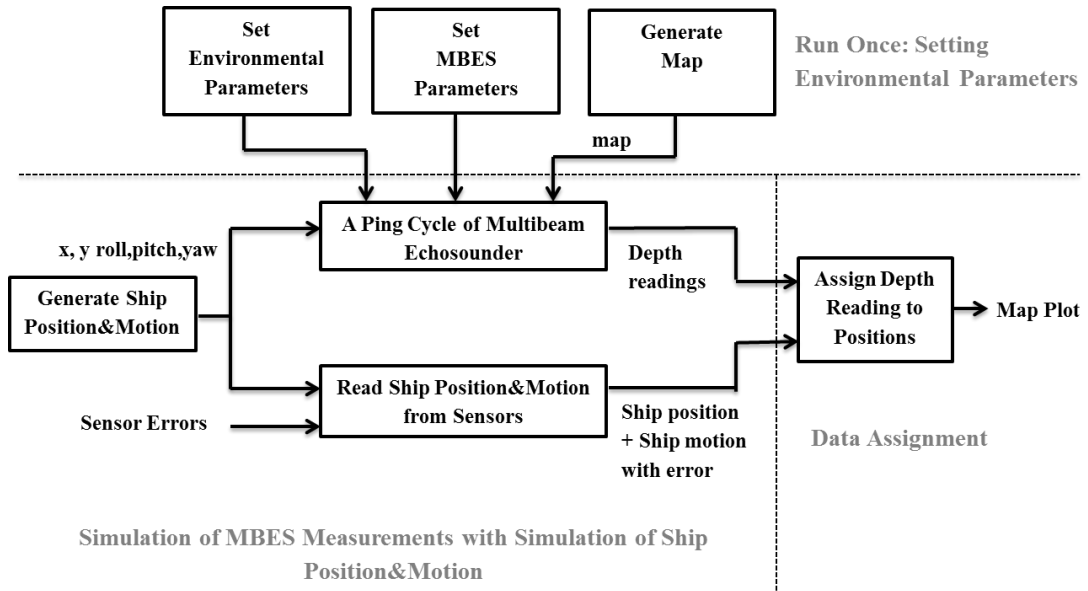
Figure 2.6. First block diagram of multibeam sonar simulation

For simulation purposes, sonar equation for each beam is considered. Amplitude of each beam direction is calculated with sonar equation. After generation of each beam, the beams are positioned on a circular plot. The circular plot edges show the maximum angle of beam steering. In Figure 2.7, the generated sonar image is shown. On the echo simulator, 160 beam echo replies are simulated. With the 160 different echo reply, 0.6° beamwidth is observed. The main purpose of the simulation is to obtain the depth value from the echo simulation. Since the expected echo level is not known due to unknown angle of incidence, thresholding is not sufficient to detect the depth value. However, the maximum echo level can be deducted as bottom echo, since the bottom is the largest object in the area of interest. The transmission loss affects the echo level on fourth power, so the near objects may have greater echo than the bottom. To avoid near objects to be detected as depth value, time varying gain can be applied. With the use of time varying gain, echoes on higher distances become on the same level with nearer objects.

a)

b)
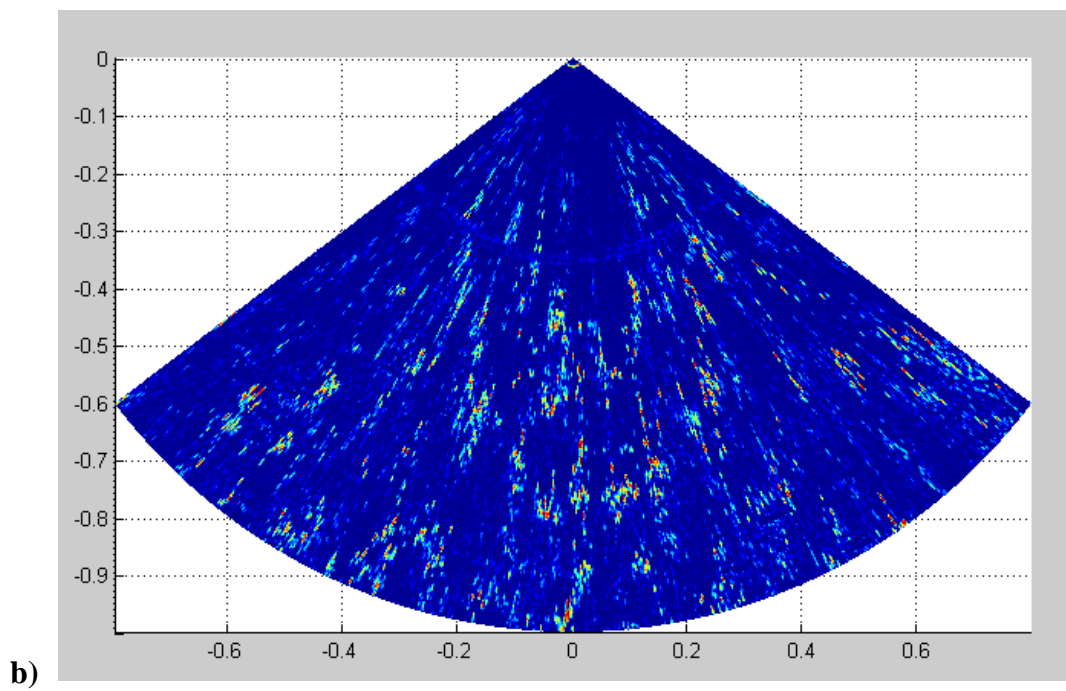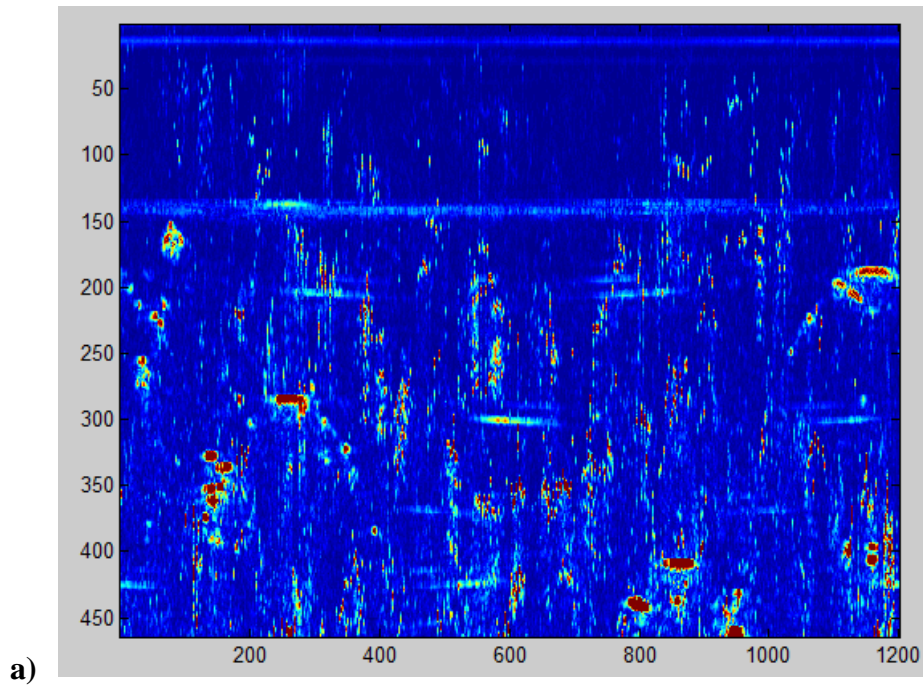
Figure 2.7. Echo simulator for simulated beam angles

a) vertically illustrated echo replies, b) echoes illustrated in polar plot
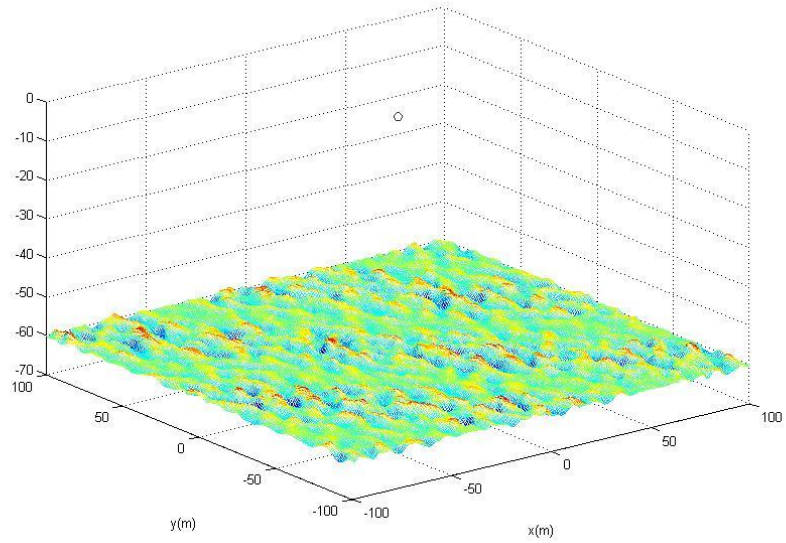
Figure 2.8. Sea bottom around the ±100 m of surface ship

On Figure 2.8, ship position is shown on (0,0,0) point. This indicates the initial position of the ship. Bottom map to be considered is shown on Figure 2.8 where the area of interest is shown as ±100 m in x and y directions.
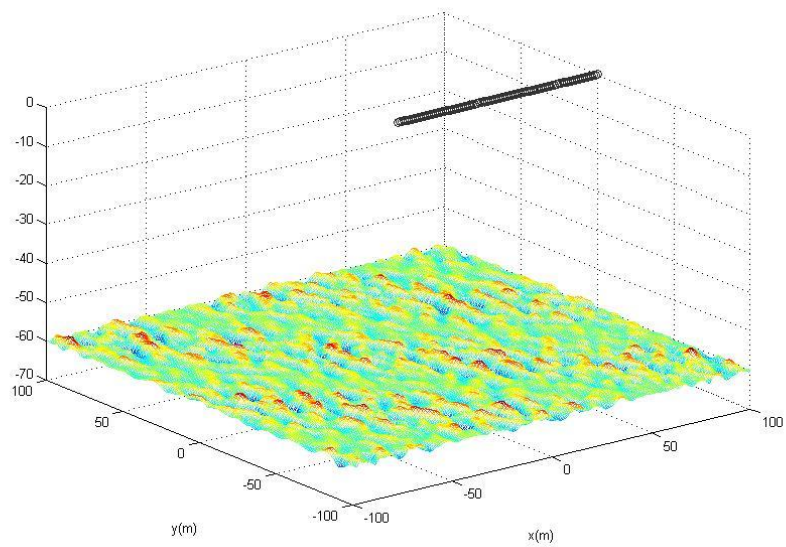
Figure 2.9. Ship route added on the map

31

In this ship referenced coordinate system, x is given as on ship movement direction and y is perpendicular axis. For a straight line of ship movement, the consecutive ship positions are shown in Figure 2.9.
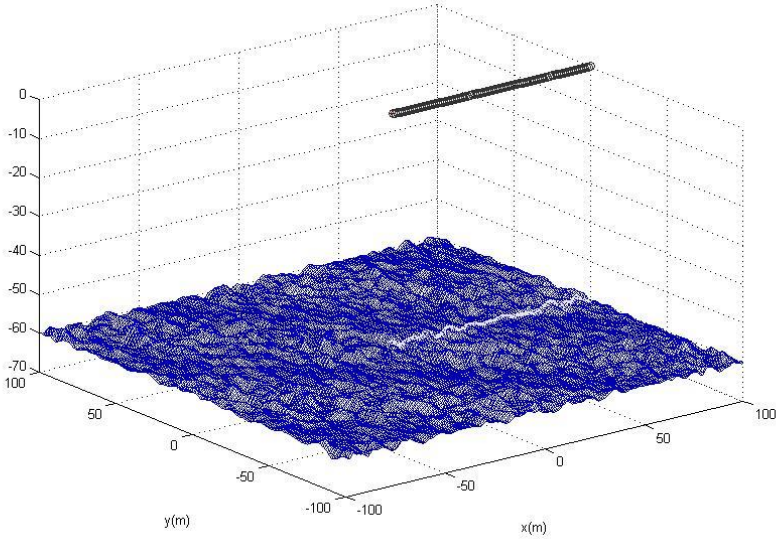
Figure 2.10. Bottom line directly under ship

The bottom line shown in Figure 2.10 is the points corresponding to directly under ship during ship motion. Bottom line is an important reference point for calculating ensonified strip positions. The roll and pitch movements are added to bottom reference points. Therefore the ensonified line can be generated.

In the simulation, ensonified area is shown as black strip. This area consists of points on sea bottom pointed by beam vectors. The ensonified strip is shown on Figure 2.11. Ensonified points give the travel distance from transmitter and return to receiver. By using the distance travelled, we can use the sonar equation to be solved.
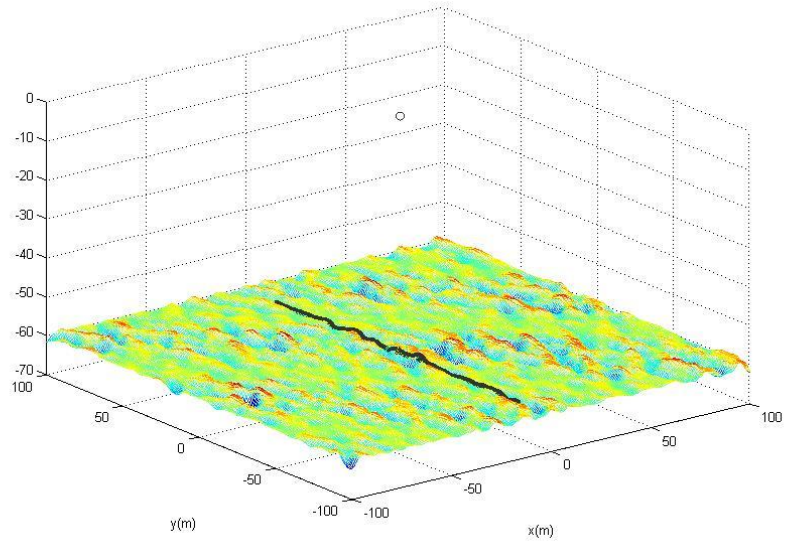
Figure 2.11. Ensonified area for a given ping cycle

Since the traveled distance does not equal to depth value for all beams, the real depth value needed to be calculated. For every beam angle, we obtain a travel time, where we get a two way travel distance. By using the angle and the travel distance, the depth values are calculated. At this point, the roll and pitch effects should be considered.
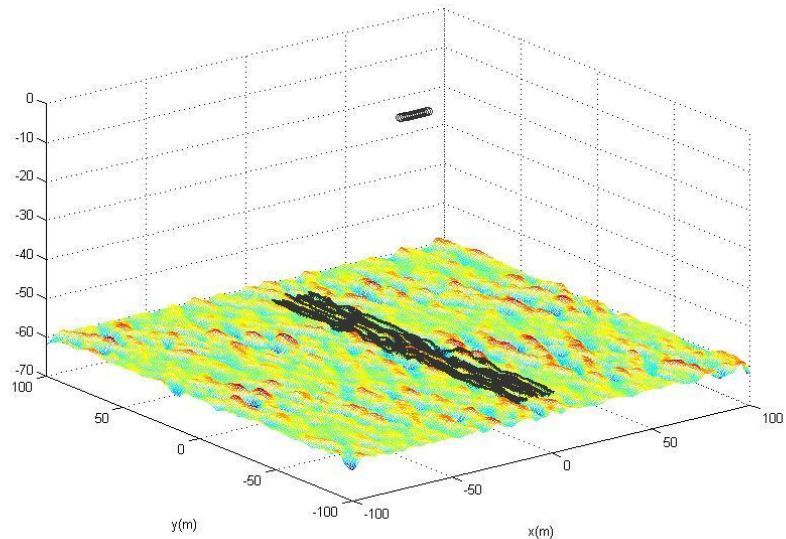
Figure 2.12. Position of depth readings affected by yaw and pitch movements

33

The roll and pitch values changes the area of ensonification. Since in this simulation the ship motion is also inserted, from ping to ping ensonified area changes the orientation. Without calculating the angular differences caused by the ship motion, the depth value assignment to positions is conducted in an erroneous way. In Figure 2.12, the depth values are assigned without consideration of roll and pitch motions. With this effect, depth measurements changes dramatically from exact depth values.

In this study, the coordinate system used is right-handed having positive x-axis pointing towards the bow, positive y-axis pointing towards starboard, and positive z-axis pointing below the vessel. Angular measurements have sign conventions according to right hand rule. Positive roll is to starboard where starboard sinks and port rises; positive pitch is nose-up where bow rises and stern sinks; and positive yaw is clockwise where bow turns to starboard. Roll (θ), pitch (φ) and yaw (γ) rotations about the x, y, and z-axes are expressed as in the following matrices:

$$R(\theta) = \begin{bmatrix} 1 & 0 & 0 \\ 0 & \cos\theta & -\sin\theta \\ 0 & \sin\theta & \cos\theta \end{bmatrix} \quad R(\phi) = \begin{bmatrix} \cos\phi & 0 & \sin\phi \\ 0 & 1 & 0 \\ -\sin\phi & 0 & \cos\phi \end{bmatrix} \quad R(\gamma) = \begin{bmatrix} \cos\gamma & -\sin\gamma & 0 \\ \sin\gamma & \cos\gamma & 0 \\ 0 & 0 & 1 \end{bmatrix}$$

The rotation is performed via matrix multiplication of the matrix and vector where following rotations are applied in a right-to-left manner. In order to explain, a roll, pitch and yaw rotation is applied via multiplication in the order as shown in the following equation.

$$\vec{V}_{rotated} = R(\gamma) \cdot R(\phi) \cdot R(\theta) \cdot \vec{V}_{original}$$

When the rotation matrices are pre-multiplied, a single rotation matrix covering the effect of all three individual rotations is obtained (ensuring that the same multiplication order is respected). Consequently, following rotation matrix is achieved:

$$R_{\theta\phi\gamma} = \begin{bmatrix} \cos\phi \cdot \cos\gamma & \sin\theta \cdot \sin\phi \cdot \cos\gamma - \cos\theta \cdot \sin\gamma & \cos\theta \cdot \sin\phi \cdot \cos\gamma + \sin\theta \cdot \sin\gamma \\ \cos\phi \cdot \sin\gamma & \sin\theta \cdot \sin\phi \cdot \sin\gamma + \cos\theta \cdot \cos\gamma & \cos\theta \cdot \sin\phi \cdot \sin\gamma - \sin\theta \cdot \cos\gamma \\ -\sin\phi & \sin\theta \cdot \cos\phi & \cos\theta \cdot \cos\phi \end{bmatrix}$$

For the correction and assignment using former and the new data, a modified block diagram is shown in Figure 2.13.
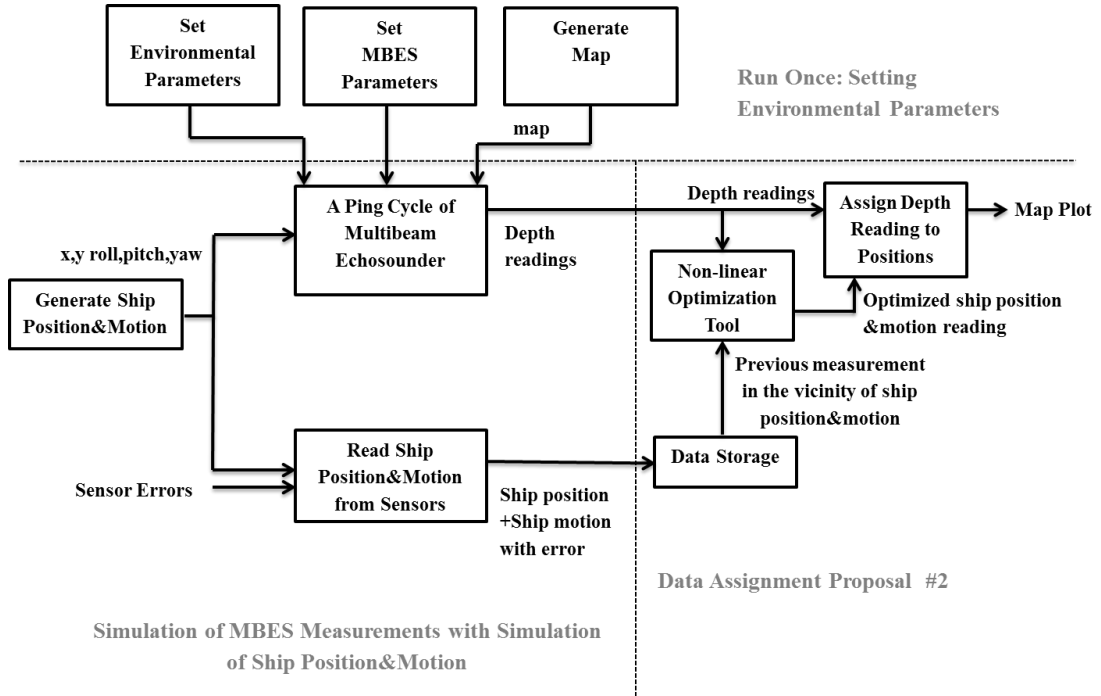
Figure 2.13. Second block diagram of multibeam sonar simulation

In this solution, a minimization problem is solved. The new measurement is fitted on the best possible orientation in order to minimize the difference between measurements.

$$\min \quad \left\| D_{former} - D_{new} \right\|^2$$

with respect to $x, y, roll, pitch, yaw$.

where

D_{former} = vector of former measurements, where each element is depth reading on the corresponding beam, $\in \mathbb{R}^N$.

D_{new} = vector of new measurements, where each element is depth reading on the corresponding beam, $\in \mathbb{R}^N$.

N = number of receiver beams, which is 161 in the simulation.

After fitting to the best position, weighted averaging is conducted. But for this, measurement quality is required to be defined. Measurement errors are analyzed in the next section. Measurement quality will be defined after a detailed analysis of error sources.

$$d_{ijn}^* = (d_{ijo}.q_{ijo} + d_{ijn}.q_{ijn}) \frac{1}{q_{ijo}+q_{ijn}}$$

where

d_{ijo} : Old depth measurement at position i, j
d_{ijn} : New depth measurement at position i, j
d_{ijn}^*: New updated depth measurement at position i, j
q_{ijo} : Old measurement quality at position i, j
q_{ijn} : New measurement quality at position i, j

CHAPTER 3

ECHOSOUNDER ERROR ANALYSIS

3.1. Single Beam Echosounding Principles

In single beam echosounders, acoustic beam is sent vertically downwards only in one direction. Therefore, these echosounders are named as single beam echosounders. Acoustic energy propagates in water medium and reaches sea bottom, reflected from bottom and travel back to the transducer. Returned echo signal is converted to digital form in the echosounder and evaluated to determine the depth value. After amplification, the returned echo is recorded as time series. These time series are echo strength versus time, which is called as echograph. Water depths are calculated from echographs with a known sound speed [39-40].

Today, depth measurements are done with an echosounder connected to a computer. A hydrography software is used to record soundings digitally. With the help of this hydrography software, depth, location sensor data are synchronized, measured depth is corrected with tide etc. effects, and real depth value is calculated [41]. Single beam echosounders mostly produce dual frequency for shallow waters. With the use of dual frequency, information about sediment structure of sea bottom can be gathered [42].

3.1.1. Beam Coverage of Single Beam Echosounders

For single beam echosounders, beam coverage of sea bottom can be calculated with the following formula. In this equation, a is the area covered by echo, d is the depth value, and φ is the beam angle [43].

$$a = 2d \tan \frac{\varphi}{2}$$
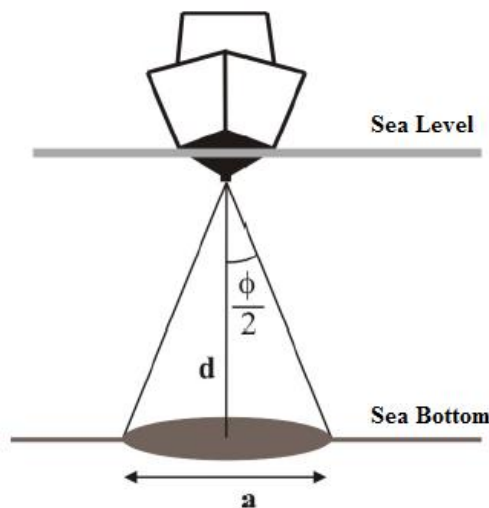
Figure 3.1. Sea bottom coverage in single beam echosounder [44]

3.1.2. Parameters of Single Beam Echosounders

For reliable and high precision and meaningful measurement, single beam echosounder parameters shall be adjusted correctly. These parameters can be listed as pulse power, pulse length, gain, measurement scale, phase scale, draft, and sound speed [45].

3.2. Error Sources in Echosounder Measurements

Error sources in depth measurements could be studied in three parts, namely structural errors, regular errors, and irregular errors. The structural errors are resulted from the defects in mechanic and electronic equipment of the echosounders. Regular errors are resulted from the movement of the measuring vessel and the errors in installation of the transducer and other sensors. These kinds of errors are detected during quality control procedures of the system and readjusted. Irregular errors remain in the depth data and they can only be determined by the statistical methods [46-47].

3.2.1. Sea Bottom Slope Related Errors

The acoustic waves sent from transducer diffuse conically and reflected from bottom and travel back to the transducer (Figure 3.2) [48]. If the sea bottom is flat, the depth is calculated from the equation below. In this equation, d is the depth value, c is the speed of sound in water, Δt is the time between the transmitted and received acoustic pulses [43].

$$d = \frac{1}{2} c \, \Delta t$$
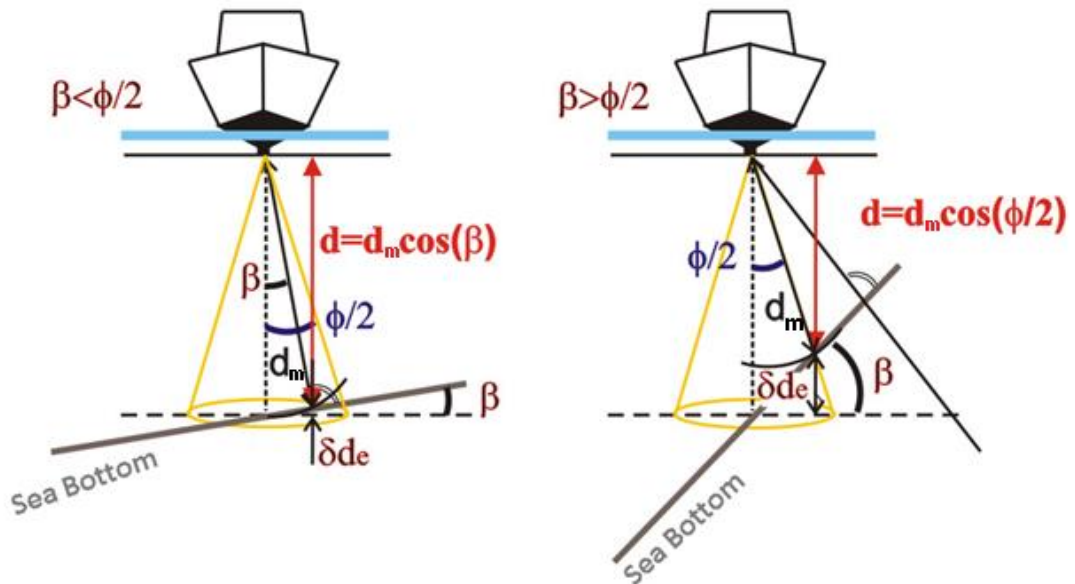
Figure 3.2. Inclined sea bottom [43]

However sea bottom is not always flat. In the case of inclined sea bottom, conically diffused waves would be edge pulse of the sound cone at the upper edge of the slope. In such cases, the error at depth measurement (δd_e) depends on beamwidth and slope of the sea bottom. In the following equations, the errors resulted from the sea bottom inclination are calculated where φ is the beam angle, β is the slope of the sea bottom, d_m is the measured depth, d is the depth [43].

$$\delta d_e = d_m \left(\frac{1}{cos\beta} - 1 \right) \quad \beta < \frac{\varphi}{2}$$

$$\delta d_e = d_m \left(\frac{1}{cos\frac{\phi}{2}} - 1\right) \quad \beta > \frac{\phi}{2}$$

Sea bottom inclination has two different effects on multibeam sonar simulation. As stated above, even if the beam is directly sent perpendicular to bottom, bottom shapes and inclinations modifies the echo. Moreover, for multibeam sonar operation, not all the beams are sent directly to the sea bottom, from the ship. When side beams are directed to bottom, even without bottom inclination, the incident angle will not be 90°. Even for an ideal fully flat bottom, different bottom backscattering levels are obtained. Backscattering level depends on bottom type and it decreases from nadir to side beams in the order of 20 dB [58].
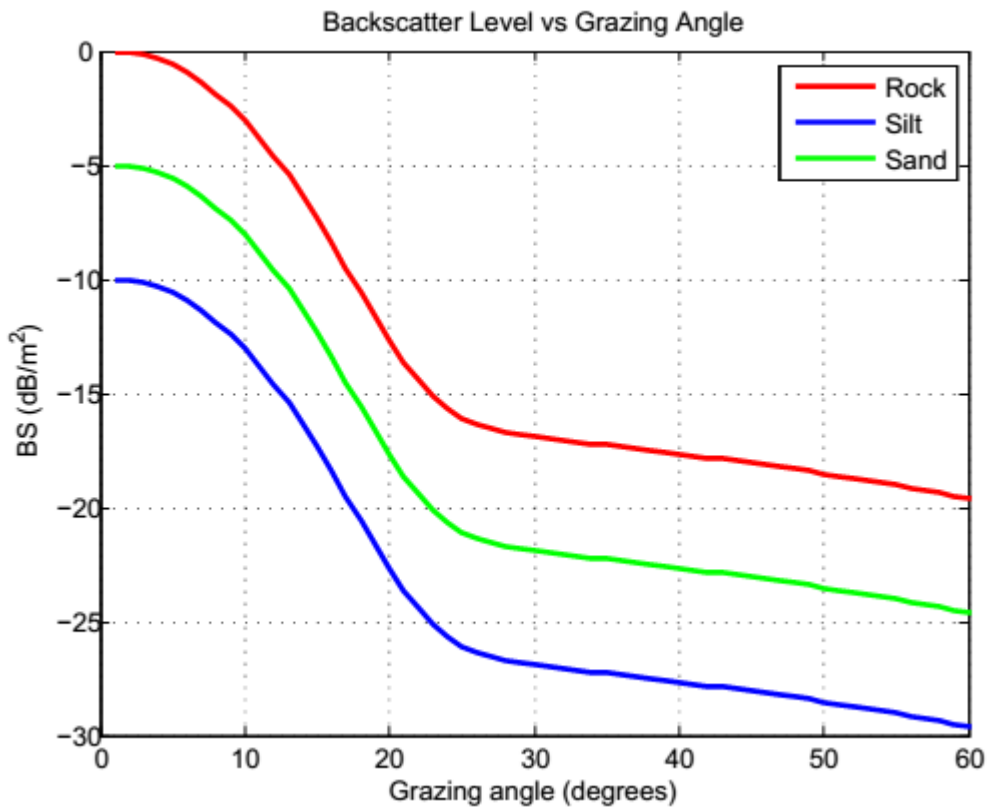
Figure 3.3. Backscattering levels versus grazing angle for different bottom types
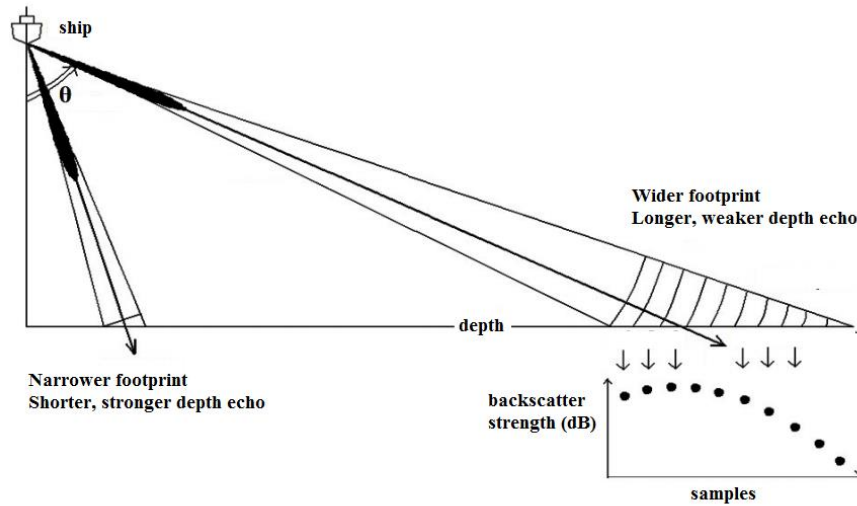
a)
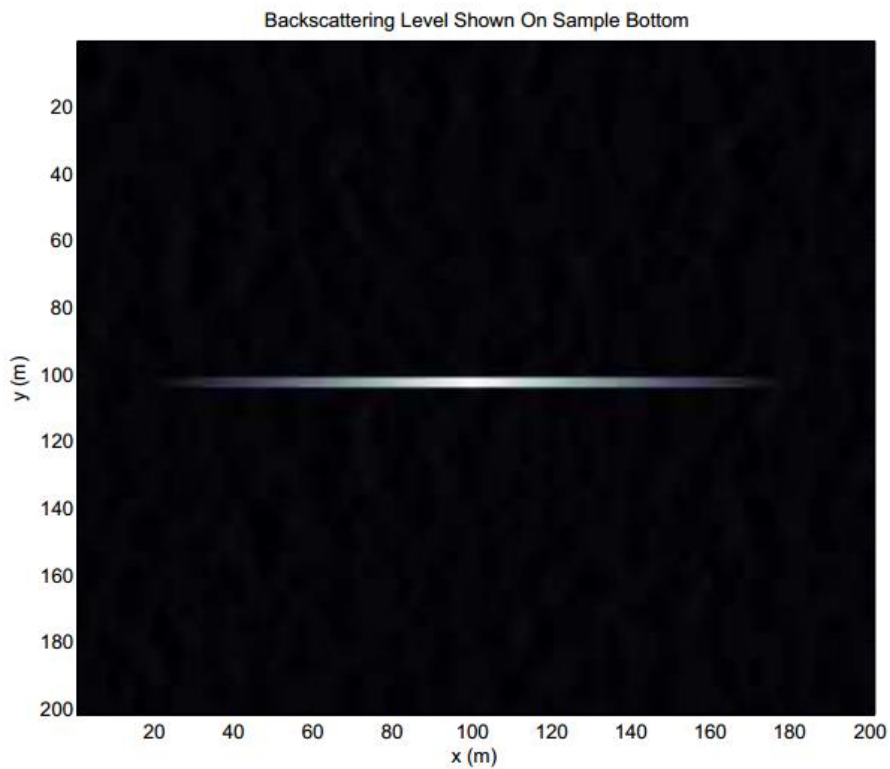
b)

Figure 3.4. Effect of grazing angle on echo shape and level

a) comparison of middle beams and end beams b) decrease of backscattering level on sides of ensonified area

Receiver array which is placed in the direction of ship axis receives signals from beams corresponding to left and right side of point directly beneath the ship. At the ends of the beams, backscattering strength is reduced. But, oblique incidence affects

not only the strength of the echo but also shape of the footprint. The area ensonified on the ends of the beams has wider footprint. This causes a longer reply echo. In 3.4 (a), this effect is illustrated. The echo reply levels give a change on backscattering levels. Backscattering levels for each beam is calculated and shown in Figure 3.4 (b).

3.2.2. Sound Velocity Related Errors

The velocity of sound in water changes with the physical parameters of the environment and the depth. If the velocity value set in the echosounder is different from the real value, then the change in depth is calculated from the following equations [43].

$$d = \frac{1}{2}ct$$

$$\delta d_c = \frac{1}{2}t\,\delta c$$

$$t = \frac{2d}{c}$$

$$\delta d_c = d\,\frac{\delta c}{c}$$

In these equations, δd_c is the error resulted from the change in sound velocity, δc is the difference between the velocity set at the echosounder and the real value, and c is the velocity set at the echosounder.

Magnitude of the error in sound velocity changes with the accuracy in determining the speed of sound, temporary changes in sound speed, and spatial variation of the speed of sound [49]. Therefore, it is crucial to measure the real sound of speed in the field where depth measurement is made. The speed of sound should be measured before and after the depth measurement.

Sound speed in sea water is a function of salinity, temperature and pressure. For 100 m of depth increase, the sound speed increases 1.7 m/s. Temperature change, which has contribution on sound velocity, is also a function of depth. Also salinity of water crucially changes the sound speed. For 1 ppt (part per thousand) increase in salinity, sound speed increases 1.4 m/s. On world oceans abundant numbers of sea trials are conducted [58]. Mackenzie stated an empirical equation with a reasonable accuracy for the world's oceans. Accuracy of the formula between 25 and 40 ppt is 0.07 m/s [59].

$$c(T, S, D) = A_1 + A_2T + A_3T^2 + A_4T^3 + A_5(S-35) + A_6D + A_7D^2 + A_8T(S-35) + A_9TD^3$$

where, T is temperature in degrees Celsius, S is salinity in parts per thousand, and D is depth in meters. Constants used in the equation are:

$A_1 = 1448.96$	$A_2 = 4.591$	$A_3 = -5.304 \times 10^{-2}$
$A_4 = 2.374 \times 10^{-4}$	$A_5 = 1.340$	$A_6 = 1.630 \times 10^{-2}$
$A_7 = 1.675 \times 10^{-7}$	$A_8 = -1.025 \times 10^{-2}$	$A_9 = -7.139 \times 10^{-13}$

From sea trials and the empirical equation given above we observe the propagation speed varies with depth. Also, the depth variation is affected by seasonal changes. Sound velocity profile given as a function of depth can be shown from real measured values on different seasons. The effect of sound velocity profile is observable on comparison of winter and summer conditions.

Sound velocity profile abruptly changes the ray of the given beam. The ray bending can be solved using ray tracing. The ray tracing simulation can be done with computer programs. The simulation data is processed using Lybin® Sonar Performance Simulation Program. The comparison of rays on ideal isovelocity case, summer sound velocity profile and winter sound velocity profile are given on simulation results.
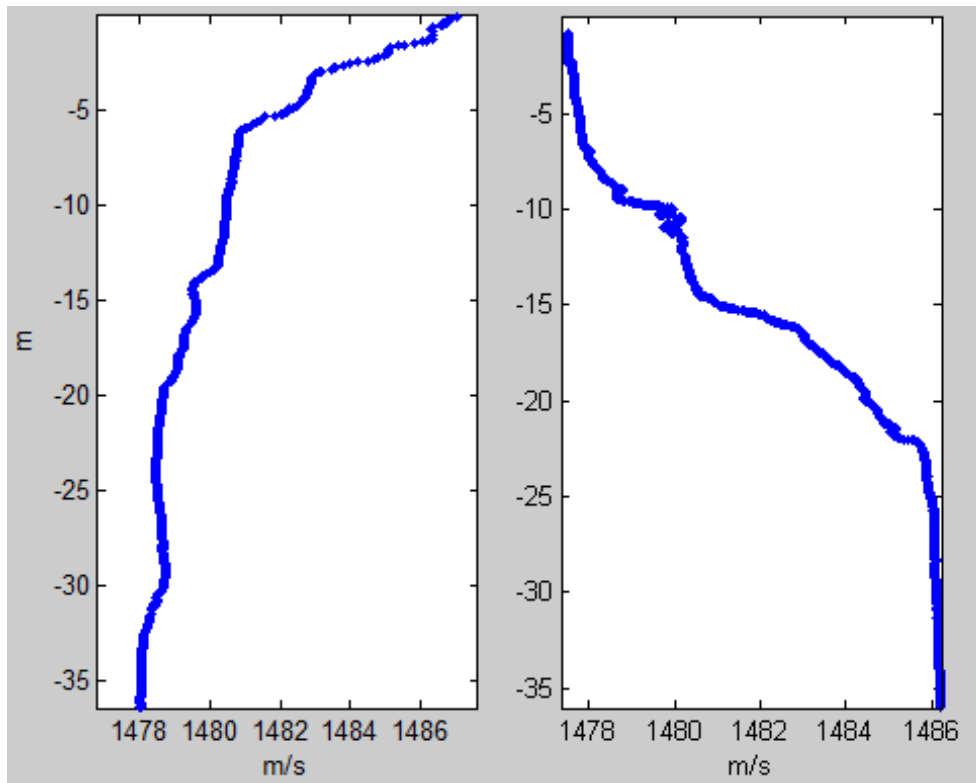
Figure 3.5. Typical summer (left) and winter (right) sound speed profiles [67]
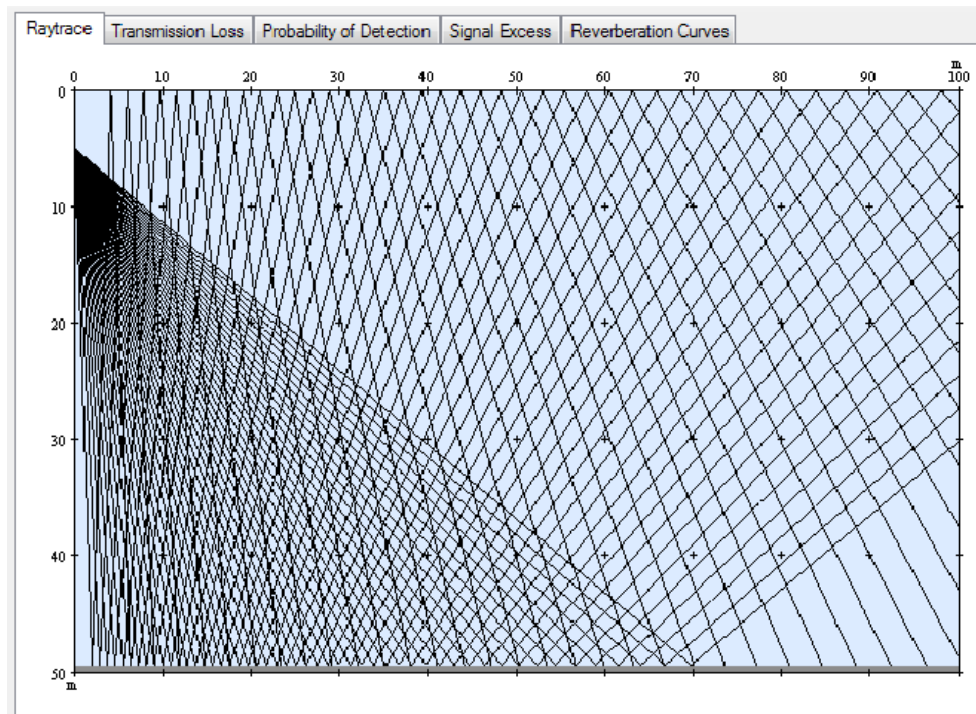
Figure 3.6. Straight rays in isovelocity water
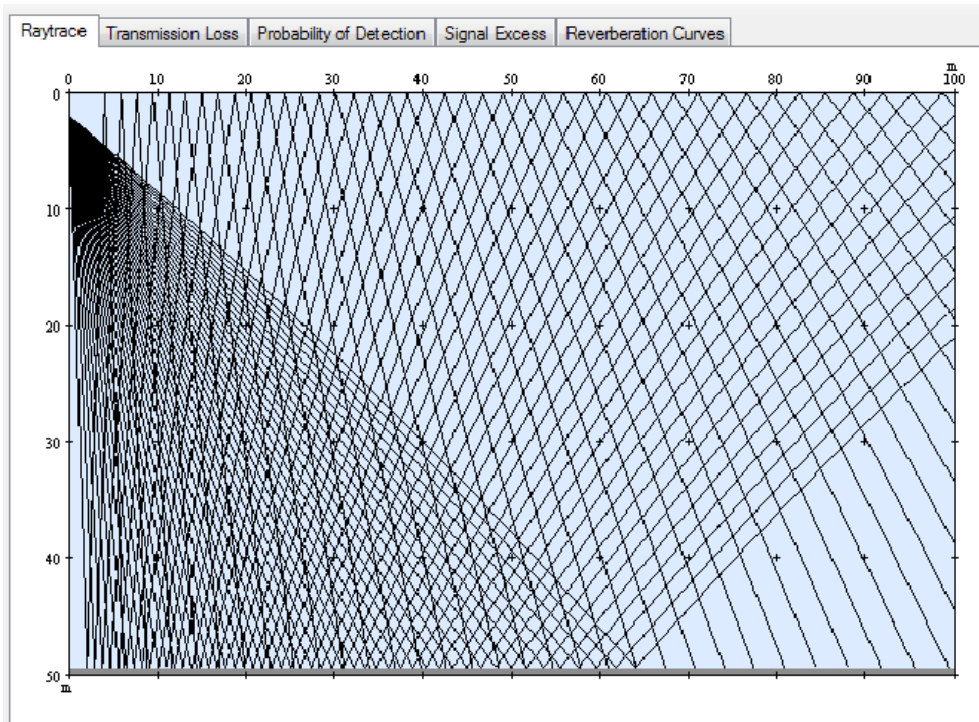
Figure 3.7. Typical summer sound velocity profile causing beams to deflect towards deeper water
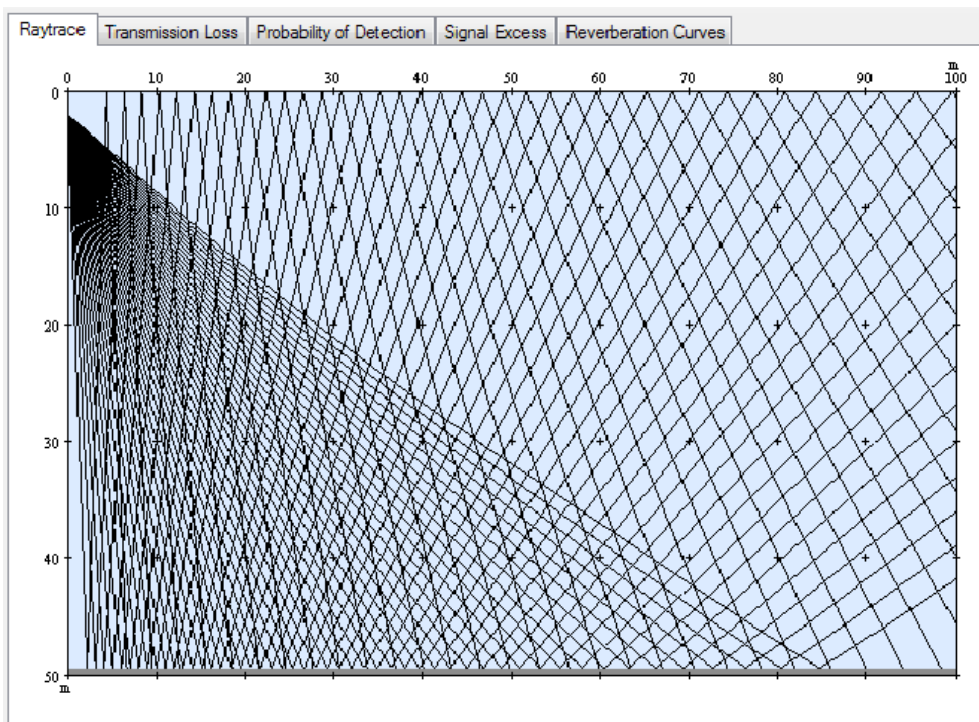
Figure 3.8. Typical winter sound velocity profile causing beams to deflect towards shallow water

From Lybin® ray tracing simulations, the change in the expected position of varies from sound velocity profile. On the outer beams, the change of illumination position may occur in the order of several meters. The interpretation of data collected becomes highly depended on sound velocity profile.

As previously stated sound velocity profile causes beam to deflect. This problem is solved by sound velocity profile measurement during survey and then applying correction using Ray Theory. The change of sound velocity in the medium can be described as a lens effect. This lens effect is inversed on calculations if the sound velocity profile is known. During multibeam operation, the sound velocity profile measurement is required in order to generate acceptable depth and position accuracy. In literature, this issue was greatly studied and some solutions are introduced. However, in the scope of this thesis we assume all sound velocity profile effects are corrected with perfect measurement of sound velocity profiler.

3.2.3. Time Related Errors

The echosounders calculate depth from the time passed from sound waves reflected from the seabed to return again the echosounder. Time related error δt directly affects the depth error resulted from time related error (δd_t). The effect of error on depth resulted from the acoustic waves' travel time difference is explained in the following formula [43].

$$\delta\, d_t = \frac{1}{2}\, c\, \delta_t$$

In modern echosounders time related error is quite low and has a constant value. This value could be determined by quality control measurements.

3.2.4. Survey Ship's Draft, Collapse, and Sitting Related Errors

Transducer assembled to survey ship is lowered to a certain depth. Measured depth is the depth beneath the transducer. The difference between the sea level and the transducer is called as draft (Figure 3.9, a). The draft value of the survey ship should be added to each measured depth value [50].

The draft is also one of the most important factors affecting total depth correctness. In a single beam echosounder measurement, if a very large survey ship is used, the factors like amount of fuel consumption largely affect the draft [51]. The draft error δd_{draft} directly affects the depth error [43].
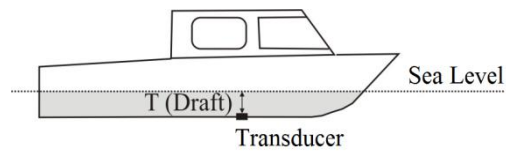
(a) draft of the survey ship
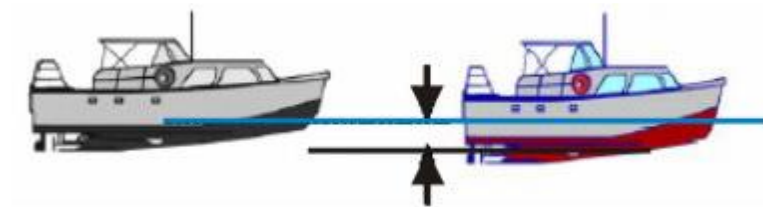
(b) sitting of the survey ship

(c) collapse of the survey ship

Figure 3.9. Draft, sitting, and collapse of the survey ship [27, 43]

Sitting of the survey ship is defined as the difference between the stable state of the ship before the measurement and the moving state of the ship at the measurement. Sitting of the survey ship affects the depth measurement as δd sitting. This effect should be taken into account at the measurements in shallow water [43].

Collapse of the survey ship could be defined as the change in draft according to velocity of the ship [27]. Collapse of the survey ship affects the depth measurement as δd collapse.

The error resulted from location of the transducer according to sea level, i.e., transducer immersion (δd_i), is calculated with the equation below [43].

$$\delta d_i = \sqrt{\delta d_{draft}^2 + \delta d_{sitting}^2 + \delta d_{collapse}^2}$$

3.2.5. Survey Ship's Movements Related Errors

The survey ship makes roll, heave, and pitch motions because of waves in the sea (Figure 3.10). Rolling motions are resulted from rotation about its longitudinal (front/back) axis, heave motion is resulted from the rotation of the ship about its vertical axis, and pitching is resulted from the rotation of the ship about its transverse (side-to-side) axis [43].

a) roll

b) heave
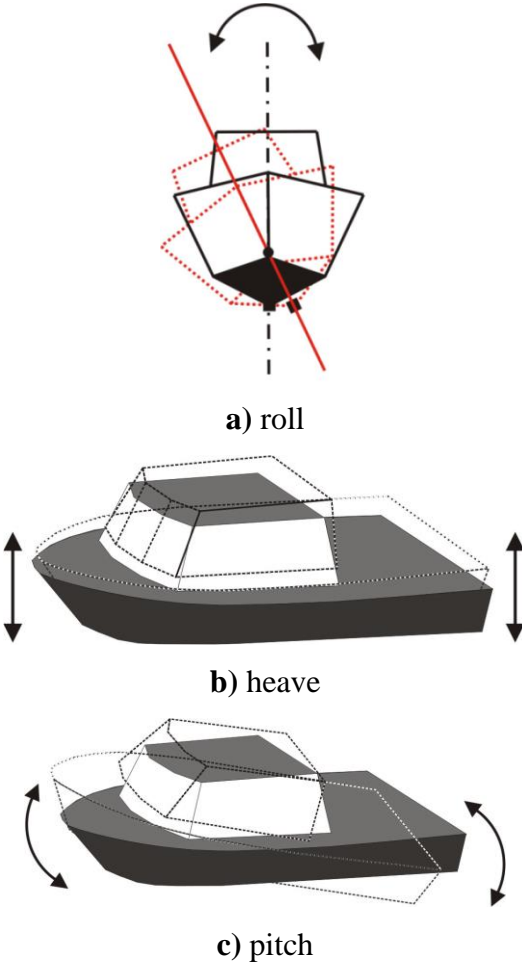
c) pitch

Figure 3.10. Rotational motions of a survey ship [43]

In a single beam echosounder, the effect of roll and pitch motions of a survey ship on depth is only applicable when roll angle (θ_R) and pitch angle (θ_P) are greater than half of beam angle ($\varphi/2$) [43]. In wide-angle echosounders, roll and pitch motions of the survey ship generally do not affect the depth.

$$\delta d_{roll} = dm\ (1 - \sec(\theta_R - \frac{\varphi}{2})) \qquad\qquad \theta_R > \frac{\varphi}{2}$$

$$\delta d_{roll} = 0 \qquad\qquad \theta_R < \frac{\varphi}{2}$$

In narrow-angle echosounders, error of δd_{roll} is determined by the equations above. As in the inclined sea bottom case, when θ_R is replaced by θ_P, the pitch error is determined with the equations above.
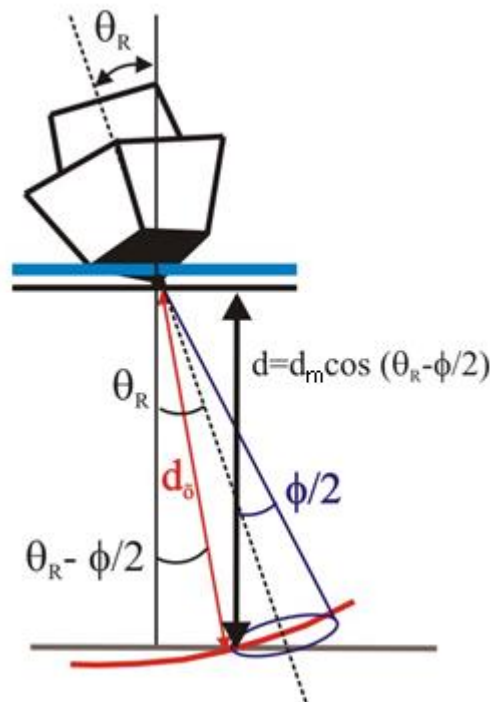
Figure 3.11. Effect of roll of a survey ship [43]

The effect of heave on depth occurs due to vertical movement of the survey ship. Especially the wavy environment causes error in depth measurements [52]. The heave effect could be determined by the heave compensators or inertial systems. The heave compensators should be placed above the transducers so as to be in the same

horizontal axis of the transducers. The measured depth value should be corrected with h_m [43].

The heave motion could be determined by the help of the inertial systems inserted closer to center of gravity of the survey ship. As the transducer is attached to the survey ship, it is in the ship's coordinate system. However, there is a slight difference in the coordinate system of the inertial system and survey ship's coordinate system. The difference between z-axis in the vertical direction of the two systems changes according to the survey ship's roll and pitch oscillations and affects heave as h_i [43]. If inertial systems are used in the survey ship, the heave motion is represented as in the following equation. In this equation, h_m is the measured heave value and h_i is the calculated heave value [43].

$$h_T = h_m + h_i$$

The heave motion caused by the difference in axis is calculated by the following equation. In this equation, coordinate values (x, y, z) are of the transducer at the survey ship's coordinate system. Heave motion is achieved from this equation [43].

$$h_i = -x \sin(\theta_P) + y \cos(\theta_P)\sin(\theta_P) + z (\cos(\theta_P) \cos(\theta_P) - 1)$$

Total error related with the heave motion is calculated with the following equation [43].

$$\delta h = \delta h_m + \delta h_i$$

3.2.6. Effect of Depth Reading Position Errors

Hereafter, error sources that affect measurement position are taken into simulation. As explained in sections 3.2.2 and 3.2.4, effects such as and sound velocity profile change and ship motion, change the position of echo taken. The measurements where these values are not known and no correction can be made cause serious mistakes.

As previously stated sound velocity profile causes beam to deflect. This problem is solved by sound velocity profile measurement during survey and then applying correction using Ray Theory. The change of sound velocity in the medium can be described as a lens effect. This lens effect is inversed on calculations if the sound velocity profile is known. During multibeam operation, the sound velocity profile measurement is required in order to generate acceptable depth and position accuracy. In literature, this issue was greatly studied and introduced some solutions. However, this issue is out of scope of this thesis study.

Previously, with ray solution, it was shown that echo reply positions may differ 10 meter because of sound velocity profile effect due to seasonal differences. These points could be corrected by taking sound velocity profile data accurately and using Ray Theory. Sound velocity change corrections are out of scope of this thesis. Sound velocity profile and Ray bending issues and analysis are much explained in the literature.

Afterwards, effect of change in ship motion is simulated. It is not proper to conduct a survey above sea state 3. Calm sea environment should be preferred for bottom mapping studies. Nevertheless, one can get 0.5° pitch 3° roll motion at sea state 3 with a mid-sized ship. How these values affect our measurement can be observed in Figure 3.12.

As shown in Figure 3.1.2, the measurement points change significantly with the ship motion. When these changes are not considered, there becomes a huge difference between the actual and obtained measurement data. The difference between the real and obtained measurements is shown in Figure 3.13.
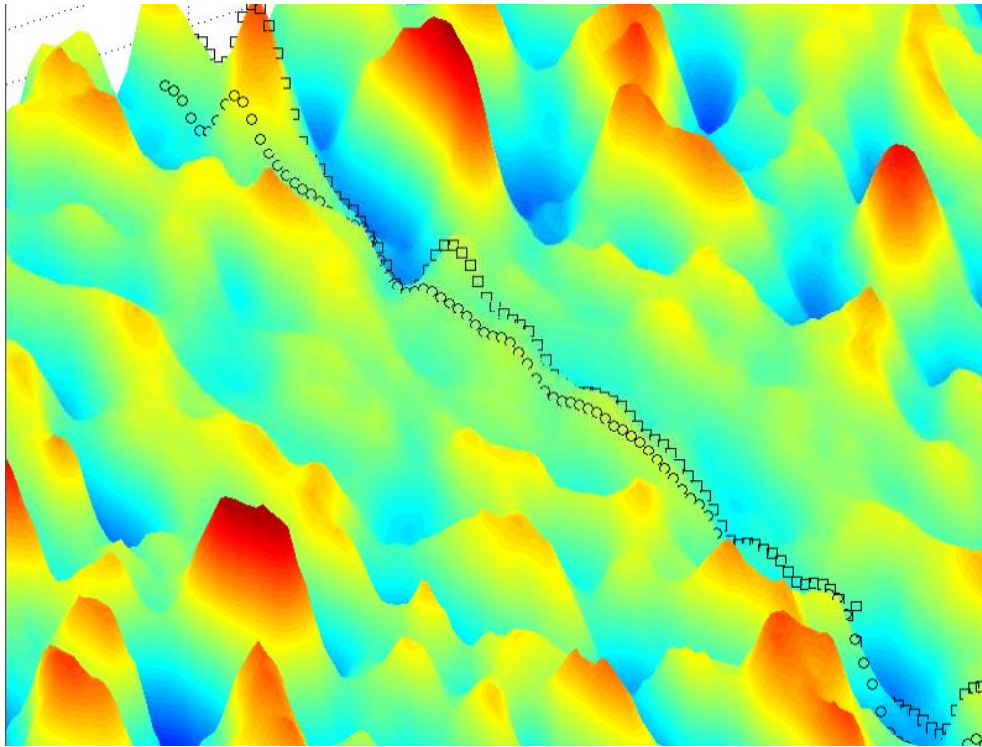
Figure 3.12. Measurement line at 0 pitch 0 roll motion and 0.5° pitch 3° roll motion on 3D Map (actual depth positions are denoted with circle and depth reading positions are denoted with square)
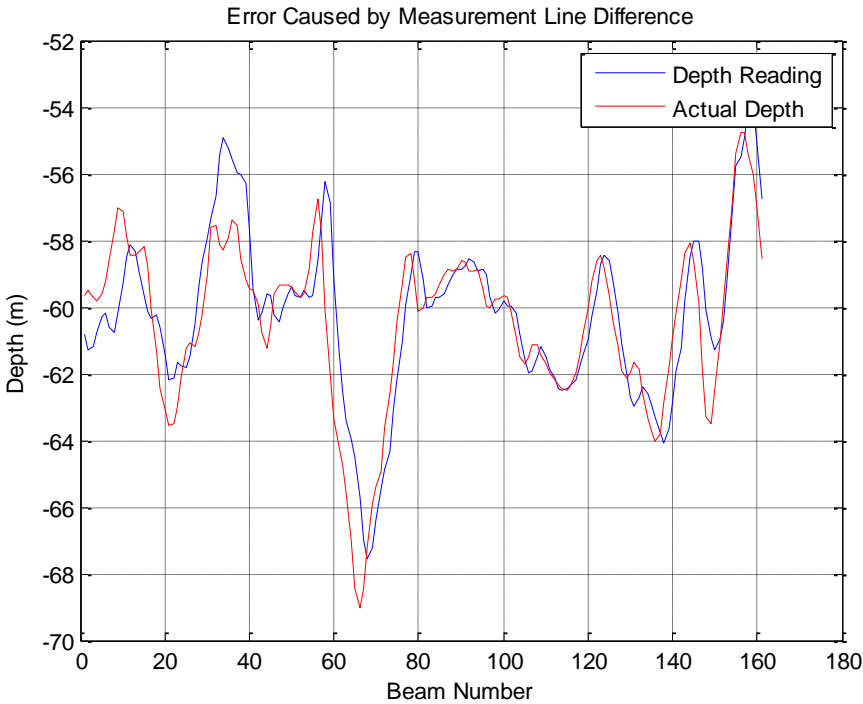
Figure 3.13. Errors caused by measurement line difference – ship motion not corrected (line of readings)
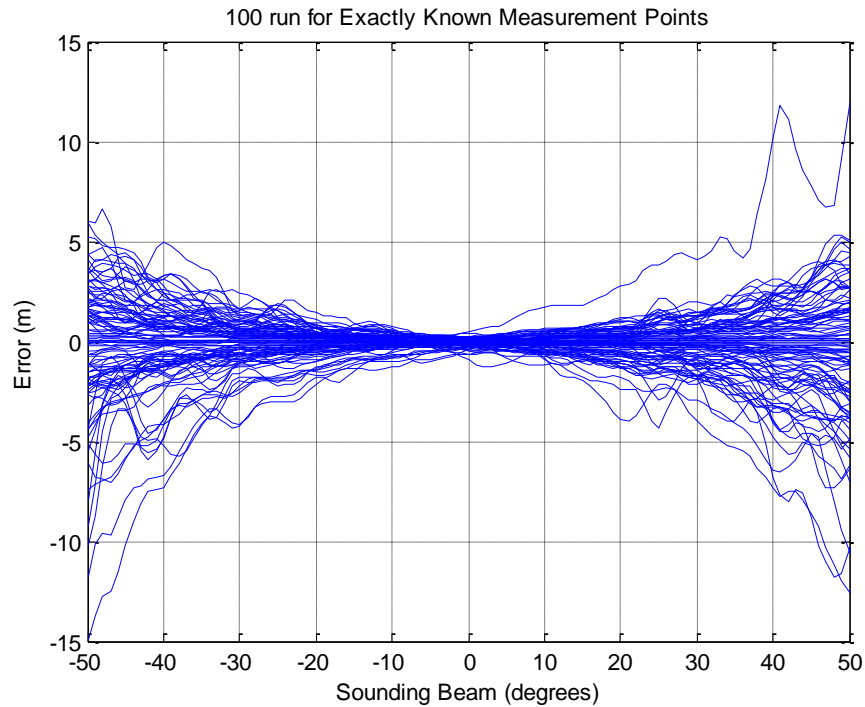
Figure 3.14. Errors caused by measurement line difference – ship motion not corrected (beam number vs error graph with 100 trials)

As shown in this comparison, the missing information about the measurement line (i.e., where the measurement line belongs to) leads to high error rates. In order to make measurements at IHO standards, high resolution motion sensors should be integrated to system during survey.

3.2.7. Simulation of Motion Sensor and GPS Readings

In present-day hydrographic surveys, high resolution motion sensors and GPSs work integrated with the multibeam echosounders. Where echo replies come from could be corrected with the help of motion sensors. Moreover, there are positional errors which could form in transformation of depth measurements into the real coordinate system. In order to prevent deviation of map information from the real value, GPS related positional errors should also be corrected. Accordingly, motion sensor and GPS value inputs are added to our simulation. In Figure 3.15, positive effect of motion corrections could be observed.

The measurements are performed with a certain error however good the motion sensors are. If ship position is expressed with x, y, z, roll, pitch, and yaw, the data taken from GPS and motion sensors can be expressed as x_{read}, y_{read}, z_{read}, $roll_{read}$, $pitch_{read}$, and yaw_{read}. This ship motion vector will be analyzed with a certain noise added onto the real ship situation. Noise amounts and obtained depth positions are shown on Figure 3.15.
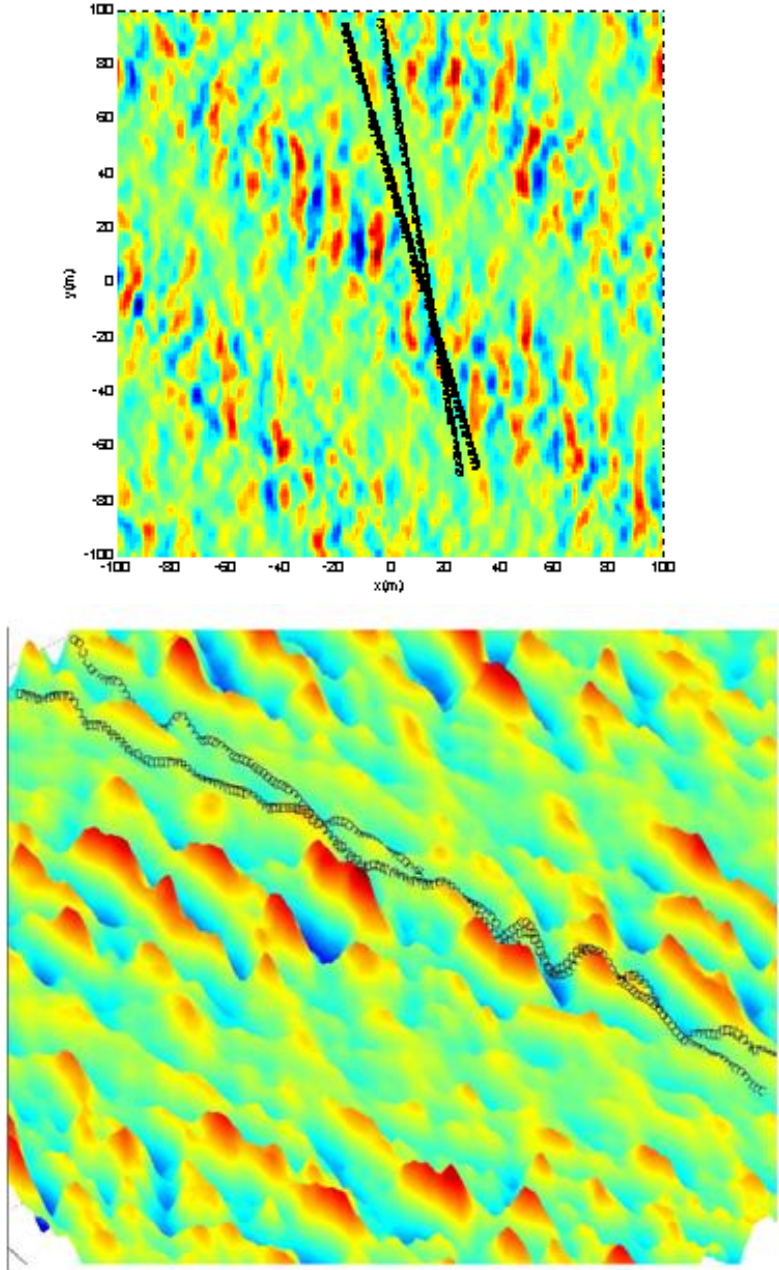
Figure 3.15. GPS, roll, pitch, yaw errors applied together (actual depth positions are denoted with circle and depth reading positions are denoted with square)
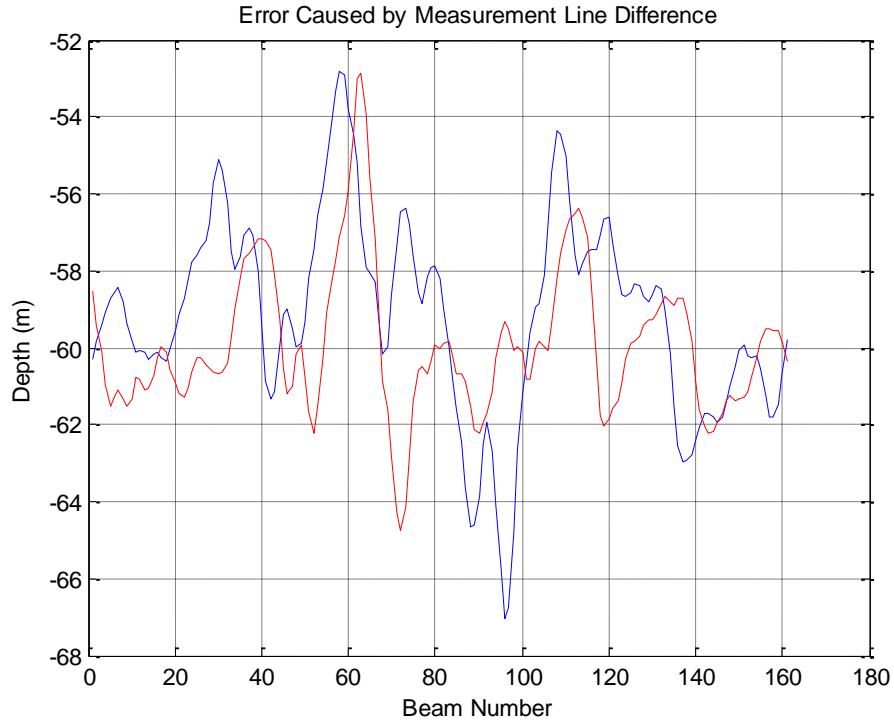
Figure 3.16. Error caused by measurement line difference $[\sigma_x, \sigma_y, \sigma_{roll}, \sigma_{pitch}, \sigma_{yaw}]$ = [5, 5, 1, 1, 1]

In order to prevent deviation of map information from the real value, motion sensor and GPS related positional errors should also be corrected.

3.2.8. Record Reading and Resolution Related Errors

In depth measurements, record readings and resolution related errors depend on the environmental conditions of the echosounder [53]. In order to get a clean vision at analog devices, necessary adjustments should be done carefully. In digital devices, the adjustments are done digitally and the results are controlled and evaluated afterwards. The error resulted in record reading after analog measurements ($\delta\ h_{reading}$) depends on experience [53].

3.2.9. Interpretation Related Error

The echoes are interpreted by the hydrographs. Wrong echoes occur when more than one echo and dual frequency transducers are used. The echo difference caused by different sediment sources at the sea bottom causes interpretation errors [54].

3.3. Motion Compensation

The echo level estimations are stored together with angle and amplitude information. Because of ship motion, the stored angles are not earth referenced measurements. The angles are given only with respect to the hydrophone array, and hydrophone array is exposed to roll, pitch and yaw motion. The motions of the hydrophone array must be corrected from all measurements. After the angle correction, the measurements can be converted to earth referenced coordinate system [55].

Using three dimensional coordinate system, with the origin on the ship's center of mass, ship motion can be described as follows:
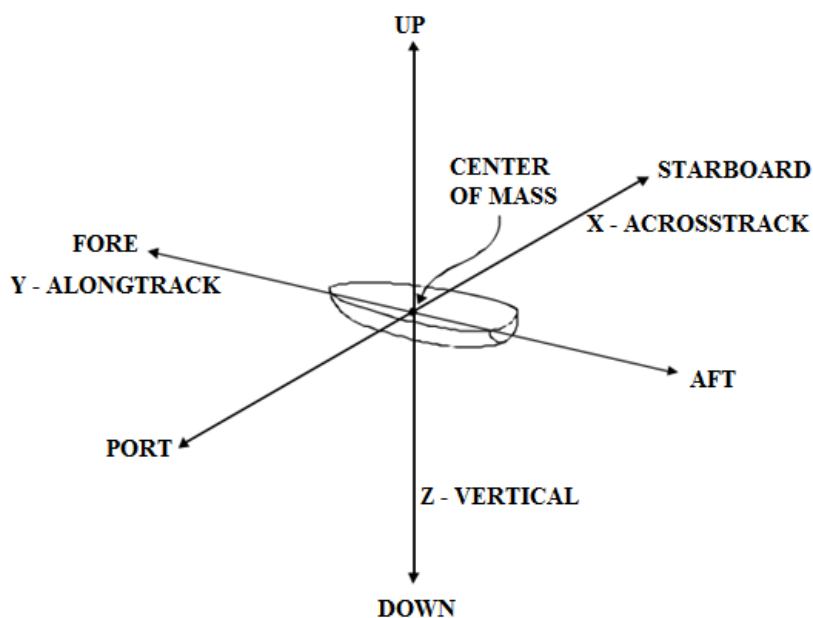
Figure 3.17. Coordinate system with an origin on ship's center of mass [64]

- x, or across-track direction – This is the direction perpendicular to the ships track and parallel to the surface of the sea.
- y, or along-track direction – This is the direction parallel to the ships direction of travel, or track.
- z, or vertical direction – This is the direction perpendicular to the surface of the sea.

There are also rotational motions around the axis of each of these coordinates:
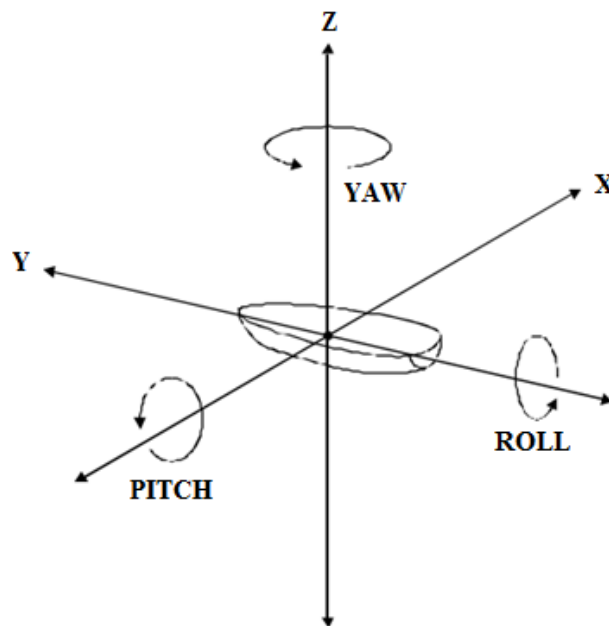
Figure 3.18. Rotational motions around x, y, z axes [64]

- Rotation about the x-direction is called pitch.
- Rotation about the y-direction is called roll.
- Rotation about the z-direction is called yaw [64].

The ship has six degrees of freedom to its motion. Motion measurement devices constantly monitor all six degrees of freedom [65]. The navigation devices record the position of the ship (latitude, longitude, and heading at time of ping) associated with surge, sway, and yaw motions. The Vertical Reference Unit (VRU) records roll, pitch, and heave information [65].
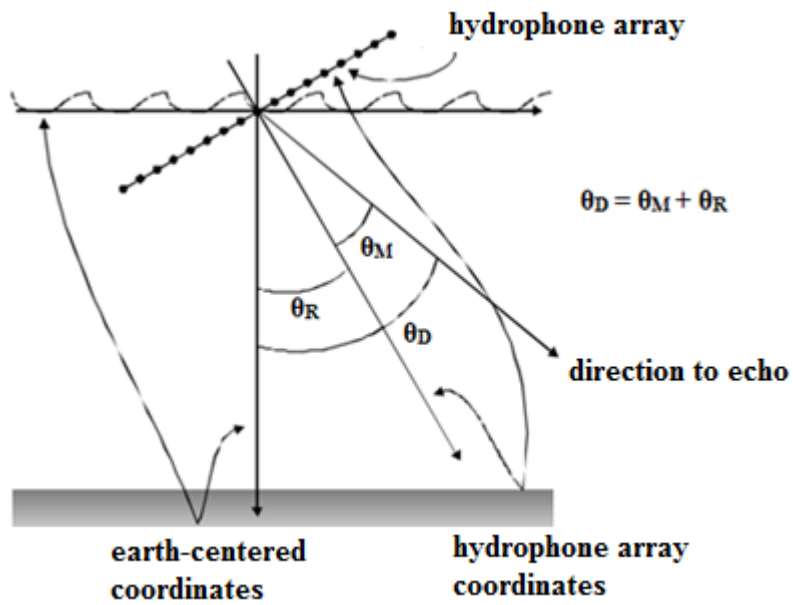
Figure 3.19. Difference of earth-centered coordinates and hydrophone array coordinates caused by roll angle [62]

In Figure 3.19, θ_M is the angle measured by hydrophone array, θ_R is the roll offset angle, θ_D is the echo in earth-centered coordinates [62].

CHAPTER 4

RESULTS AND DISCUSSIONS

4.1. Properties of Simulation Map

In the context of bathymetry simulation, we need a realistic sea bottom surface. With more realistic sea bottom characteristics, bottom shape induced error is added to simulation. Most sea bottoms have sand wave shapes on. For a bottom similar to such a shape, a wavy surface is generated [66].

In order to determine map resolution required in depth mapping, the resolution involved in these measurements should be handled carefully. The depth data corresponding to coordinates of the region where measurements are taken on bottom profile determine return time of the return echo. Accordingly, the actual map should be known well with a high resolution in order to analyze the reflection's turn points in the simulation. Bottom shape can be used for the desired mean depth value. With the addition of a mean depth value, the depth values to be detected are obtained. Depth value for given x and y positions are considered as exact values. The exact bottom depth values are used for error calculation. The multibeam sonar measurement performance can be given as the difference of depth readings and exact depth values.

By the help of the samples on the map, the depth values in the inner-sample region could be assigned to a value by interpolation. An assumption can be made on the map which is called as the original depth image and could be later used as data source in the simulation.

It is assumed that the depth values at inter-sample points and the depth values taken via spline interpolation are equal.

For absolute original map, it is not possible to define the depth for every position. Simulation has a sampled data set, but in order to realize the echo simulation from bottom for every point, inter-sample depth data is needed. This data will be assumed to be the original map, therefore, interpolated values will be assumed for real data. This assumption covers only the generated map, which does not affect the validity of the simulator. Cubic spline interpolation is used on the map generation since cubic splines produce an interpolated function that is continuous up to second derivatives which causes fewer oscillations between the points. This gives a smoother interpolating function.

The cubic spline function is denoted as $S_3(x)$ and is written as sum of the B_k terms.

$$S_3(x) = \sum_{k=-1}^{N+1} a_k B_k(x)$$

In the formula, B_k terms are basis functions defined for continuity conditions. For interpolation in the $[x_0, x_N]$ region B functions are defined as:

$$B_0(x) = \begin{cases} 0 & x \leq x_0 - 2h \\ \frac{1}{6}(2h + (x - x_0))^3 & x_0 - 2h \leq x \leq x_0 - h \\ \frac{2h^3}{3} - \frac{1}{2}(x - x_0)^2(2h + (x - x_0)) & x_0 - h \leq x \leq x_0 \\ \frac{2h^3}{3} - \frac{1}{2}(x - x_0)^2(2h - (x - x_0)) & x_0 \leq x \leq x_0 + h \\ \frac{1}{6}(2h - (x - x_0))^3 & x_0 + h \leq x \leq x_0 + 2h \\ 0 & x \geq x_0 + 2h \end{cases}$$

$$B_k(x) = B_0(x-kh+x_0)$$

where;

$$h = x_{k+1} - x_k = \frac{x_N - x_0}{N}$$

Using the definitions of B_k terms it can be written as:

$$B_k(x_k) = B_0(x_0) = \frac{2h^3}{3}$$

$$B_{k-1}(x_k) = B_0(x_0+h) = \frac{h^3}{6}$$

$$B_{k+1}(x_k) = B_0(x_0-h) = \frac{h^3}{6}$$

$$B_{k+2}(x_k) = B_0(x_0-2h) = 0$$

Then, the coefficients are found by solving the equation below:

$$
\begin{pmatrix}
1 & 0 & 0 & & & & \\
1 & 4 & 1 & 0 & 0 & \cdots & 0 \\
0 & 1 & 4 & 1 & 0 & \cdots & 0 \\
\vdots & & \ddots & & & & \\
0 & 0 & & & 1 & 4 & 1 \\
0 & 0 & & & & 0 & 1
\end{pmatrix}
\begin{pmatrix}
a_0 \\
a_1 \\
a_2 \\
\vdots \\
a_{N-1} \\
a_N
\end{pmatrix}
= \frac{1}{h^3}
\begin{pmatrix}
f(x_0) \\
6f(x_1) \\
6f(x_2) \\
\vdots \\
6f(x_{N-1}) \\
f(x_N)
\end{pmatrix}
$$

After finding $a_0...a_N$ coefficients, the spline function defining the value on interpolated points can be found using $S_3(x)$. The reason of choosing cubic spline functions is for their properties of continuity and cubic interpolation can be conducted easily on MATLAB.

Spline interpolation is preferred due to no oscillation requirement at the values obtained at inter-sample points. The data obtained from spline interpolation are counted as the real depth values. Accordingly, the simulated depth is a depth map where the samples are known and the values at inter-sample areas and from spline interpolation are known to be equal.

Figure 4.1. Simulated bottom map showing the 100 m vicinity of operation point
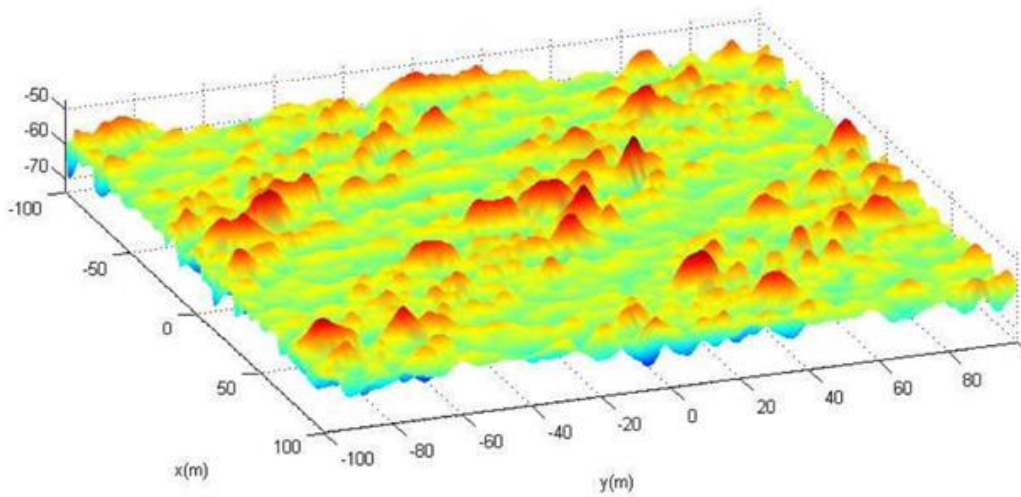
Figure 4.2. Interpolated bottom map is used for higher accuracy simulation

The resolution used in depth map generation should be better than the depth resolution taken from multibeam echosounder. There is no need for resolution less than 1 meter since the objects larger than 1 meter are desired to be detected in accordance with IHO object detection standards.

Table 4.1. IHO S-44 definition of orders and related requirements [42]

	Special Order	Order 1a	Order 1b	Order 2
Description of areas	Areas where under-keel clearance is critical	Areas shallower than 100 meters where under-keel clearance is less critical but features of concern to surface shipping may exist	Areas shallower than 100 meters where under-keel clearance is not considered to be an issue for the type of surface shipping expected to transit the area	Areas generally deeper than 100 meters where a general description of the sea floor is considered adequate
Maximum allowable vertical uncertainty Allowable vertical uncertainty: $\pm\sqrt{a^2 + (b \times depth)^2}$	a = 0.25 m b = 0.0075	a = 0. 5 m b = 0.013	a = 0.5 m b = 0.013	a = 1 m b = 0.023
Feature Detection	Cubic features > 1 meter	Cubic features > 2 meters, in depths up to 40 meters; 10% of depth beyond 40 meters	Not applicable	Not applicable

The multibeam echosounder depth measurement resolution to be used in simulation should also be higher than 1 meter. Accordingly, narrow beam is preferred to fulfill this requirement. Current studies use arrays with a 0.25° beamwidth. Nevertheless, in this study an echosounder working with 1° receive beamwidth is preferred to create a model inspiring from commercial products. In mapping at 50 m, the desired image resolution can be achieved with this echosounder. In deeper waters, a system with a narrower receive beamwidth should be used to get this mapping resolution. In

IHO order 1, the need for object detection for 2 meter-cubic features is up to 40 meter depth and object detection for size of depth's 10% up to 100 meter depth. Cubic feature of 1 meter is only specified in IHO special order. The regions specified at IHO special order are harbors and critical channels which are shallow waters.

Bottom shape can be used for the desired mean depth value. With the addition of a mean depth value, the depth values to be detected are obtained. Depth value for given x and y positions are considered as exact values. The exact bottom depth values are used for error calculation. The multibeam sonar measurement performance can be given as the difference of depth readings and exact depth values.

Military forces often require detection of features smaller or deeper than those required for the safety of navigation. For example, some strive to detect features with a volumetric size of 0.5 m on the continental shelf in depths to 200 m. Mine warfare forces, using specialized sensors, aim to detect and classify even smaller features. Whilst these reflect particular capabilities not normally required of the surveyor employed in nautical charting, there is a resultant effect on the development of systems capable of achieving them becoming available on the commercial market.

4.2. Measurement at the Points with Exactly Known Positions

The error sources were explained in the previous chapter. The error sources are modeled as random fluctuations, where zero mean Gaussian noise is used. The quality of the measurement is assigned as inverse of its standard deviation. The value measured can also be affected by a bias. For example, an angular bias can be due to misalignment of arrays. The refraction caused by the effect of sound velocity profile is also a bias that can be corrected during post-processing. With the sound velocity related depth error, time related depth error, heave related depth error, immersion related depth error, depth reading interpretation error and the tide effect, the total error can be written as:

$$\sigma_z^2 = \sigma_{zc}^2 + \sigma_{zt}^2 + \sigma_h^2 + \sigma_i^2 + \sigma_r^2 + \sigma_{tide}^2$$

These components are assumed to be independent. Therefore the total error can be modeled as the quadratic sum of these components [73].

Measurement taken points are directly beneath the ship, where roll, pitch, heave motions do not affect the position of the depth reading, which is the starting point in our simulation. Firstly, let's analyze the data when the ship is in flat position. Then, let's compare the obtained data with the original data. After putting measurement data from each single beam side by side, travelling distance versus beam angle graph is obtained.
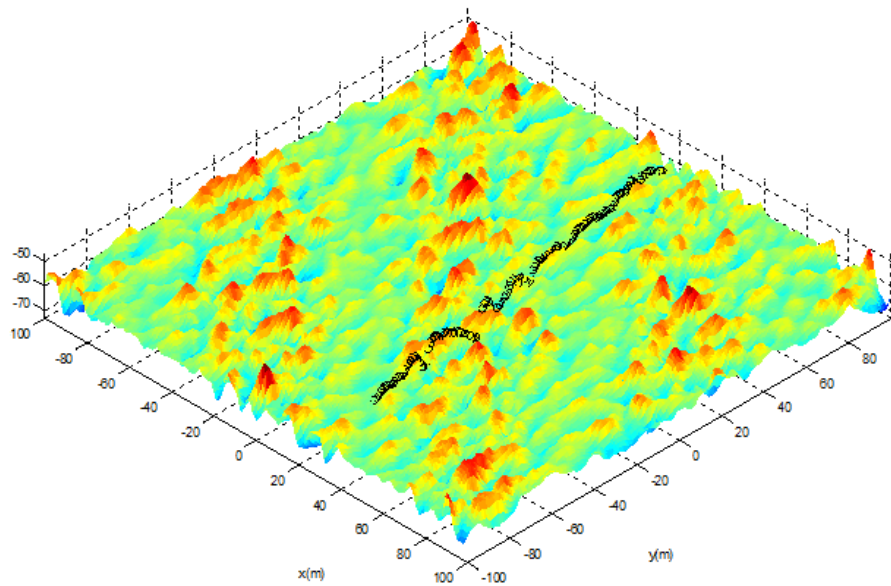
Figure 4.3. Illustration of depth reading positions for a ping cycle
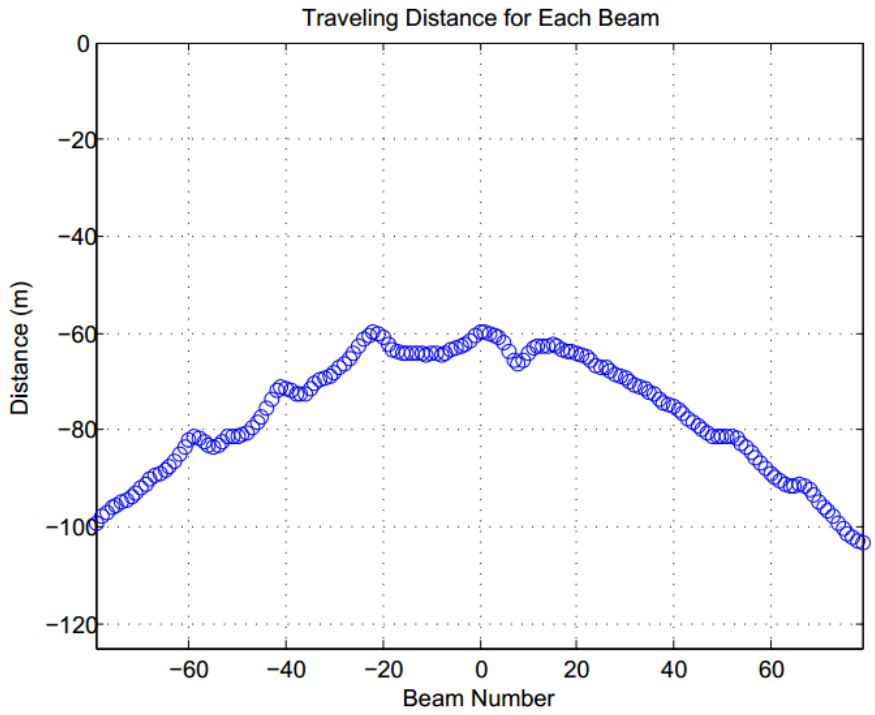
Figure 4.4. Traveling distance vs beam angle for given ping cycle
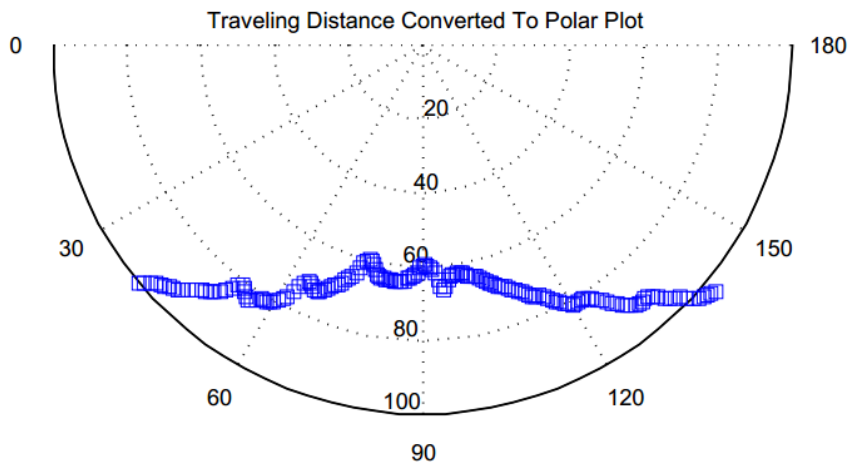
Figure 4.5. Traveling distance on polar plot for given ping cycle
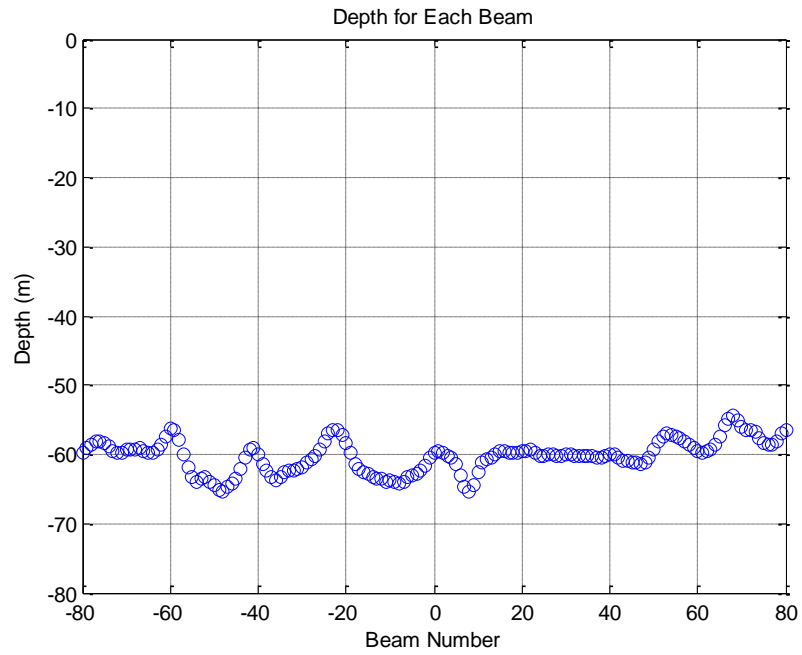
Figure 4.6. Depth vs beam angle for given ping cycle

The depth values can be obtained from these measurements since angle of every single beam is known. This transposition could be seen from the graph. In the second graph, the red depth values show real values. The difference in-between is error resulted from stationary measurement. Hence, graph of error versus beam angle can be obtained from here.
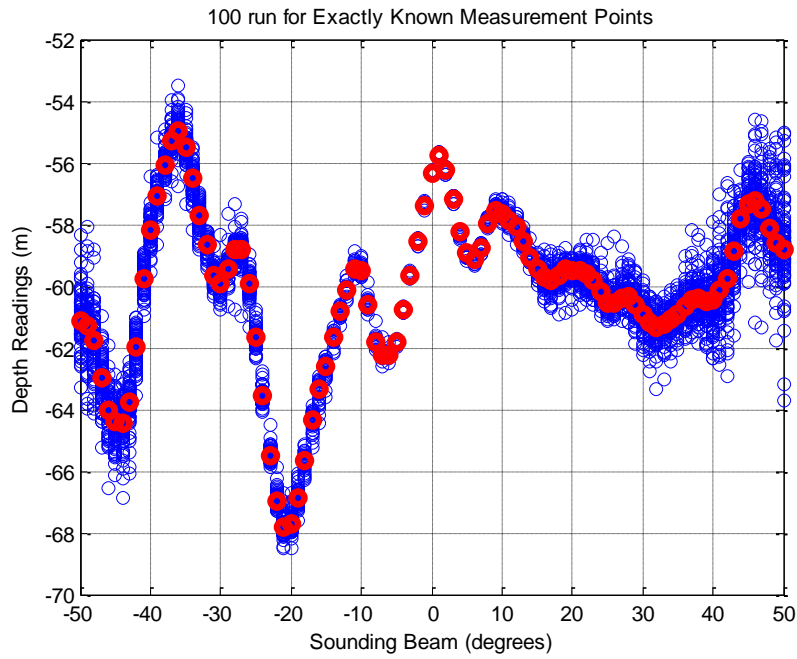
Figure 4.7. Measurement on exactly known positions conducted 100 times where ship movement/position effects are not included (red dots are absolute truth, blue dots are depth measurements)
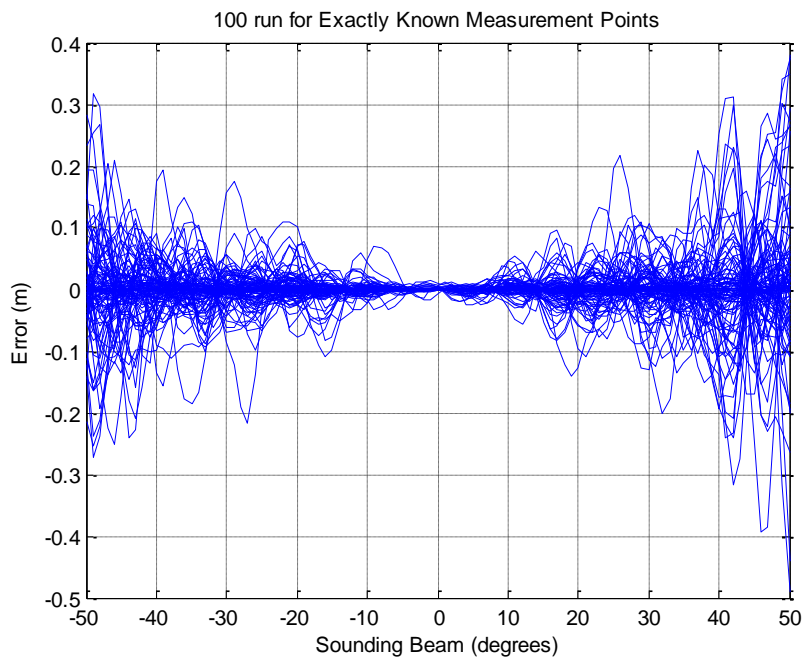
Figure 4.8. Error rates for a measurement with exactly known measurement data points for given ping cycle where ship movement/position effects are not included

This value increases up to the next beam and becomes the lowest in the middle beam. The values at this graph show the best measurement results to be achieved in case ship motion is well compensated.

4.3. Analysis of Position Errors Caused by Motion Sensor Errors

In the previous chapter, error source due to bottom inclination is examined. With addition of surface waves the bottom inclination is added to the simulation. Bottom shape affects not only the scattering strength, but also the time delays due to the fact that distance travelled changes. Moreover, with realistic bottom surface, the effect of ship motion can be observed for all potential scenarios.

Effect of changes in ship motion is simulated. It is not proper to conduct a survey above sea state 3. Calm sea environment should be preferred for bottom mapping studies. Nevertheless, one can get 0.5° pitch 3° roll motion at sea state 3 with a mid-sized ship. How these values affect our measurement could be seen below:
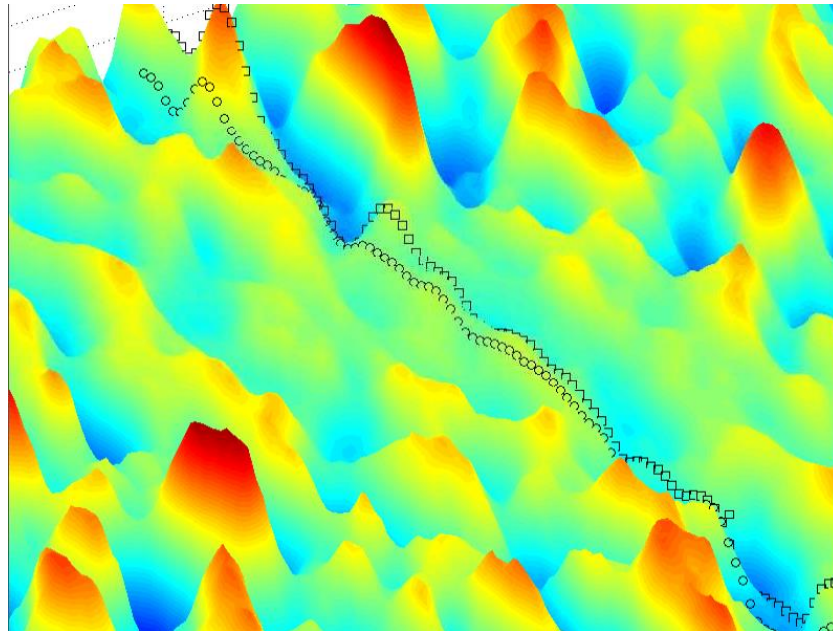
Figure 4.9. Measurement line at 0 pitch 0 roll motion and 0.5° pitch 3° roll motion on 3D Map (actual depth positions are denoted with circle and depth reading positions are denoted with square)

As shown in Figure 4.9, the measurement points change significantly with the ship motion. When these changes are not considered, there becomes a huge difference between the real and obtained measurement data. The difference between the real and obtained measurements is shown in Figure 4.10.
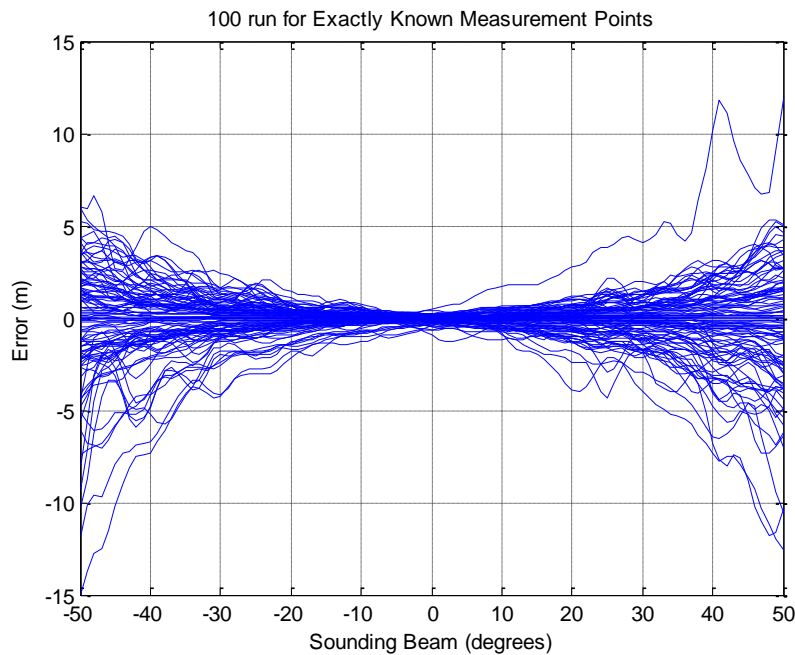
Figure 4.10. Errors caused by measurement line difference – ship motion not corrected (beam number vs error graph with 100 trials)

As shown in this comparison, the missing information about the measurement line (i.e., where the measurement line belongs to) leads to high error rates. In order to prevent deviation of map information from the real value, GPS related positional errors should also be corrected. Accordingly, motion sensor and GPS value inputs are added to our simulation.

The measurements are performed with a certain error however good the motion sensors are. If ship position is expressed with x, y, z, roll, pitch, and yaw, the data taken from GPS and motion sensors can be expressed as x_{read}, y_{read}, z_{read}, $roll_{read}$, $pitch_{read}$, and yaw_{read}. This ship motion vector will be analyzed with a certain noise added onto the real ship situation. Noise amounts and taken depth positions are shown on the Figure 4.11.
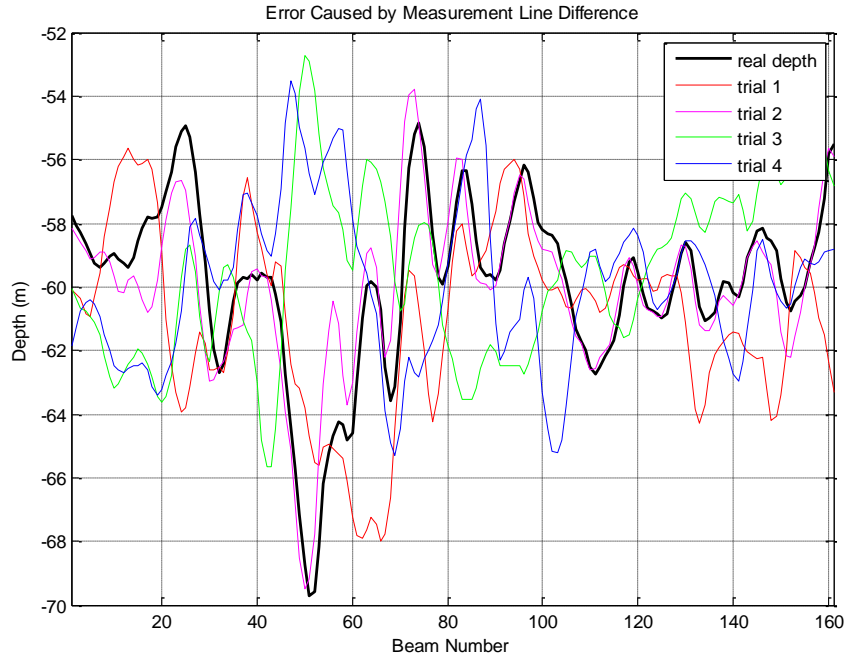
Figure 4.11. Error caused by measurement line difference $[\sigma_x, \sigma_y, \sigma_{roll}, \sigma_{pitch}, \sigma_{yaw}]$ = [5, 5, 1, 1, 1]
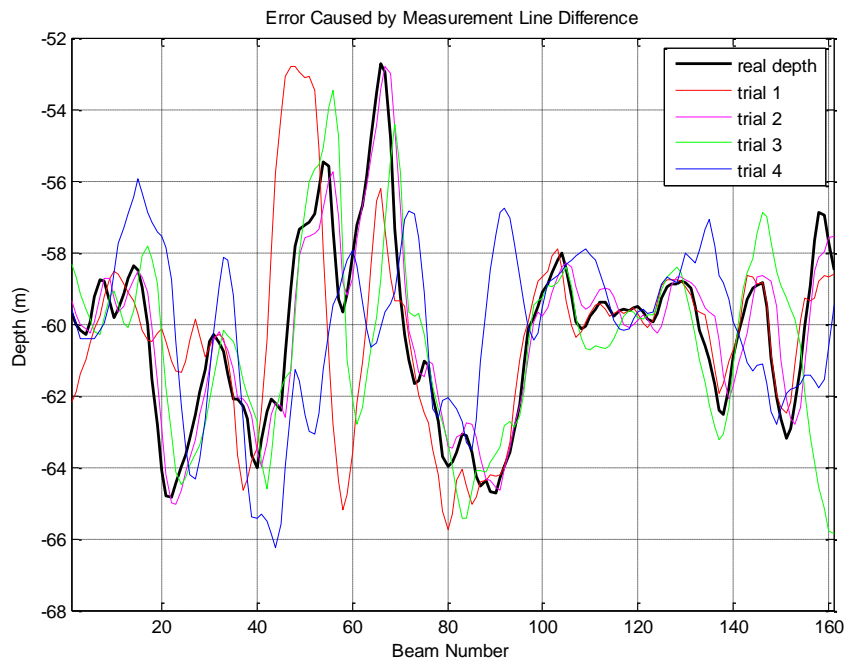
Figure 4.12. Error caused by measurement line difference $[\sigma_x, \sigma_y, \sigma_{roll}, \sigma_{pitch}, \sigma_{yaw}]$ = [1, 1, 1, 1, 1]
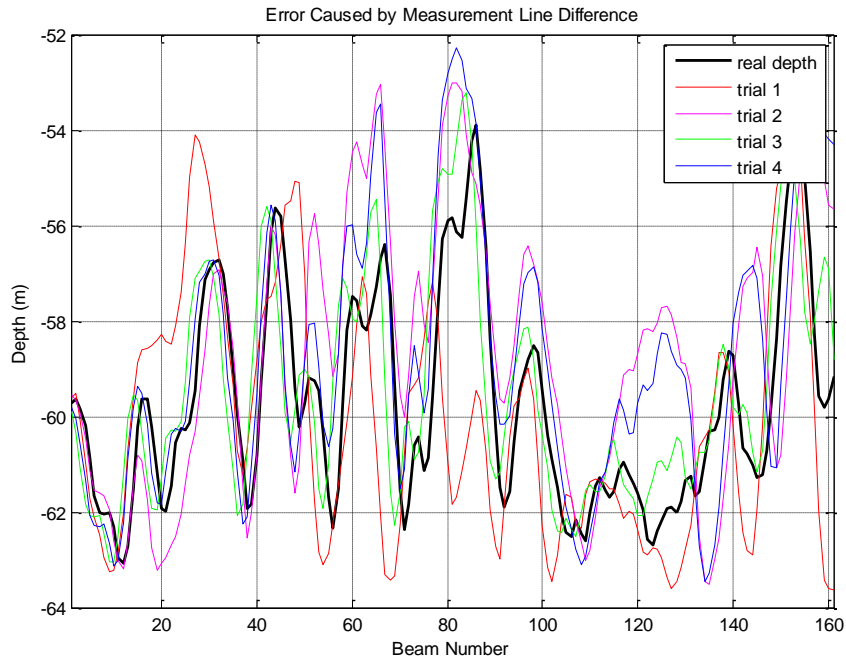
Figure 4.13. Error caused by measurement line difference $[\sigma_x, \sigma_y, \sigma_{roll}, \sigma_{pitch}, \sigma_{yaw}] =$
$[1, 1, 0.5, 0.5, 0.5]$
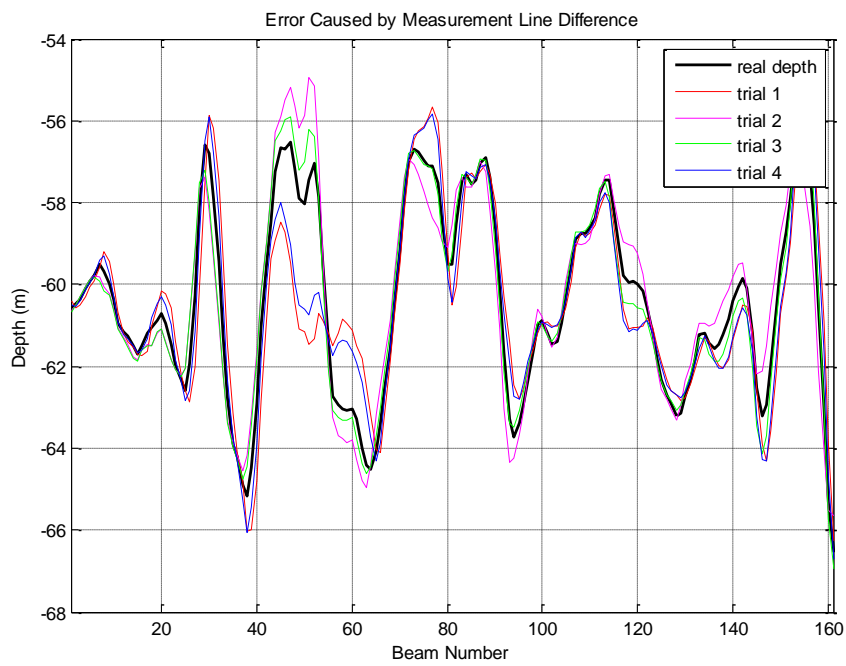
Figure 4.14. Error caused by measurement line difference $[\sigma_x, \sigma_y, \sigma_{roll}, \sigma_{pitch}, \sigma_{yaw}] =$
$[0.5, 0.5, 0.2, 0.2, 0.2]$
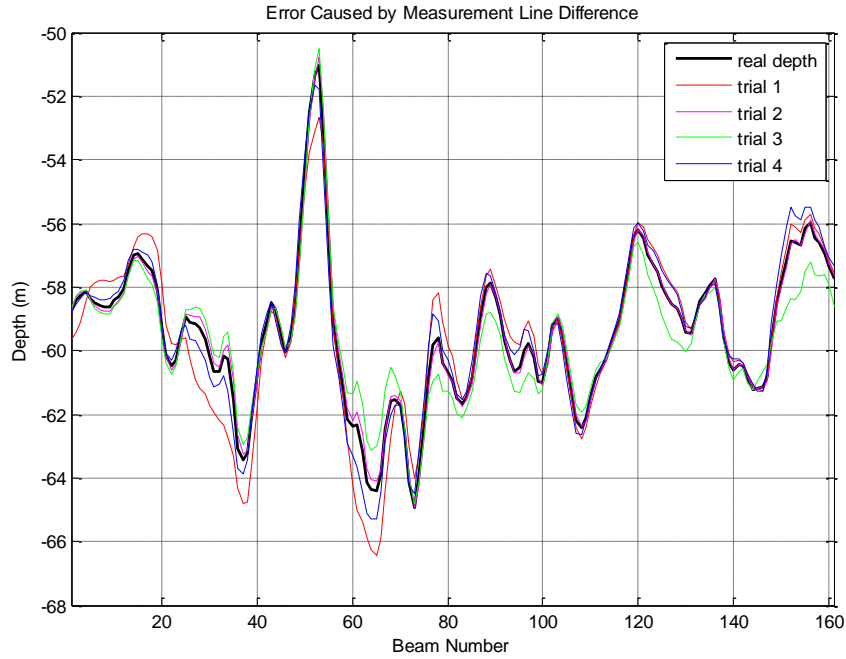
Figure 4.15. Error caused by measurement line difference [σ_x, σ_y, σ_{roll}, σ_{pitch}, σ_{yaw}] = [0.25, 0.25, 0.1, 0.1, 0.1]

According to graphs, measurement accuracy defined in IHO standards can be obtained with accurate GPS data and motion sensor data. It can be concluded that this simulation needs a GPS receiver with 0.5 m accuracy and motion sensor accuracy with at most 0.2 degrees.

4.4. Correction of the New Measurement Position

In the previous section, it was explained how accurate sensors needed to get high accuracy multibeam echosounder measurements during a hydrographic survey. The parameters in simulation were set to comply with the IHO standards for a survey. In order to ensure measured accuracy stated by IHO special order and first order, characteristics of depth, resolution, and beam type were foreseen. Moreover, roll and pitch sensors with a known accuracy and GPS sensors were modeled to investigate motion and position effects. The simulation was fed with the modeled sensor output information. Accuracy of information of the required sensor information was investigated to be able to comply with the IHO standards.

In this section, we will analyze how to make improvements in case the specifications are not met for a measurement. Therefore, the measurements will be analyzed for making improvements by taking measurements in the same region. With the help of a map taken from an area where measurements were done, the previous map will be analyzed for how to use in case of re-measurement.

Previous measurement points and new measurement points are impossible to meet exactly on the same point. Even in case the same route is scanned with the same speed, it is still not possible to take the same points. Here, positional errors don't affect which position the data is taken from. It is impossible that two similar measurements to occur repeatedly when the speed of sound is the same, and ship roll and pitch motions are completely the same. Even if it is possible, there is a certain error rate in multibeam echosounder data which are taken from motion sensor and GPS data shown in simulation. Even if it is possible to take data at the right positions, the position of the data could not be known exactly in new measurements. In Figure 4.16, the transmissions at the same positions, at the same ship motions, at the same roll, pitch, and yaw angles ensonify the same location. However, as seen in the figure, the information of where the ship performs these measurements depends on GPS error, roll, pitch and yaw reading errors.

It is summarized that it is unlikely to get the same depth measurement positions as in the previous data. Hence, there is need for a simulation where orientation and sample points of the new measurements are not the same. In the most general sense, we should have a process in which new measurements are only needed to be inside of the former measurement area.

We will achieve the former data at the position of the new data with interpolation over the former map. In addition to the data achieved from the former map by interpolation, interpolated variance values of the former map should be obtained. In the previous section, it was stated that ship's exact orientation and position are not known by the ship. When new measurements are obtained after the previous one, position values will be improved by using the measurement values.
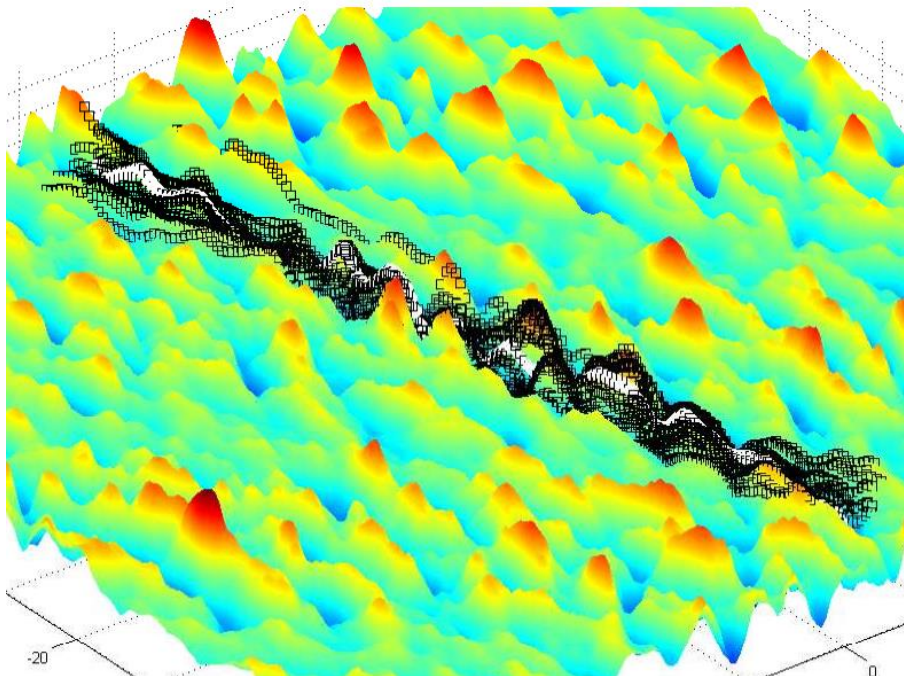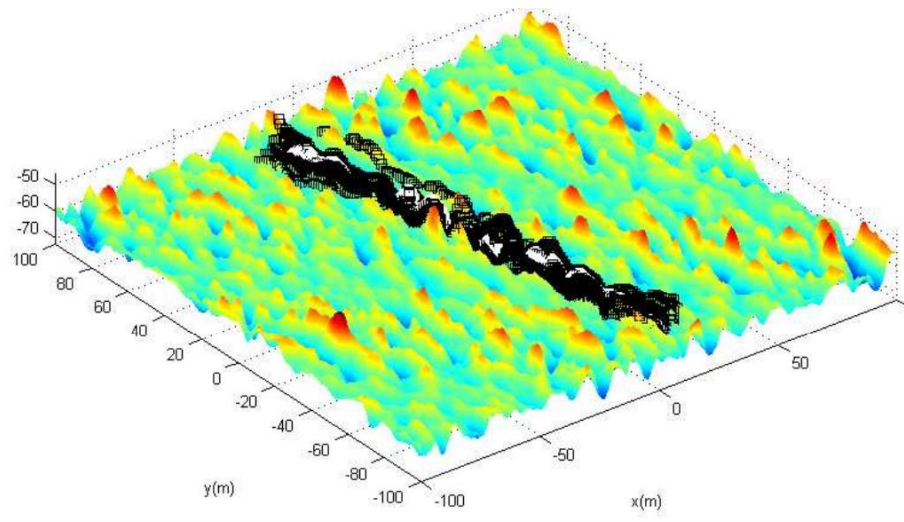
Figure 4.16. On the same location and same roll, pitch, and yaw – the position of depth readings varies with changing motion sensor errors (white denotes the assigned positions for error-free motion sensor)

The new value could be overlapped with the old value by sliding and rotating it in the vicinity ranged in error value. While identifying measurement position, x_{read}, y_{read}, z_{read}, $roll_{read}$, $pitch_{read}$, and yaw_{read} values should be improved. New measurement position will be oriented by changing these sensor data between the range of the error amount. When new measurement position value is closest to real x,

y, z, roll, pitch, and yaw values, array of depth reading will be nearest to the array of depth readings at former measurements.

$$\min \ \left\| D_{former}(x_{est}, y_{est}, roll_{est}, pitch_{est}, yaw_{est}) - D_{new} \right\|^2$$

with respect to $x_{est}, y_{est}, roll_{est}, pitch_{est}, yaw_{est}$.

within the boundaries:

$$x_{read} - 3\,\sigma_x \leq x_{est} \leq x_{read} + 3\,\sigma_x$$
$$y_{read} - 3\,\sigma_y \leq y_{est} \leq y_{read} + 3\,\sigma_y$$
$$roll_{read} - 3\,\sigma_{roll} \leq roll_{est} \leq roll_{read} + 3\,\sigma_{roll}$$
$$pitch_{read} - 3\,\sigma_{pitch} \leq x_{est} \leq pitch_{read} + 3\,\sigma_{pitch}$$
$$yaw_{read} - 3\,\sigma_{yaw} \leq yaw_{est} \leq yaw_{read} + 3\,\sigma_{yaw}$$

where;

D_{former}: vector of former measurements, where each element is depth reading calculated using $x_{est}, y_{est}, roll_{est}, pitch_{est}, yaw_{est}$ on the corresponding beam

D_{new}: vector of new measurements on the corresponding beam, where each element is depth reading on the corresponding beam

σ_x, σ_y, σ_{roll}, σ_{pitch}, σ_{yaw} : Standard deviations of motion sensor and GPS readings

Estimated position of new measurement is a function of x, y, z, roll, pitch, and yaw. As x, y, z, roll, pitch, and yaw expected values approach to the real motion values, the cost function will be minimized. Therefore, we can write an optimization code to solve for x, y, z, roll, pitch, and yaw. Using the resulting motion data, the echosounder measurement positions will be set.

Run 1: Perfect Depth Measurement – Error on Ship Motion&Position Sensors

This run is to check if the optimization for ship motion & position sensor assures the best when the depth reading position is the same with estimated ship position given from optimization tool.

Iteration 2 - Depth Reading and
Former Measurement Calculated at Estimated Positions

a)

Iteration 7 - Depth Reading and
Former Measurement Calculated at Estimated Positions

b)

Iteration 9 - Depth Reading and
Former Measurement Calculated at Estimated Positions

c)

Iteration 14 - Depth Reading and
Former Measurement Calculated at Estimated Positions

d)

78
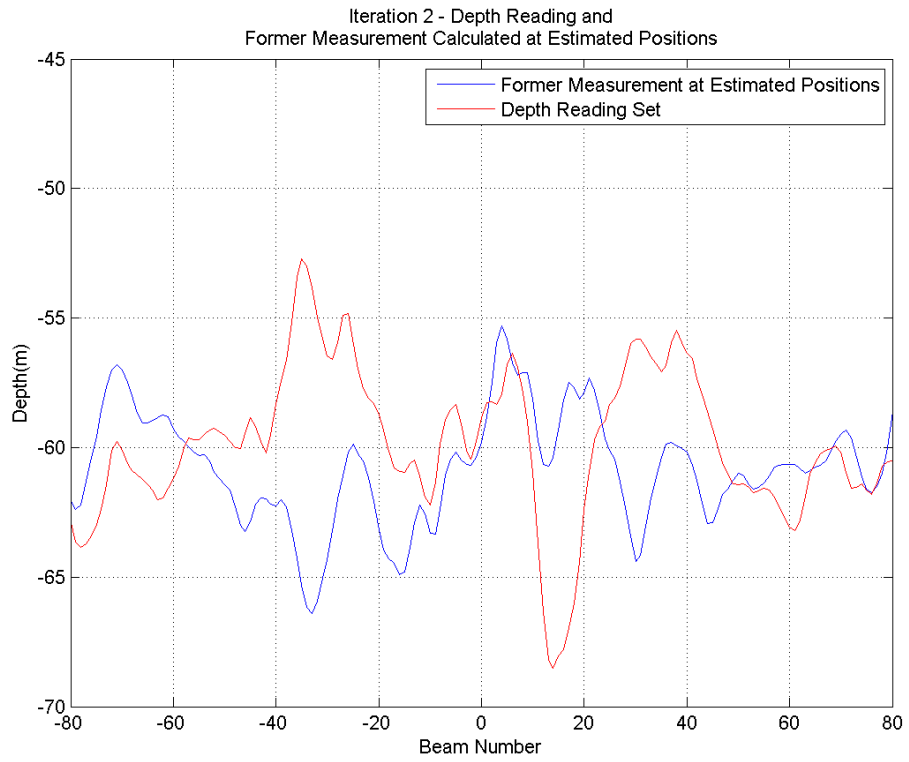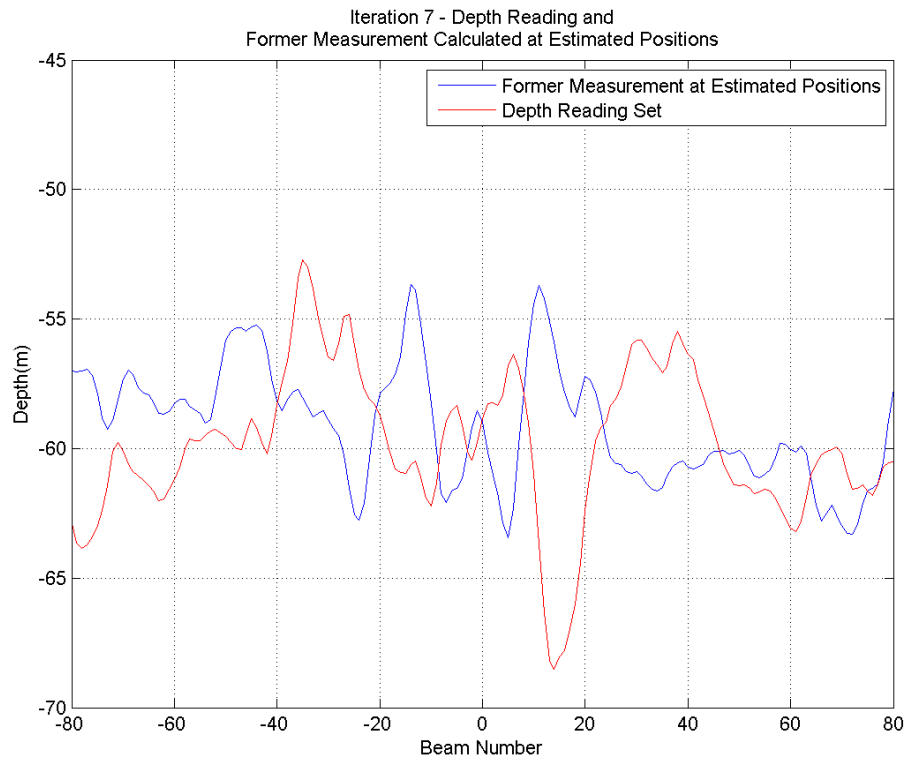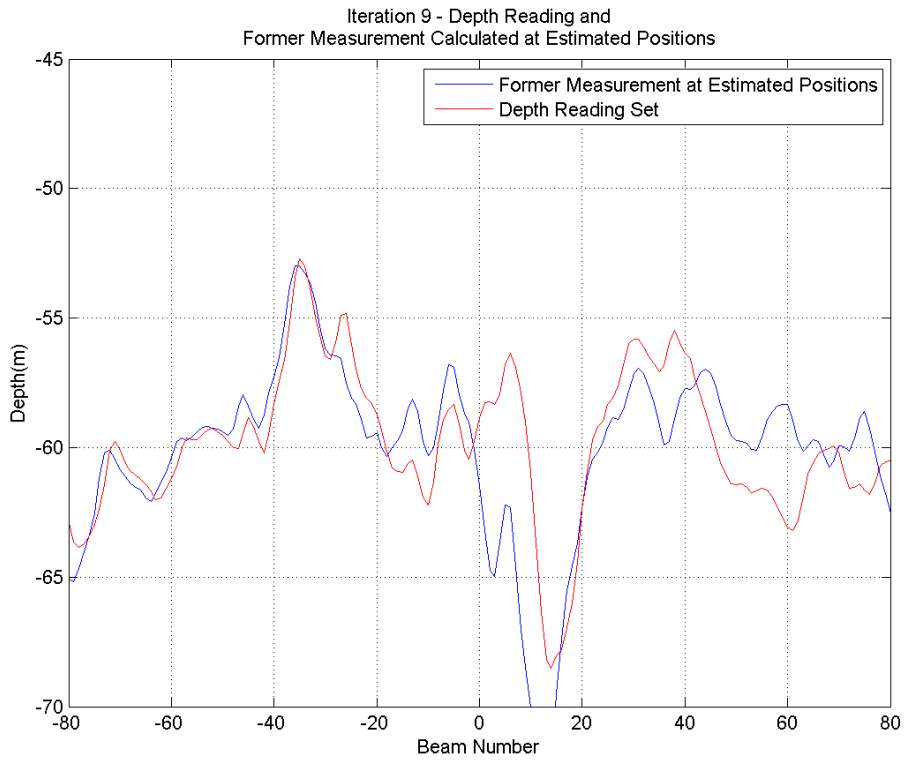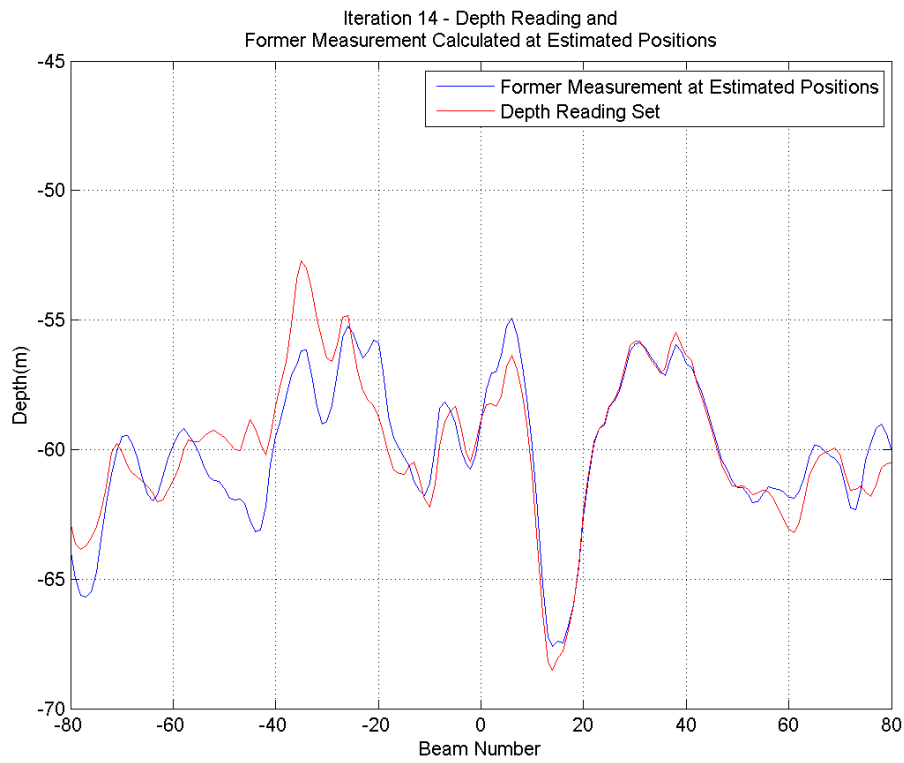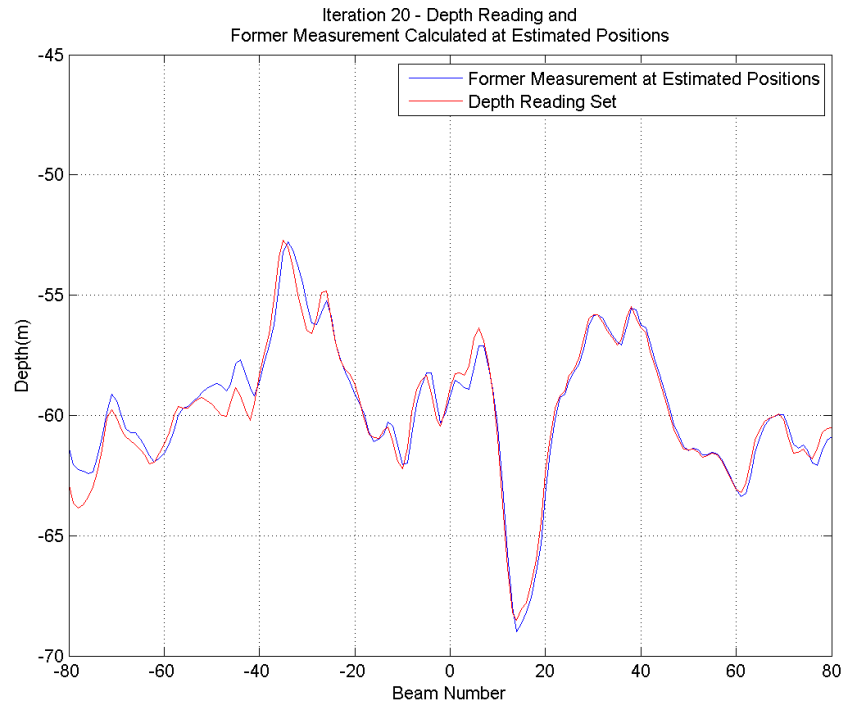
e)
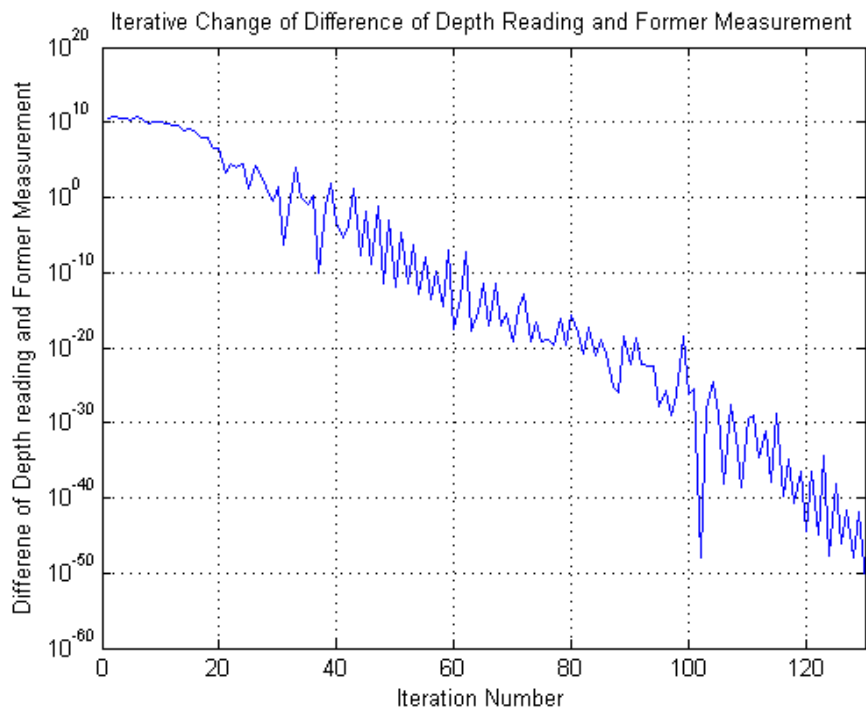
f)

Figure 4.17. Optimization run error on both depth measurement and ship motion&position sensors (**a, b, c, d, e** are former measurement and depth reading, **f** is iterative change of difference of depth reading and former measurement)

79

Run 2: Error on both Depth Measurement and Ship Motion&Position Sensors

This run is the real concern of this study; estimated ship position given from the optimization tool gives a better positional assignment.

a)

b)

Iteration 20 - Depth Reading and
Former Measurement Calculated at Estimated Positions

c)

Iteration 40 - Depth Reading and
Former Measurement Calculated at Estimated Positions

d)

Iteration 60 - Depth Reading and
Former Measurement Calculated at Estimated Positions

e)

Iteration 158 - Depth Reading and
Former Measurement Calculated at Estimated Positions

f)

82
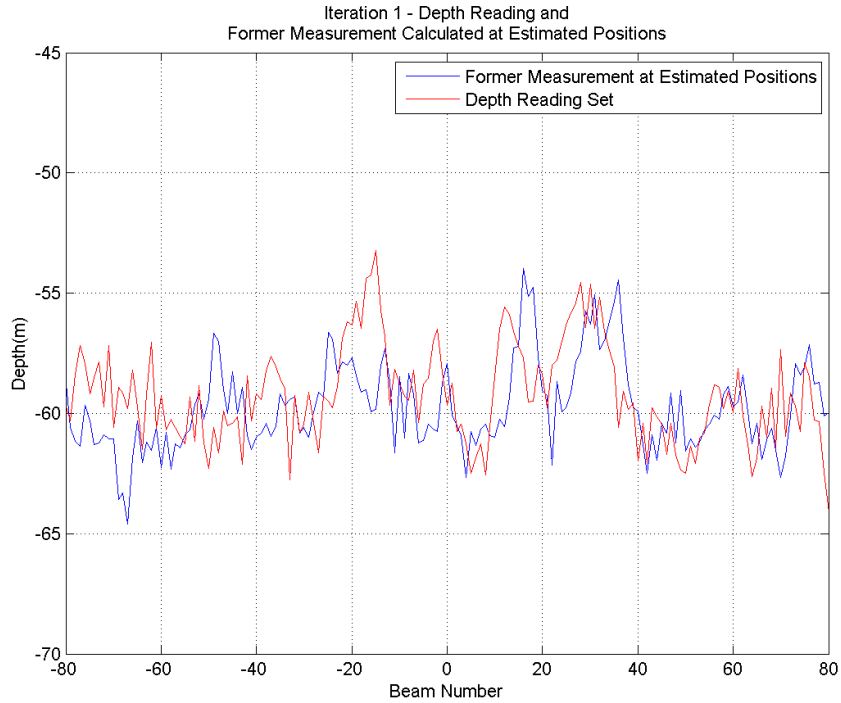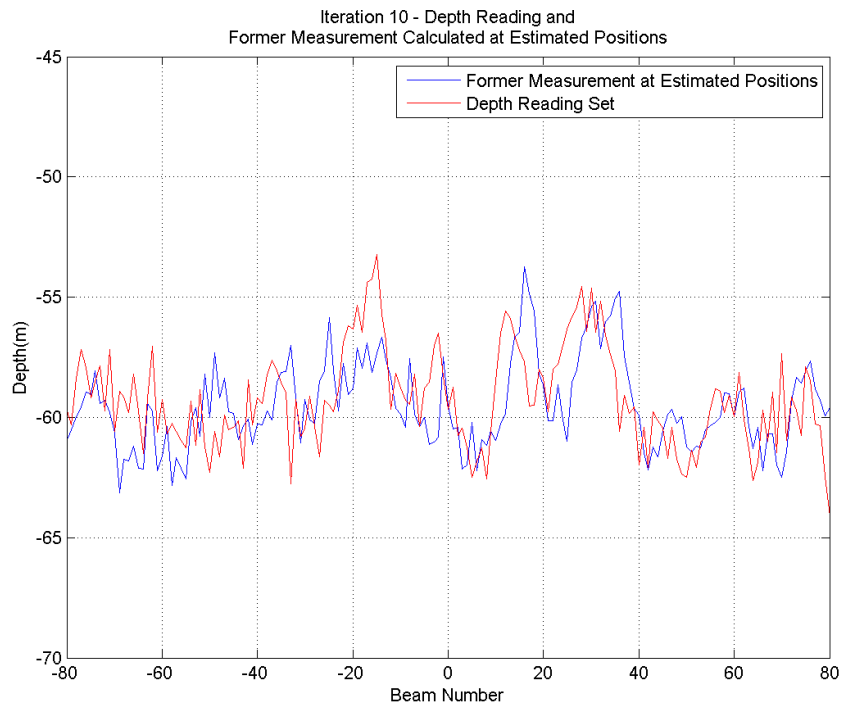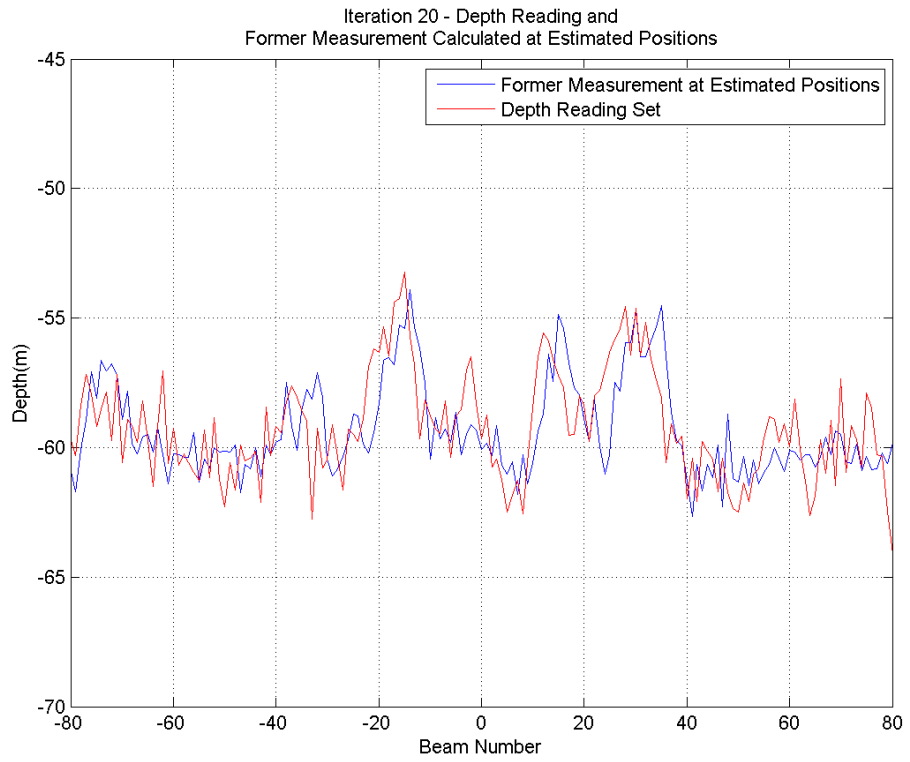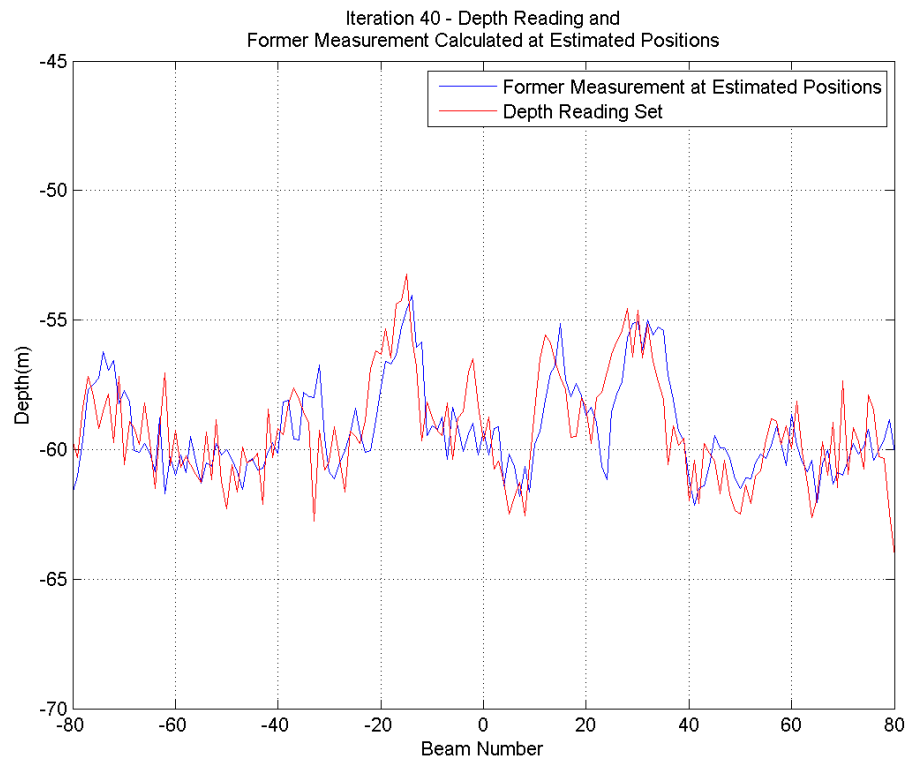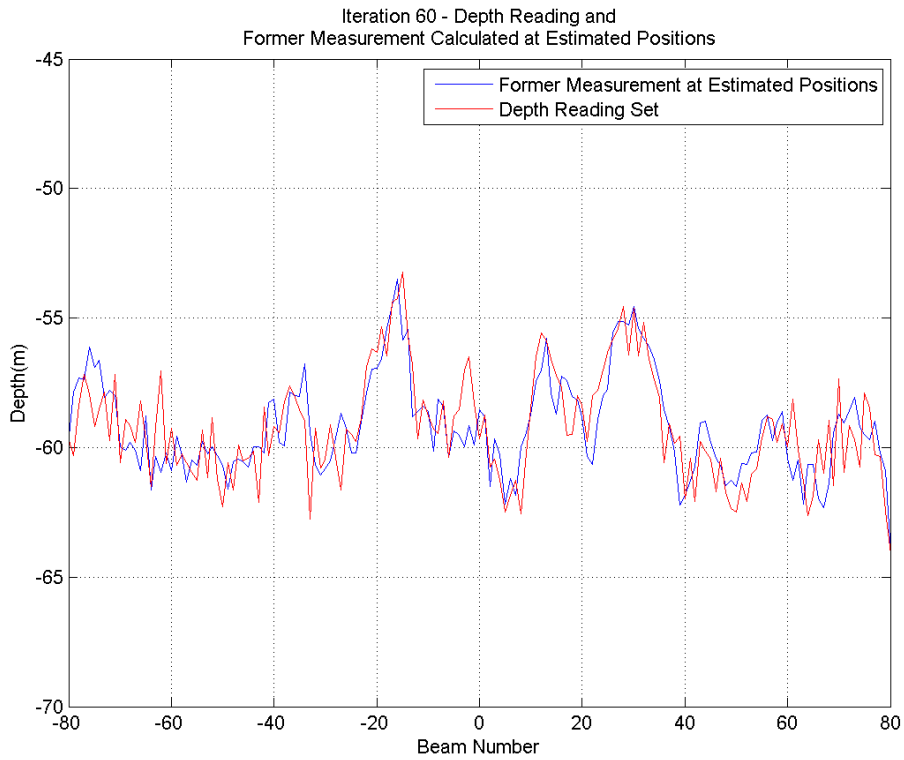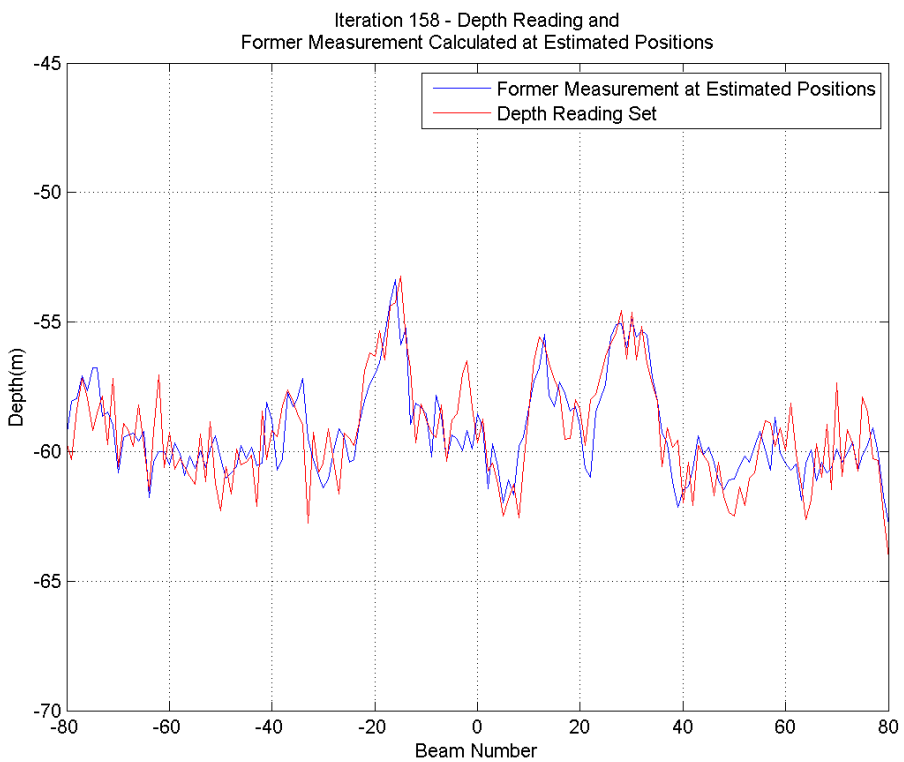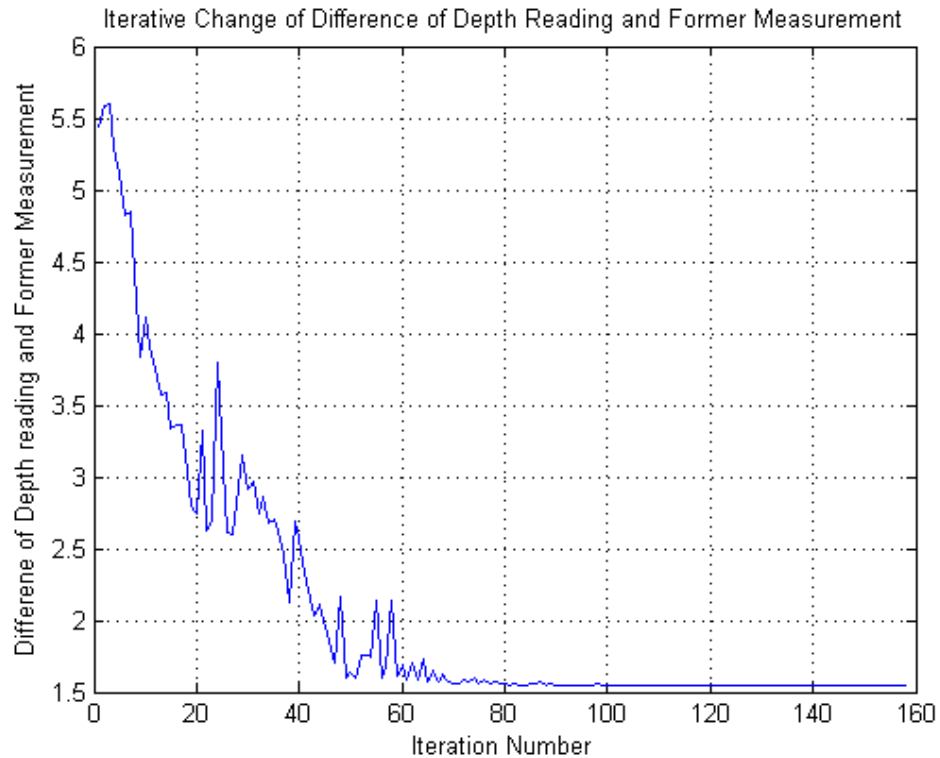
g)

Figure 4.18. Optimization run about error on both depth measurement and ship motion&position sensors (**a, b, c, d, e, f** are former measurement and depth reading, **g** is iterative change of difference of depth reading and former measurement)

4.5. Updating the Measurement Using Quality Weighted Averaging

The measurements will be analyzed for making improvements by taking measurements in the same region. With the help of a map taken from an area where measurements were done, the previous map will be analyzed for how to use in case of re-measurement.

The previous measurement data should have characteristics of the map achieved with simulation in the previous section. Hence, map information with a certain error rate and error variance value at every single point is stored in the map achieved by simulation. The error rate at new measurements will be lowered by using previous measurement values and variance value at every single point in the map. The measurement will be improved by taking the weighted average of the value of the point at re-measurement and previous measurement.

$$d^*_{ijn} = \left(d_{ijo} \; \frac{1}{\sigma^2_{ijo}} + d_{ijn} \; \frac{1}{\sigma^2_{ijn}} \right) \frac{1}{\frac{1}{\sigma^2_{ijo}} + \frac{1}{\sigma^2_{ijn}}}$$

d$_{ijo}$: Calculated old depth measurement obtained for interpolating at position i, j

d$_{ijn}$: New depth measurement at position i, j

d$_{ijn}$*: New updated depth measurement at position i, j

σ$_{ijo}$: Calculated old measurement error standard deviation obtained for interpolating at position i, j

σ$_{ijn}$: New measurement error standard deviation at position i, j

If measurement points exactly meet with the defined positions at the previous map, measurements can be corrected easily with this formula. However, previous measurement points and new measurement points are impossible to meet exactly on the same point. Therefore, we need to use the fitting position algorithm defined in the previous section. After applying the position correction using the optimization, we can apply the formula to improve measurements.
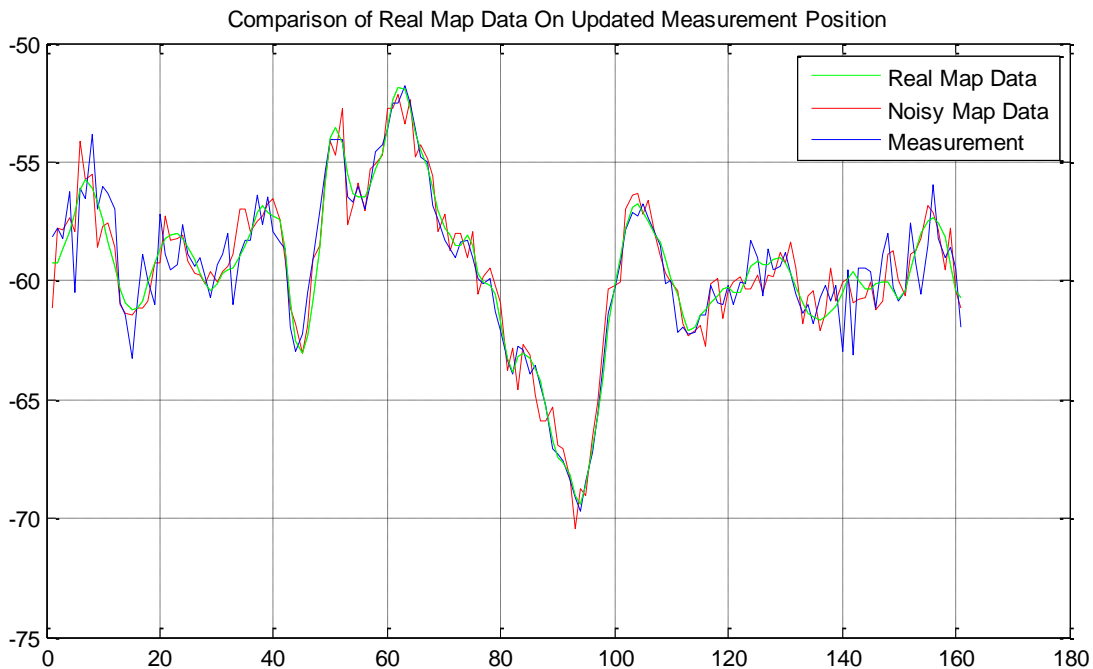
Figure 4.19. Comparison of map data on updated measurement position
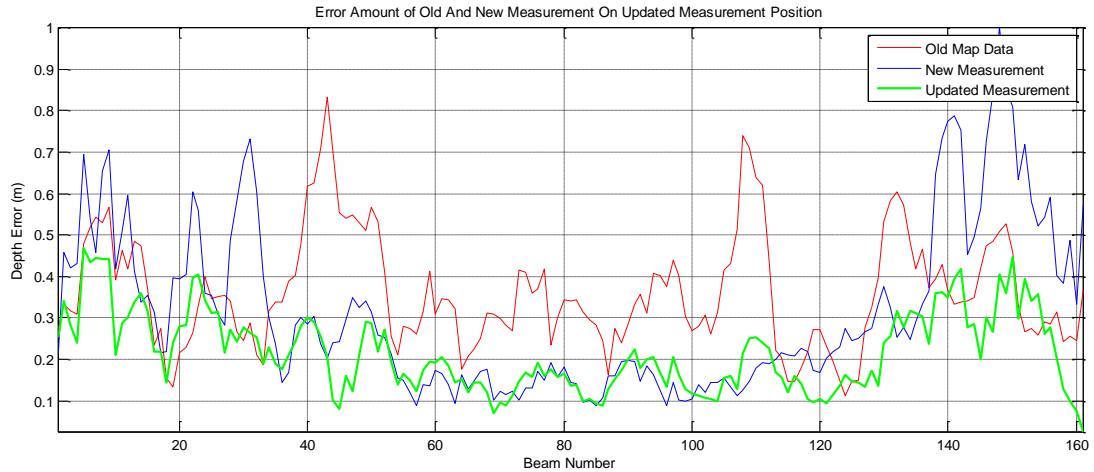
Figure 4.20. Error amount of old and new measurement and error of updated measurement position

Sum of error square for previous measurement:

$$\|D_{old} - D_{real}\|^2 = 31,89$$

Sum of error square for new measurement fitted on the optimized position:

$$\|D_{new} - D_{real}\|^2 = 28,56$$

Sum of error square for updated measurement:

$$\|D_{new}^* - D_{real}\|^2 = 16,47$$

It is seen from sum of error squares, with updating map data, we can decrease error on measurements significantly.

Hydrographic studies are conducted around the world oceans. Our measurement update method can be useful for this kind of measurements.

4.6. Total Error on Mapping Process

In the total mapping process, the effects of ship motion, the effect of sound velocity profile, depth measurement related errors, sea bottom slope related errors are considered. On the simulation, the hydrographic survey on a straight line is studied. As seen on Figure 4.21, the depth values on the area underneath of the ship are

obtained. The effects of ship motion can be seen from the studied area. Across the ship axis, the soundings are shown to be oscillating on y direction, caused by roll effect of ship. Along ship axis, the pitch variations cause some parts of the bottom not to have been covered.
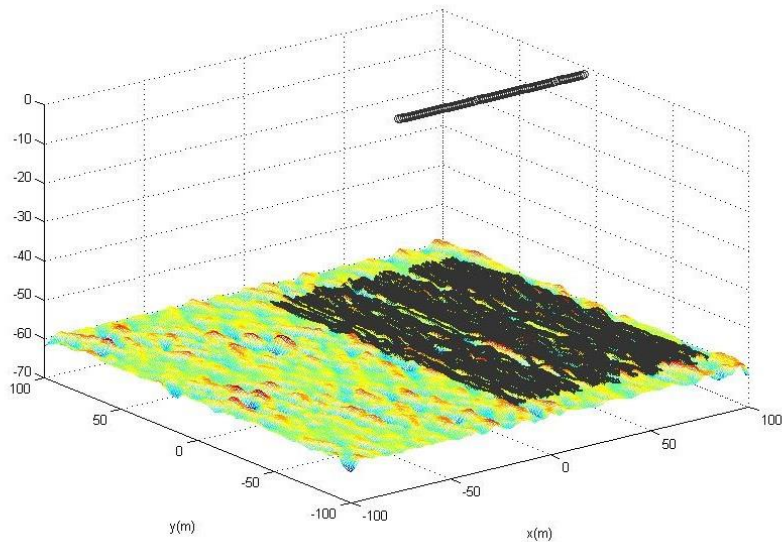
Figure 4.21. Total coverage area under ship motion

During this mapping process the data obtained from measurement is updated with the method applied in Chapters 4.4 and 4.5. The results for one ping cycle were shown to have successful effects on error rates. In this part, the moving ship collects different depth lines from successive swaths.

By conducting simulation on different parts of the map, several extreme situations are observed. These cases can be described as, unexpected increase of error on the new measurement, unexpected high error on the previous bathymetric data and the case where the results of update algorithm have higher error than the measurement.
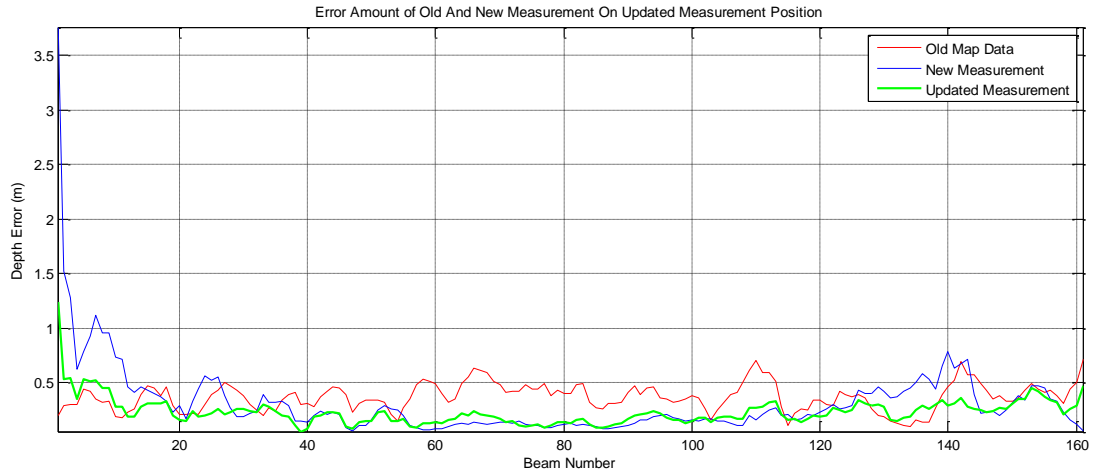
Figure 4.22. The case where the new measurement on sides have high error rate

On one extreme condition, the new measurement on one side is taken with high error rate. Since the weight of new data on the side beam is much smaller than the old measurement, the result is closer to the old map data error.

Furthermore, for the sum of the beams it can be seen that the error is reduced on the total.

Sum of error square for old map data:

$$\|D_{old} - D_{real}\|^2 = 24,91$$

Sum of error square for new measurement fitted on the optimized position:

$$\|D_{new} - D_{real}\|^2 = 33,11$$

Sum of error square for updated measurement:

$$\|D_{new}^* - D_{real}\|^2 = 18,13$$
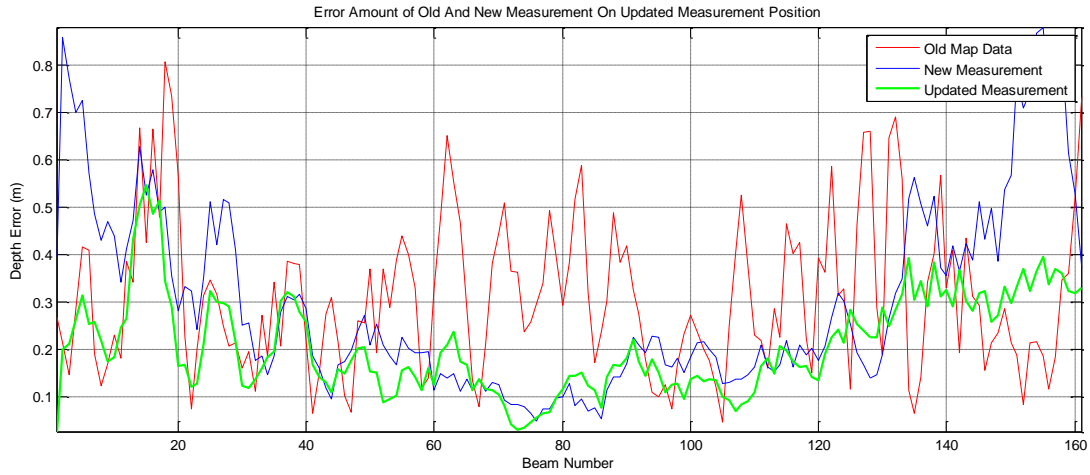
Figure 4.23. The case where some old map data has high error rate

On another extreme condition where the old bathymetric data on the received beam position is worse than the average bathymetric data, the result is seen on Figure 4.23. It is seen that on middle beams, the new measurement position is highly reliable. Since the weighting of middle beam on the new measurement is higher, the averaging process gives results closer to new measurement data.

Sum of error square for old map data:

$$\|D_{old} - D_{real}\|^2 = 37,94$$

Sum of error square for new measurement fitted on the optimized position:

$$\|D_{new} - D_{real}\|^2 = 27,26$$

Sum of error square for updated measurement:

$$\|D_{new}^* - D_{real}\|^2 = 17,31$$
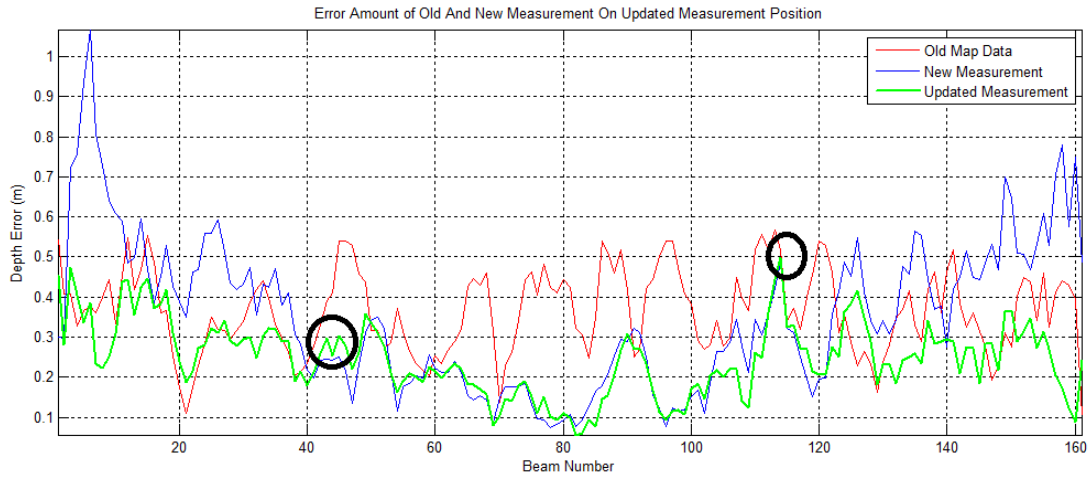
Figure 4.24. The case the update process fails to improve measurement quality

In the case where the old and new data has similar error, the obtained data may have high errors. However, this can happen for only few samples. When the sign of the error is the same on old and new measurements, the update error is inevitably small.

Sum of error square for old map data:
$$\|D_{old} - D_{real}\|^2 = 31,31$$

Sum of error square for new measurement fitted on the optimized position:
$$\|D_{new} - D_{real}\|^2 = 37,68$$

Sum of error square for updated measurement:
$$\|D_{new}^* - D_{real}\|^2 = 18,83$$

From the results on the overall mapping process, the optimization and averaging process is observed to have successful results. The updated measurement has nearly half of the error rate of the new and old measurements. There are extreme conditions on which the error is increased after averaging. For these beams, the improvement cannot be achieved due to the nature of the problem. However this effect is observed in only some beams where the measurement line for the given ping is improved in average of the overall line.

CHAPTER 5

CONCLUSION

In this thesis, acoustic methods which are the most practical methods in underwater mapping are explained. Bathymetric measurements conducted with multibeam echosounder have the capability of both efficient swath coverage and mapping from shallow water to deep ocean. In this thesis study a simulation program is developed on depth measurements with a multibeam sonar. On some places in the world, where navigational or under sea applications are vital, repeated multibeam echosounder measurements are documented. However, mapping process is heavily affected by the positional errors. Because of the positional errors, consecutive depth measurements are not suitable for improvement in depth accuracy. In this thesis, process of positioning the new measurements on old bathymetric data is studied. After fitting the new measurements on the old bathymetric data, different measurements taken on different times are corrected together.

In the first part of the thesis study, the sonar simulation basics are explained. The array and parameters of multibeam echosounder geometry are modeled. Environmental parameters affecting simulation are explained mathematically and added to simulation. Ship movement and location sensors which are the positional error sources are modeled.

For each beam, conversion of the travel time information to depth value using the geometry is modeled in the simulation. The error occurred during estimation of travel time is modeled with the effect of grazing angle on the scatterer, the effect of sound velocity and the effect of draft, collapse and sitting of the ship. The effect of ship motion and the effect of ship position information on depth reading location are modeled.

Error amount results which occur during positional error related reading differences are shown. In order to investigate the positional error effects in detail, a realistic seabed environment is formed. Since it is aimed to show IHO requirements are satisfied on the data gathered on realistic seabed, studies are performed on a surface with an average 60 m depth.

The depth readings are extracted on 100 run for the case of stationary ship, for the case of moving ship without motion sensor and GPS and for the case of moving ship with motion sensor and GPS with error. It is concluded that in order to get a measurement suitable to standards, GPS receiver with 0.5 meter accuracy and motion sensor with 0.2° accuracy are needed.

The proposed method, the use of data which are obtained from consecutive measurements is added to simulation. For this, positional improvement is conducted to eliminate the positional difference of new and old measurements. The location of each measurement on old bathymetric data is calculated. Around the 3(sigma) of x, y, roll, pitch, yaw variables, optimization algorithm is conducted. By this method, the x, y, roll, pitch, yaw sensor readings are corrected. With the corrected motion and position sensor data, the depth reading position errors are minimized. In this work, the ship motion is simulated by generating the roll and pitch values. Roll and pitch values are generated as zero-mean white Gaussian noise. By modeling the ship structure, forces created by waves and currents, the frequencies of roll and pitch values can be set. With this model, the uncertainty of the roll and pitch motion can be minimized. During the data association process, ship motion estimation algorithm can be used to decrease the error amounts on ship motion sensors. This interpretation can help optimization process on positioning the readings on correct locations.

After overlapping the new measurements on the old measurements, the depth value is calculated with weighted averaging method. Weights of the measurements are determined with the quality of measurement which is calculated as the inverse of the error variance. The mapping process is updated with obtained data from weighted averaging.

Error rate on old bathymetric data, error rate on new measurement and error rate on the data obtained from weighted averaging are compared. The error amounts are calculated from the sum of the squares of the differences from absolute truth fed on simulation. On the comparison, weighted averaging results are obtained as nearly half of the error rates of old bathymetric data and the new measurement. On the simulation, the positional correction with optimization algorithm and weighted averaging is shown to have successful results.

To conclude, this study suggests that developed methods are useful in underwater mapping with high accuracy. Therefore the methods in the simulation would be beneficial in hydrography and bathymetry sciences including hydrographic mapping, coastal engineering and scientific application fields.

During this study, multibeam echosounder real measurements taken from sea floor were not available. For further study, the correction process can be conducted using real data. The real data collected from ASELSAN test facilities will be available in near future. It is important to include sound speed profile correction in order to give precise positioning, where precise positioning is vital before weighted averaging. Former bathymetric data and the new data can be both taken from sea surveys. With real measurements, the measurement quality should also be recorded. With the real data, measurement errors that are simulated in the program would occur naturally. Therefore this natural measurement error would be minimized with the proposed methods.

Without the real data, the simulation can also be improved by adding water column data simulation. In this thesis, echosounding is conducted to generate depth values on each beam. But addition of water column features, simulation can be developed for underwater structures such as shipwrecks or underwater archeological sites. Echoes from the water column is mostly unused for bathymetric measurements since the water column echoes are caused by fish, planktons and other living creatures which are eliminated to get the correct depth measurements. Since the sea bottom has the highest backscattering strength, the methods for eliminating the echoes other than the bottom are easy to implement. However, in some cases the water column data is

needed for seabed mapping, if the seabed has underwater structures in the scope of interest. In this case, eliminating the echoes other than the sea bottom will cause losing the information of interest. To simulate the water column data in the simulation, a detailed study is required in both simulating the echoes for each beam and reconstruction of the underwater structures.

The depth measurement correction and improvement method studied in this thesis can also be implemented on AUV based bathymetric measurements. This position assignment and fitting algorithm can be conducted on side-scan sonar or synthetic aperture sonar imaging. For AUV based mapping applications, the imaging for deeper bottoms with higher resolution is possible. Since the underwater vehicle is positioned on a certain depth, the sonar beams are closer to sea bottom, which provides higher spatial resolution. Another advantage of this application arises from discarding the effect of surface waves. While the surface ships are vulnerable to surface waves, on underwater vehicles, amount of ping to ping change of roll, pitch and yaw changes are much smaller. For position assignment and fitting, not only slices of measurements are used but also patches created with several slices can be used for fitting on the previous bathymetric data. By using an area to position on the map, the depth and position correction can be further improved.

REFERENCES

[1] D.G. Dallmeyer, "Values at sea: ethics for the marine environment", Athens, Ga.: University of Georgia Press, 2003.

[2] H.M. Dierssen and A.E. Theberge, "Bathymetry: Assessing Methods," in Encyclopedia of Ocean Sciences. New York: Taylor and Francis Group, 2014.

[3] A.E. Theberge, "Sounding Pole to Sea Beam", in ASPRS/ACSM Annual Convention, 1989.

[4] C.H. Sherman and J.L. Butler, *Transducers and arrays for underwater sound*. New York: Springer, 2007.

[5] J.A. Fornshell and A. Tesei, "The Development of SONAR as a Tool in Marine Biological Research in the Twentieth Century", *International Journal of Oceanography*, vol. 2013, pp. 1-9, 2013.

[6] J.D. Mudie, W.R. Normark and E.J. Cray, "Direct Mapping of the Sea Floor Using Side-Scanning Sonar and Transponder Navigation", *Geol. Soc. America Bull*, vol. 81, no. 5, pp. 1547-1554, 1970.

[7] A.S. Lanier, "A comparison of seafloor sonar classification methods through the use of error matrices and 3 dimensional GIS visualization: a multibeam sonar investigation of Nehalem Bank", M.S. thesis, Marine Resource Manage., Oregon State Univ., Corvallis, USA, 2006.

[8] S.E. Reutebuch, H. Andersen and R. McGaughey, "Light detection and ranging (LIDAR): an emerging tool for multiple resource inventory", *Journal of Forestry*, vol. 103, no. 6, pp. 286-292, 2005.

[9] C. Malzone, D. Lockhart, T. Meurling and M. Baldwin, "The progression and impact of the latest generation of multibeam acoustics upon multidisciplinary hydrographic-based applications", *Underwater Technology*, vol. 27, no. 4, pp. 151-160, 2008.

[10] J.C. Brock and S.J. Purkis, "The Emerging Role of Lidar Remote Sensing in Coastal Research and Resource Management", *Journal of Coastal Research*, no 53, pp. 1-5, 2009.

[11] R.A. Pickrill and B.J. Todd, "The multiple roles of acoustic mapping in integrated ocean management, Canadian Atlantic continental margin", *Ocean & Coastal Management*, vol. 46, no. 6-7, pp. 601-614, 2003.

[12] S. Bateman, "Hydrographic surveying in the EEZ: differences and overlaps with marine scientific research", *Marine Policy*, vol. 29, no. 2, pp. 163-174, 2005.

[13] J.A. Roelvink, "Coastal morphodynamic evolution techniques", *Coastal Engineering*, vol. 53, no. 2-3, pp. 277-287, 2006.

[14] D. Cauquil, "3D seismic and AUV data integration for deepwater geohazard assessment: Application to offshore northwest Borneo, Brunei," in Offshore Technology Conference, Kuala Lumpur, Malaysia, 2014.

[15] A. Dulip, "Offshore Environmental Monitoring Around Oil and Gas Installations on the Western Continental Shelf, Arabian Sea, India," in SPE/EPA/DOE Exploration and Production Environmental Conference, Texas, 2003.

[16] B. Lachman, P. Schirmer, D.R. Frelinger, V.A. Greenfield, M.S. Tseng and T. Nichols (2007). *Installation mapping enables many missions* [Online]. Available: http://www.rand.org/pubs/monographs/MG552.html.

[17] J. Simley and W. Carswell. (2009). *The national map—Hydrography* [Online]. Available: http://pubs.usgs.gov/fs/2009/3054/.

[18] S. Turchetti, "Sword, Shield and Buoys: A History of the NATO Sub-Committee on Oceanographic Research, 1959-19731", *Centaurus*, vol. 54, no. 3, pp. 205-231, 2012.

[19] M. Lepparanta and K. Myrberg, *Physical oceanography of the Baltic Sea*. Berlin: Springer/Praxis Pub., 2009.

[20] E. Hutin, Y. Simard and P. Archambault, "Acoustic detection of a scallop bed from a single-beam echosounder in the St. Lawrence", *ICES Journal of Marine Science*, vol. 62, no. 5, pp. 966-983, 2005.

[21] K.E. Sawaya, L.G. Olmanson, N.J. Heinert, P.L. Brezonik and M.E. Bauer, "Extending satellite remote sensing to local scales: land and water resource monitoring using high-resolution imagery", *Remote Sensing of Environment*, vol. 88, no. 1, pp. 144-156, 2003.

[22] R. Smith, M. Schwager, S. Smith, B. Jones, D. Rus and G. Sukhatme, "Persistent ocean monitoring with underwater gliders: Adapting sampling resolution", *Journal of Field Robotics*, vol. 28, no. 5, pp. 714-741, 2011.

[23] O. Andrejev, A. Sokolov, T. Soomere, R. Värv and B. Viikmäe, "The use of high-resolution bathymetry for circulation modelling in the Gulf of Finland", *Estonian J. Eng.*, vol. 16, no. 3, pp. 187-210, 2010.

[24] R. Timmermann, A. Le Brocq, T. Deen, E. Domack, P. Dutrieux, B. Galton-Fenzi, H. Hellmer, A. Humbert, D. Jansen, A. Jenkins, A. Lambrecht, K. Makinson, F. Niederjasper, F. Nitsche, O. Nøst, L. Smedsrud and W. Smith, "A consistent data set of Antarctic ice sheet topography, cavity geometry, and global bathymetry", *Earth Syst. Sci. Data*, vol. 2, no. 2, pp. 261-273, 2010.

[25] C. de Moustier, "Beyond bathymetry: Mapping acoustic backscattering from the deep seafloor with Sea Beam", *The Journal of the Acoustical Society of America*, vol. 79, no. 2, pp. 316-331, 1986.

[26] J. Becker, D. Sandwell, W. Smith, J. Braud, B. Binder, J. Depner, D. Fabre, J. Factor, S. Ingalls, S. Kim, R. Ladner, K. Marks, S. Nelson, A. Pharaoh, R. Trimmer, J. Von Rosenberg, G. Wallace and P. Weatherall, "Global Bathymetry and Elevation Data at 30 Arc Seconds Resolution: SRTM30_PLUS", *Marine Geodesy*, vol. 32, no. 4, pp. 355-371, 2009.

[27] *Engineering and Design-Hydrographic Surveying*, U.S. Army Corps of Engineers, Wasington, DC, 2002.

[28] R. Dashen, *Sound transmission through a fluctuating ocean.* Cambridge: Cambridge University Press, 2010.

[29] M. Malik. (2011). *Gulf of Mexico Expedition 2011*. [Online]. Available: http://oceanexplorer.noaa.gov/okeanos/explorations/ex1105/welcome.html.

[30] E. Kammerer, "New Method for the Removal of Refraction Artifacts in Multibeam Echosounder Systems," Ph.D. dissertation, Dept. Geodesy and Geomatics Eng., University of New Hampshire, Durham, NH, 2000.

[31] C. Moustier, "Field evaluation of sounding accuracy in deep water multibeam swath bathymetry," in MTS Oceans Conf., HI, 2001, pp. 1761-1765.

[32] J.V. Gardner. (2002). *Multibeam mapping of the west Florida shelf, Gulf of Mexico*. [Online]. Available: http://pubs.usgs.gov/of/2002/0005/.

[33] C. Brown and P. Blondel, "Developments in the application of multibeam sonar backscatter for seafloor habitat mapping", *Applied Acoustics*, vol. 70, no. 10, pp. 1242-1247, 2009.

[34] P. Fernandes, "Autonomous underwater vehicles: future platforms for fisheries acoustics", *ICES Journal of Marine Science*, vol. 60, no. 3, pp. 684-691, 2003.

[35] D. Anthony and J. Leth, "Large-scale bedforms, sediment distribution and sand mobility in the eastern North Sea off the Danish west coast", *Marine Geology*, vol. 182, no. 3-4, pp. 247-263, 2002.

[36] L. Hamilton, "Acoustic seabed segmentation for echosounders through direct statistical clustering of seabed echoes", *Continental Shelf Research*, vol. 31, no. 19-20, pp. 2000-2011, 2011.

[37] K. Marks and W. Smith, "An uncertainty model for deep ocean single beam and multibeam echo sounder data", *Marine Geophysical Researches*, vol. 29, no. 4, pp. 239-250, 2008.

[38] J Behrens, "Surveying of Waters in the FRG by the Federal Waterways and Shipping Administration," in *New Technology for a New Century*, Seoul, Korea, 2001.

[39] A. Nikolovska, "Acoustic methane seepage quantification model design, experiments and deep-sea application," in *OCEANS 2007-Europe*, Bremen, Germany, 2007.

[40] C. Cofaigh, P. Dunlop and S. Benetti, "Marine geophysical evidence for Late Pleistocene ice sheet extent and recession off northwest Ireland", *Quaternary Science Reviews*, vol. 44, pp. 147-159, 2012.

[41] K. Haris, B. Chakraborty, C. De, R. Prabhudesai and W. Fernandes, "Model-based seafloor characterization employing multi-beam angular backscatter data—A comparative study with dual-frequency single beam", *The Journal of the Acoustical Society of America*, vol. 130, no. 6, pp. 3623-3632, 2011.

[42] *Manual on Hydrography,* 1st ed., International Hydrographic Bureau, Monaco, 2005.

[43] Y. Pailhas, K. Brown, C. Capus and Y. Petillot, "Design of artificial landmarks for underwater simultaneous localisation and mapping", *IET Radar, Sonar & Navigation*, vol. 7, no. 1, pp. 10-18, 2013.

[44] A. Amiri-Simkooei, M. Snellen and D. Simons, "Principal Component Analysis of Single-Beam Echo-Sounder Signal Features for Seafloor Classification", *IEEE Journal of Oceanic Engineering*, vol. 36, no. 2, pp. 259-272, 2011.

[45] X. Wu, G. Eleftheriades and T. van Deventer-Perkins, "Design and characterization of single- and multiple-beam mm-wave circularly polarized substrate lens antennas for wireless communications", *IEEE Transactions on Microwave Theory and Techniques*, vol. 49, no. 3, pp. 431-441, 2001.

[46] W. Maleika, "The influence of track configuration and multibeam echosounder parameters on the accuracy of seabed DTMs obtained in shallow water", *Earth Sci. Inform.*, vol. 6, no. 2, pp. 47-69, 2013.

[47] W. Smith and D.T. Sandwell, "Global Sea Floor Topography from Satellite Altimetry and Ship Depth Soundings", *Science*, vol. 277, no. 5334, pp. 1956-1962, 1997.

[48] M. Stojanovic and J. Preisig, "Underwater acoustic communication channels: Propagation models and statistical characterization", *IEEE Commun. Mag.*, vol. 47, no. 1, pp. 84-89, 2009.

[49] D. Rothrock and M. Wensnahan, "The Accuracy of Sea Ice Drafts Measured from U.S. Navy Submarines", *J. Atmos. Oceanic Technol.*, vol. 24, no. 11, pp. 1936-1949, 2007.

[50] C. Wang, J. Corbett and J. Firestone, "Modeling Energy Use and Emissions from North American Shipping: Application of the Ship Traffic, Energy, and Environment Model", *Environmental Science & Technology*, vol. 41, no. 9, pp. 3226-3232, 2007.

[51] G. Yufit and E. Maillard, "The influence of ship motion on bathymetric sonar performance in FM mode of operation," in *OCEANS 2011*, Waikoloa, HI, 2011, pp. 1-5.

[52] V. Ernstsen, R. Noormets, D. Hebbeln, A. Bartholomä and B. Flemming, "Precision of high-resolution multibeam echo sounding coupled with high-accuracy positioning in a shallow water coastal environment", *Geo-Mar. Let.t*, vol. 26, no. 3, pp. 141-149, 2006.

[53] R. Aubauer, M. Lammers and W. Au, "One-hydrophone method of estimating distance and depth of phonating dolphins in shallow water", *The Journal of the Acoustical Society of America*, vol. 107, no. 5, pp. 2744-2749, 2000.

[54] A. Thompson and B. Taylor, *Guide for the use of the International System of Units (SI)*. Gaithersburg, M.D.: National Institute of Standards and Technology, 2008.

[55] M.P. Hayes and P.T. Gough, "Synthetic Aperture Sonar: A Review of Current Status", *IEEE Journal of Oceanic Engineering*, vol. 34, no. 3, pp. 207-224, 2009.

[56] L. Brekhovskikh and I. Lysanov, *Fundamentals of ocean acoustics*. New York: Springer, 2003.

[57] J. Robert, *Principles of underwater sound.* New York: McGraw-Hill Book Company, 1983.

[58] R. Hodges, *Underwater acoustics*. Hoboken, NJ: Wiley, 2010.

[59] W. Burdic, *Underwater acoustic system analysis*. Englewood Cliffs, NJ: Prentice-Hall, 1991.

[60] John E. Piper, "Beamforming Narrowband and Broadband Signals," in *Sonar Systems,* InTech, 2011.

[61] C. Jong, *Multibeam sonar theory of operation*. Delft: Delft University Press, 2002.

[62] H. Sastry, *Proceedings of the International Conference on Sonar Sensors of Systems*. Kochi, India: Allied Publishers*, 2002.

[63] D. Stewart, "A platform with six degrees of freedom", *Proceedings of the Institution of Mechanical Engineers*, vol. 180, no. 1, pp. 371-386, 1965.

[64] R. Loweth, *Manual of offshore surveying for geoscientists and engineers*. London: Chapman & Hall, 2012.

[65] C. Huang, "Acoustic wave scattering from rough sea surface and seabed", M.S. thesis, Inst. of Undersea Technol., National Sun Yat-sen Univ., Kaohsiung, Taiwan, 1998.

[66] FarSounder Inc. (2011, July 11). *DAMUS: FarSounder's Sonar Performance Prediction Tool* [Online]. Available: http://www.farsounder.com/technology/blog/sonar_performance_prediction.

[67] P. Etter, *Underwater Acoustic Modeling and Simulation*, New York: Spon Press, 2003.

[68] National Centers for Environmental Information, National Oceanic and Atmospheric Administration. (2015). *Bathymetric Surveys* [Online]. Available: https://maps.ngdc.noaa.gov/viewers/bathymetry/.

[69] J. Zhao, J. Yan, H. Zhang, Y. Zhang and A. Wang, "A new method for weakening the combined effect of residual errors on multibeam bathymetric data", *Marine Geophysical Research*, vol. 35, no. 4, pp. 379-394, 2014.

[70] A. Flinders, L. Mayer, B. Calder and A. Armstrong, "Evaluation of arctic multibeam sonar data quality using nadir crossover error analysis and compilation of a full-resolution data product", *Computers & Geosciences*, vol. 66, pp. 228-236, 2014.

[71] A. Schimel, D. Ierodiaconou, L. Hulands and D. Kennedy, "Accounting for uncertainty in volumes of seabed change measured with repeat multibeam sonar surveys", *Continental Shelf Research*, 2015.

[72] H. Saç, K. Leblebicioğlu and G. Bozdağı Akar, "2D High-frequency forward-looking sonar simulator based on continuous surfaces approach", *Turk. J. Elec. Eng. & Comp. Sci.*, vol. 23, pp 2289-2303, 2015.

[73] X. Lurton, *An introduction to underwater acoustics*. London: Springer, 2004.